Diagnosis of Feline Infectious Peritonitis

by

Yen-Chen Juan

A dissertation submitted to the Graduate Faculty of
Auburn University
in partial fulfillment of the
requirements for the Degree of
Doctor of Philosophy

Auburn, Alabama
May 8, 2018

Keywords:
Polymerase Chain Reaction, Assay Performance

Copyright, 2018 by Yen-Chen Juan

Approved by

Bernhard Kaltenboeck, Chair, Professor, Dept. of Pathobiology
Paul Walz, Professor, Dept. of Pathobiology
Kellye Joiner, Associate Professor, Dept. of Pathobiology
Chengming Wang, Professor, Dept. of Pathobiology

Abstract

Feline infectious peritonitis (FIP), a fatal immune-mediated disease, is caused by feline infectious peritonitis virus (FIPV), the high-virulence pathotype of Feline coronavirus (FCoV). It is believed that the FIPV is an accumulation of mutations of the low-virulence feline enteric coronavirus (FECV) favored by extensive viral replication and transmission in a multi-cat environment. However, the complete extent of such etiological mutations has remained unestablished. The absence of FIP-specific clinical signs and laboratory parameters further aggravates the diagnosis of FIP. Currently, an accurate FIP ante-mortem diagnostic assay is unavailable. In this study, we aimed to establish a highly sensitive FIP diagnostic PCR assay.

In the course of the investigation, we developed several quantitative real-time PCRs (qRT-PCR) targeting different genomic regions of FCoV, detecting FCoV via either mRNA or genomic RNA (FIP M gene mRNA qRT-PCR, FIP N gene mRNA qRT-PCR, and FIP MN gene qRT-PCR). We subsequently evaluated the performance of the PCRs by the use of the developed dual-labeling immunofluorescence (IF) assay as the gold standard. We concluded that the FIP MN gene qRT-PCR is the most accurate FIP diagnostic assay, with 84% sensitivity at 100% specificity, resulting in 100% positive and 47% negative predictive value. Upon discovering a symmetrical distribution of the results in the MN gene qRT-PCR and the IF assay, we evaluated the performance of the IF assay by using the MN gene qRT-PCR as the gold standard. The IF assay generated a 44% sensitivity at 100% specificity, resulting in 100% positive and 21% negative predictive value. Additionally, we pinpointed a serum albumin to globulin ratio of ≤ 0.5 was the most FIP-pertinent clinical correlate. We also determined that mutations of the furin cleavage motif within the FCoV spike protein that largely abrogate furin cleavage are associated with 58% of cases of FECV to FIPV conversion.

On the basis of this study, we established the FIP MN gene qRT-PCR as a robust single assay that greatly overcomes the ante-mortem diagnostic challenge of FIP. By demonstrating the co-localization of FIP viral vesicles with macrophages, the high resolution IF assay can be used as confirmatory FIP assay with 100% specificity.

Acknowledgments

The six years of my PhD life is not only the most brainstorming years in my life but also the most struggling years as a young adult. There is an old Chinese saying: mentors are those who convey the truth, pass on the knowledge, and clarify the confusions. I would like to thank my mentor Dr. Bernhard Kaltenboeck, being in his role, surfed with me through all the highs and lows. What a ride!

I would like to thank my committee members Dr. Kellye Joiner, Dr. Ken Macklin, Dr. Paul Walz, and Dr. Chengming Wang for letting me revisit the saying that knowledge is power that being able to apply the learned knowledge in the real world is an amazing thing.

I would like to thank Ms. Ludmila Kaltenboeck for her tremendous help with the PCRs and her emotional support. I would like to thank Ms. Dongya Gao for all the technical support. I would also like to thank Ms. Sabrina van Ginkel for her help with the Confocal microscope.

I would like to Dr. John Dennis for his knowledgeable lectures of immunofluorescence and his beautiful awesome friendship, which I cherish dearly. Salute to my fellow lab members: Dr. Erfan Chowdhury, Dr. Shamsur Rhaman, Dr. Anil Poudel, for their patient guidance. I would like to thank my everyday companies, Mr. Anwar Kalalah, the Giant, for showering me with his endless humor and free coffee, of course! Mr. Ramon Alejandro Zegpi Lagos for his amazing 24/7 comfort food supply chain, and Ms. Yuan Kang, for her warm friendship.

Lastly, I would like to pay my special thank you to Dr. Frederik van Ginkel, an outstanding teacher who cared about his students genuinely. Lastly, I would like to thank my family and my furry kids for, everything! Now the silence is broken, and the ocean is no longer calm. Time to sail, Cheers!

Table of Contents

List of Tables

List of Figures

List of Abbreviations

A/G	Albumin to globulin ratio
A1F1	Allograft 1 factor 1
AA	Amino acid
ALP	Alkaline phosphate
ALT	Alanine aminotransferase
AUC	Area under the curve
BUN	Blood urea nitrogen
CCoV	Canine coronavirus
cDNA	Complementary DNA
CNS	Central nervous system
DIF	Direct immunofluorescence
dL	deciliter
ER	Endoplasmic reticulum
ERGIC	Endoplasmic reticulum-Golgi intermediate compartment
FC	Furin cleavage
FCoV	Feline coronavirus
FECV	Feline enteric coronavirus
FIPV	Feline infectious peritonitis virus
FITC	Fluorescein isothiocyanate
FN	False negative
FP	False positive
H&E	Hematoxylin and eosin stain
IF	Immunofluorescence
IFN-α	Interferon alpha
IH	Immunohistology
IHC	Immunohistochemistry
IIF	Indirect immunofluorescence

Kb	Kilobase
M	Membrane
mRNA	messenger RNA
N	Nucleocapsid
NPV	Negative predictive value
Nsps	Non-structural protein
Nt	Nucleotide
ORF	Open reading frame
PCR	Polymerase chain reaction
Poly (A)	Polyadenylated
pp	Polyprotein
PPV	Positive predictive value
PRF	Programmed ribosomal frameshifting
RBC	Red blood cell
RdRp	RNA dependent RNA polymerase
RT	Reverse transcription
RT	Reverse transcription
RTC	Replication-transcription complex
S	Spike
S1	Spike protein domain 1
S2	Spike protein domain 2
Se	Sensitivity
Sg	Subgenomic
Sp	Specificity
TGEV	Transmissible gastroenteritis virus
$\boldsymbol{T}_{\mathrm{m}}$	Melting temperature
TN	True negative
TNC	total nucleated cells

TNCC	Total nucleated cell count
TP	True positive
TRITC	Tetramethyl rhodamine isothiocyanate
TRS	Translational regulatory sequences
UTR	Untranslated region
VLPs	Virus like particles
WBC	White blood cell

CHAPTER 1 LITERATURE REVIEW

1.1 BIOLOGY OF FELINE CORONAVIRUS

Classification and genome structure. Feline coronavirus (FCoV) belongs to the family *Coronaviridae*, order *Nidovirales*. Together with porcine transmissible gastroenteritis virus (TGEV) and canine coronavirus (CCoV), FCoV belongs to the subfamily of *Coronaviridae*, genus *Alphacoronavirus*, species *Alphacoronavirus 1*. Feline coronavirus is an enveloped, non-segmented single-stranded positive-sense RNA virus. It contains a large genome of ~30 kb in length, consisting of 11 putative open reading frames (ORFs). The structural and accessory proteins occupies only about one-third, 10 kb, of the viral genome, whereas the replicase gene encoding the nonstructural proteins (Nsps) makes up two-third, about 20 kilobase (kb) of the genome (Fehr and Perlman, 2015). The 5′ end of the genome is capped and comprises an untranslated region (UTR) and a leader sequence that is responsible for RNA replication and transcription along with a 3′ polyadenylated tail, allowing it to function as mRNA for translation of the replicase and polyproteins (Fehr and Perlman, 2015). Genome organization of FCoV is 5′- leader – UTR - replicase - Spike (S) - Envelope (E) - Membrane (M) - Nucleocapsid (N) - 3′ UTR - poly (A) tail, with accessory genes (3a-c, 7a and 7b) interspersed within the structural genes at the 3′ of the genome (**Fig. 1.1.1**).

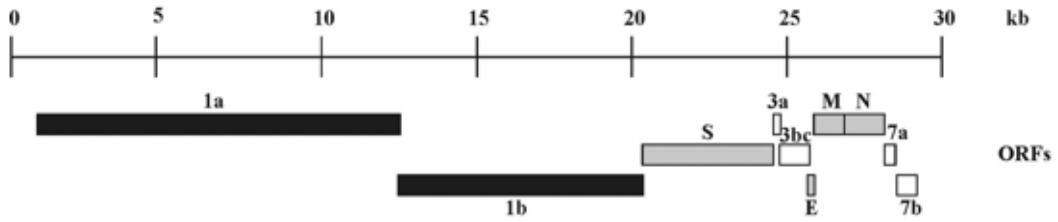

Figure 1.1.1. ***Feline coronavirus genome organization*.** FCoV has a genome size of ~30 kb in length, consisting of 11 putative open reading frames. The nonstructural proteins, ORF 1a and 1b occupies two-thirds, nearly 20 kb of the genome; the remaining structural and accessory proteins make up only about one-third, approximately 10 kb of the genome. (From *Tekes et al., 2008*).

Virion structure. The FCoV virion is nearly 125 nm in diameter as depicted in Fig. 1.1.2. It consists of 4 structural proteins: spike (S) protein, membrane (M) protein, nucleocapsid (N) protein, and envelope (E) protein.

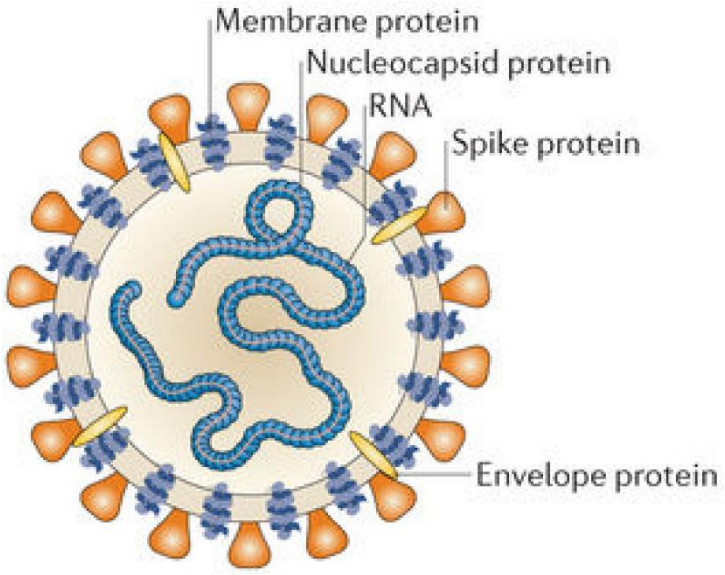

Figure 1.1.2. ***Feline coronavirus (FCoV) virion structure*.** The size of FCoV virion is about 125 nm in diameter. It contains 4 structural proteins: spike (S) protein, membrane (M) protein, nucleocapsid (N) protein, and envelope (E) protein. (From *Graham et al., 2013*).

The envelope is constituted of the S protein, a 180- to 200-kDa glycoprotein arranged in peplomers, which forms a large, bulbous surface projections of the virion, and thus give it the appearance of a royal crown, giving the name, coronavirus. The S protein

is critical for cell entry and determination of cell tropism, and thus is also the most variable protein in the coronavirus genome (Licitra et al., 2013). It is a type I transmembrane protein cleaved by a host cell furin protease into a N-terminal (S1) domain responsible for initial host cell attachment and binding, and a C-terminal (S2) domain responsible for the subsequent fusion of host cellular and viral membrane. Due to the function of the S protein, the S gene is considered the most variable region in the FCoV genome (Wu et al., 2009). In particular, the S1 domain is more variable than the S2 domain due to the intensive immune-selective pressure from host antibodies.

Several studies have investigated the correlation of functional mutations within the S gene and a change of cell tropism of the coronavirus (Chang et al., 2012; Licitra et al). Different amino acid changes have been identified, yet not a single one has been confirmed as the sole mutation that is responsible for the pathogenesis of feline infectious peritonitis (FIP), which is caused by the pathogenic FCoV. The M protein (~25-30 kDa) is a smaller protein with 3 transmembrane domains (Kuo et al., 2016). This protein is the most abundant protein in the virion (Fehr and Perlman, 2015) and the essential component involved in virion morphogenesis (Neuman et al., 2011; Fehr and Perlman, 2015, Kuo et al., 2016). The major function of the M protein is virion assembly and capture of other structural proteins at the budding sites (Neuman et al., 2011). Also, the M gene is one of the highly conserved regions of the coronavirus genome and therefore being used as a target sequence for PCR testing (Simons et al., 2005). By detecting messenger RNA (mRNA) of the M gene, the PCR is able to detect the active replication of the virus in specimens, which is thought to be specific for FIP diagnosis (Simons et al., 2005).

The N protein (~ 50kDa) chaperones and packages the viral RNA genome to form the flexible, helically symmetrical nucleocapsid (Fehr and Perlman, 2015). Its interaction with M protein also enhances the efficiency of virion assembly (McBride et al., 2014; Fehr and Perlman, 2015). As another conserved region of the coronavirus genome, the N gene is also a target region for PCR design (Dye et al., 2008; Kiss et al., 2000; Battilani et al., 2003; Sharif et al., 2011; Bálint et al., 2012). The E protein (~9 kDa) is a small protein that facilitates virion assembly and release (Kipar and Meli, 2014). Other properties of E protein include anti-apoptosis during infection (Dediego et al., 2011) and an ion channel function (Ruch and Machamer, 2012). Unlike M and N genes, the E gene is generally highly divergent (Ruch and Machamer, 2012), however, whether this polymorphism of the E protein sequence affect its function remains undetermined.

Life cycle. Infection of the host cell is initiated by interaction between the S protein and its receptor on the host cell surface (Licitra, 2015). The S protein is cleaved by a host protease into an N-terminal receptor binding domain (S1) and a C-terminal fusion domain (S2). The interaction between the S1 domain and the host cell surface receptor dictates the viral cell tropism and host selection. This interaction triggers the furin proteolytic cleavage of the S2 domain at two sites within the protein. The first cleavage enables the separation of the receptor binding domain (S1) and the fusion domain (S2); the second cleavage enables the exposure of fusion peptide that insert into the host membrane (Ruch and Machamer, 2012). Subsequently, an antiparallel six-helix bundle is formed that allows the fusion of the viral and host membranes. The viral nucleocapsid is then released into the host cytoplasm where replication occurs (Ruch and Machamer, 2012).

The next step is to translate the replicase gene from the viral genomic RNA. The replicase gene encodes two large ORFs, ORF1a and ORF1b, which express 2 co-terminal polyproteins, pp1a and pp1ab. In order to express two polyproteins from a single mRNA, the virus utilizes a programmed –1 ribosomal frameshifting (–1 PRF) machinery involves using the pseudoknot structure and slippery sequence (5′-UUUAAAC-3′), which enables differential protein translation of an mRNA sequencing by changing the ORF (Li et al., 2013). This frameshift only occurs in approximately 10% of the replicase translations, with the ribosome uncoiling the pseudoknot structure allowing the translation to continue until it meets the ORF1a stop codon (Ruch and Machamer, 2012). Occasionally, the ribosome is not able to uncoil the pseudoknot structure while it is translating the mRNA. As a consequence, the ribosome shifts back by 1 nucleotide and translates a new frame-shifted ORF. By utilizing the –1 PRF machinery, the virus is able to deliver the precise ratios of polyproteins required for efficient viral replication (Plant, 2010). These polyproteins are then cleaved into separate Nsps, which are subsequently assembled into the viral replication-transcription complex (RTC) (Sawicki, 2007).

Upon synthesis of a full-length negative-sense RNA by RTC, a discontinuous transcription follows and produces a nested set of sub-genomic negative-sense RNAs (Stadler et al., 2003). It is believed that during the transcription, RNA dependent RNA polymerase (RdRp) pauses randomly at any one of the body translational regulatory sequences (TRS) and either continues elongation to the next TRS or switches to transcribe the leader sequences at the 5′ end of the genome (**Fig. 1.1.3**) (Fehr and Perlman, 2016). These newly synthesized negative-sense intermediates serve as templates for the synthesis of positive-sense messenger RNAs (mRNAs) (Wu and Brian, 2010). This transcription

mechanism ensures that each produced mRNA has the same leader sequence, and thus PCR that target the leader sequence along with a downstream gene-specific primer would allow, via subgenomic (Sg) mRNA detection, the identification of replicating FCoV (Simons et al., 2005).

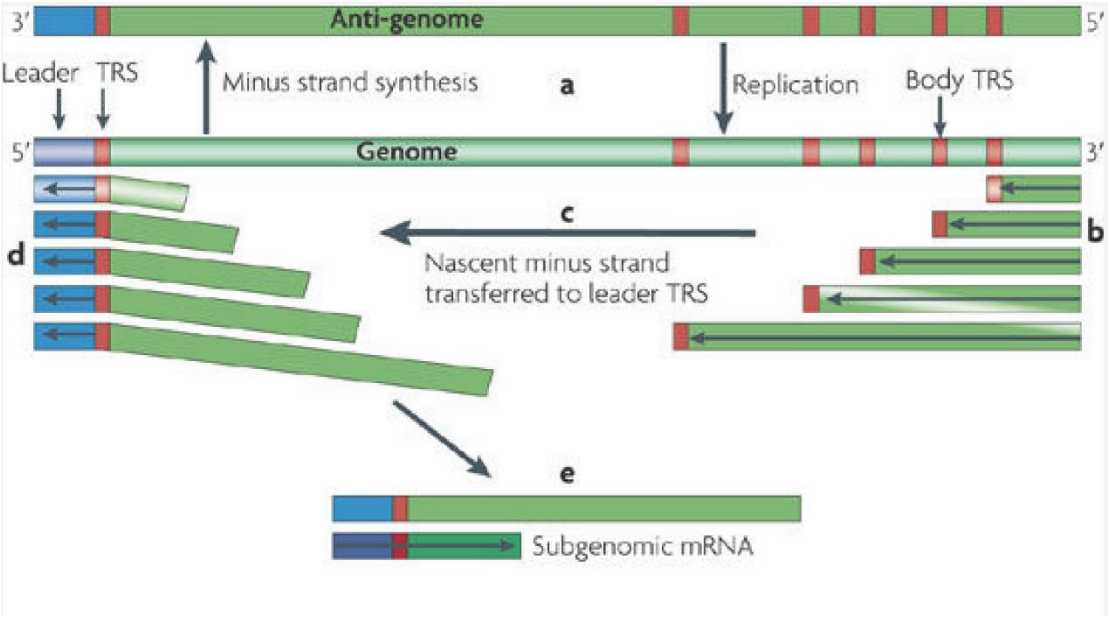

Figure 1.1.3. ***FCoV RNA replication mechanism.*** During replication, FCoV produces a nested set of sub-genomic negative-sense mRNAs that all possess identical 5′ leader sequence and 3′ poly (A) tails. Via discontinuous transcription, RNA dependent RNA polymerase (RdRp) encounters one of the body translational regulatory sequences (body TRS) and either continues elongation to the next TRS or switches to transcribe the leader sequences at the 5′ end of the genome. These subgenomic mRNAs then serve as templates for the synthesis of viral mRNAs. (From *Perlman and Netland, 2009*).

These positive-sense mRNAs are then translated into viral structural proteins S, E and M, which are inserted and folded into the endoplasmic reticulum (ER), where N protein is translated in the cytoplasm. (Fung and Liu, 2014). S, E, and M proteins migrate along the secretory pathway into the endoplasmic reticulum-Golgi intermediate compartment (ERGIC) for virion assembly. Protein-protein interactions play an important role in virion assembly. Virus like particles (VLPs) are only efficiently produced and released when

both E and N protein are co-expressed with M protein (Siu, 2008; Fehr and Perlman, 2016). S protein is not involved in virion assembly, yet it is incorporated into virions by interacting with M protein. Following virion assembly, mature virions bud into the ERGIC and are exported via the secretory pathway in smooth-wall vesicles and released by exocytosis (Fung and Liu, 2014). For FCoV in particular, a portion of the S protein is inserted into the plasma membrane instead of being incorporated into the virion. These S proteins mediate fusion of the infected cell with adjacent uninfected cells, resulting in formation of a syncytium, a large, multinucleated cell. This allows the virus to spread without being released into the extracellular space (Fung and Liu, 2014).

Serotypes. FCoV has 2 serotypes: type I and type II based on spike protein homology (Motokawa et al., 1996). Type I strains are exclusively feline, whereas type II strains are more closely related to CCoV than type I strains according to the sequence similarity of S protein (Motokawa et al., 1996; Wesseling et al., 1994). Other than S protein, comparative sequence analyses have demonstrated that type I and type II strains share high sequence similarity in the genes encoding ORF 7ab, M, and N proteins (Herrewegh et al., 1998). Collectively, the evidence suggests that type II FCoV strains are continuously generated by homologous RNA recombination between CCoVs and type I FCoV strains (Herrewegh et al.1998, Motokawa et al., 1996; Wesseling et al., 1994). This serotype classification is not necessarily related to the virulence since each biotype is comprised of low virulence feline enteric coronavirus (FECV) strains and high virulence feline infectious peritonitis virus (FIPV) strains (Borschensky and Reinacher, 2014).

However, some studies showed potentially conflicting evidence for association of either type I or type II FCoV with FIP. Kummrow et al. (2005) found that type I strains

induced higher antibody titers than type II strains, and predominantly associated with FIP clinical manifestation, whereas Lin et al. (2009) found that type II strains were more associated with FIP disease manifestation. Most studies reported that type I strains are more prevalent in the cat population worldwide (Addie et al, 2003; Benetka et al., 2004; Kummrow et al., 2005; Lin et al., 2009; Wang et al., 2014), however, mixed infections of both type have also been reported (An et al., 2011). Unfortunately, the field predominant type I strains have been proven very difficult to grow *in vitro*, which hinders the study of type I strain field infections (Benetka et al., 2004; Kummrow et al., 2005; Lin et al., 2009).

1.2 FELINE CORONAVIRUS INFECTIONS AND PATHOGENESIS OF FELINE INFECTIOUS PERITONITIS (FIP)

Feline coronavirus (FCoV) infection is ubiquitous in domestic cat populations, particularly in multi-cat environments (Pedersen et al., 2014). Two pathotypes of FCoV have been described: the low virulent FECV resides only in enteric cells, and usually causes either mild or asymptomatic infection, whereas the high virulent FIPV replicates in monocytes/macrophages and usually results in a fatal systemic immune-mediated infection (Cahn and Line, 2010; Pedersen et al., 2009) termed feline infectious peritonitis (FIP). FECV infection is mild and has little clinical significance. On the other hand, FIPV infection has gained research attention since its first report in the 1960s (Kim et al., 2016).

It has been postulated that mutations of FECV in individual cats alter the cell tropism of FECV allowing effective infection of monocytes/macrophages, which results in devastating systemic FIPV infection (Chang et al., 2012; Dedeurwaeder et al, 2013; Pedersen, 2014; Pedersen et al., 2009; Poland et al., 1996; Vennema, 1999; Vennema et al., 1998).

Several genes have been associated with the conversion of FECV to the FIPV biotype. These genes include accessory genes ORF 3c (Borschensky et al, 2014; Chang et al., 2010; Dedeurwaeder et al, 2013, 2014; Hora et al., 2016; Pedersen et al., 2012; Thiel et al., 2014; Vennema et al., 1998), 7a (Borschensky et al, 2014; Dedeurwaeder et al, 2013, 2014) and 7b (Borschensky et al., 2014; Dedeurwaeder et al, 2013, 2014; Lin et al., 2009); as well as among structural genes the spike protein gene (Chang et al., 2012; Licitra et al, 2013; Porter et al., 2014).

Mutations in the ORF 3c gene. An ORF 3c mutation of FECV associated with conversion into FIPV was first mentioned by Vennema et al. (1998). The study compared the sequence of 1.2- to 8.9-kb segments on the 3′ end of the genome of both FECV and FIPV isolates. The high sequence similarity between FECV and FIPV isolates indicated that it was likely the two strains share the same ancestry. Meanwhile, the deletions of ORF 3c and ORF 7b of some FIPV isolates but not FECV isolates implied that FIPV is a mutant of FECV. Chang et al. (2010) compared the sequence of ORF 3c genes from naturally occurring FECV and FIPV variants from fecal specimens collected from 27 apparently healthy cats and 28 FIPV infected cats confirmed by pathological examination. The results demonstrated that all FECVs variants had intact ORF 3c genes, whereas 20 out of 28 FIPV infected cats showed small in-frame insertions or deletions within the ORF 3c genes. It was not known whether these small mutations would alter the function of the ORF 3c proteins, however, it was certain these mutations would cause premature termination of translation and severe truncation of ORF 3c polypeptides. The study concluded that ORF 3c protein was required for successful replication of FCoV in the intestinal environment but dispensable for systemic infection. Several studies supported the findings that mutation of ORF 3c is a major determinant for the biotype conversion of FECV to FIPV (Borschensky et al., 2014; Hora et al., 2016; Pedersen et al., 2009, 2012), while other studies showed evidence to the contrary (Dedeurwaeder et al., 2013; Thiel et al., 2014).

Mutations in the ORF 7a and 7b genes. By comparing the sequences of field and laboratory FIPV strains, Herrewegh et al. (1995) found intact ORF 7b genes in all field FIPV strains but deletions in ORF7b genes only in laboratory propagated FIPV strains, and thereby they concluded that ORF 7b protein may play an important role in natural FIP

infections. Dedeurwaeder et al. (2013) investigated whether the deletion of ORF 3abc, ORF7ab, or both had an effect in the viral replication in monocytes. The study found that deletion of ORF 7ab abolished its replication in monocytes while the deletion of ORF 3c had a less pronounced effect on viral replication in monocytes. This finding is consistent with the hypothesis that an intact ORF 3c protein is important for viral replication in intestinal epithelium rather than in monocytes/macrophages. The same researchers further investigated the function of ORF 7ab protein and found that ORF 7a protein was indispensable for the evasion of the host IFN-α antiviral response. Interestingly, ORF 7a protein could exert the function only in the presence of ORF 3c protein. Another study suggested that deletion of ORF 7b may have decreased the virulence of laboratory FIPV strains (Pedersen, 2014). Since ORF 7b was well-conserved in all FCoV field strains, mutations of ORF 7b may not be involved in converting FECV to FIPV.

Mutations in the spike protein (S) gene. While some studies focused on mutations in accessory FCoV genes, other studies investigated whether mutations of structural proteins have an impact on conversion of FECV to FIPV (Chang et al., 2012; Licitra et al., 2013; Porter et al. 2014). Chang et al. (2012) reported the first mutations in the S gene that were associated with the conversion of FECV to FIPV. They first sequenced the full genome of 11 FECV-FIPV pairs, and found that the S gene harbored the most polymorphic sequences. They then sequenced the S gene region of hundreds of other FCoVs and found 2 alternative amino acid sequences, M1058L and S1060A, encoding the fusion peptide of the spike protein that distinguished FIPV from FECV in most cases. . The study concluded that it is likely that mutations within the S gene, maybe along with other mutations, account for the change to macrophage tropism that favors FIPV infections.

However, accroding to Porter et al. (2014), one of the mutation M1058L that Chang et al. (2012) proposed did not serve as one of the critical mutations that converts FECV to FIPV.

Another study examined the functional perspective of a furin cleavage site within the boundary of the S1 and S2 region (Licitra et al., 2013). They believed that mutations within S1/S2 region would alter the cleavage susceptibility of S protein, thus modulate the S fusogenic properties, leading to the change in cell tropism and ultimately to FIP. They first compared the sequences of this region from isolates of both pathotypes, and then confirmed that the observed mutations were functionally associated with susceptibility to furin cleavage. The study showed that mutations within the furin cleavage site of S gene influenced furin cleavage activity, and thus potentially change the cell tropism of the virus, leading to FIP disease manifestation (Licitra et al., 2013).

While some studies that focused on mutations of the virus appear to contradict each other, other studies investigated whether the host genetic background is the factor that drives the fatal systemic FIP infection. It is believed that a successful immune response, particularly with cell-mediated immunity, at the early stage of the infection, is able to rescue the host from ensuing fatal systemic infection (Kim et al., 2016; Vermeulen et al., 2013). However, up to date, not a single host factor has been genetically associated with fatal FIPV infection. Collectively, the response to an infection is complex and involves both the host and the virus. The combinations of factors from both entities can be highly variable and unpredictable. Therefore, it is plausible that there is no single factor that results in an FIPV infection. Rather, a combination of host factors such as stress level of the host and concomitant infections may determine the potential for successful immune response. But most importantly, it may be the FCoV infectious dose that drives the

potential of the virus for a stochastic mutation in a single virus genome that converts FECV into FIPV. Such mutant viruses may survive extraintestinally in the face of an ineffective immune response, ultimately precipitating FIP.

1.3 EPIDEMIOLOGY AND PATHOLOGICAL MANIFESTATIONS OF FELINE INFECTIOUS PERITONITIS

Prevalence and transmission. FCoV primarily infects enterocytes and mainly resides in the colon (Kipar et al., 2010). Virus shedding in feces occurs either persistently or intermittently (Kipar et al., 2010). Consequently, the prevalence of FCoV infection is usually influenced by the density of the feline host population. As a result, FCoV infection is generally highly prevalent in multi-cat environments, such as shelters, catteries, and pet stores (Kipar et al., 2010; Cahn and Line, 2010). Interestingly, despite the high prevalence of FCoV infection in such environments, only less than 5% of the cat population actually develops FIP, a disease with a virtually 100% mortality (Cahn and Line, 2010; Pedersen, 2009). The major risk factors include the amount of transient/chronic FCoV carriers and the overall frequency of virus shedding in the environment (Kipar and Meli, 2014). In order to cause FIP, FECV has to first gain access to monocytes/macrophages to trigger a subsequent systemic infection, which means that a critical change of cell tropism of FECV must take place. By its nature as a RNA virus, FCoV is prone to mutate at a high frequency, generating quasispecies (Addie et al., 2003). Under consistent high viral shedding, and infection and re-infection, the chance of mutational conversion of one of the highly polymorphic FECV quasispecies to FIPV is greatly increased.

Other than the virus itself, the individual and breed host genetic background also plays an essential role in FIP development, as well as age and gender of the affected animals. Most cats that develop FIP are 3 months to 3 years of age (Kipar and Meli, 2014; Pesteanu-Somogyi et al., 2005). Studies have reported that cats of pure breeds such as the Norwegian forest cat, Scottish fold, British Shorthair, Devon Rex, and Abyssinian are more

predisposed to FIPV infections than mixed-breed cats (Rohrbach et al., 2001; Soma et al., 2013; Worthing et al., 2012). Other potential predisposed breeds include Australian Mist Bengal, Birman, Himalayan, Cornish Rex, and Ragdoll (Cahn and Line, 2010; Norris et al., 2005). Male cats were reported having a higher incidence of FIP than female cats (Norris et al., 2005; Rohrbach et al., 2001; Soma et al., 2013; Worthing et al., 2012), in particular intact male cats (Rohrbach et al., 2001).

Gross lesions and clinical presentations. In 1966, feline infectious peritonitis was first reported from 16 cases, upon examination by abdominal necropsy, which found severe peritonitis with yellowish to gray fibrinous and granulomatous serositis, pyogranulomatous lesions on kidneys and livers, and effusive protein-rich exudate (Wolfe and Griesemer, 1966). Based on the gross pathological findings, the disease was termed Feline Infectious Peritonitis (FIP). However, the virus by no means is restricted to the peritoneum. Three forms of FIP were distinguished later: 1) a ″wet form″ with effusive exudate; 2) a non-effusive ″dry form″ with granulomatous lesions in parenchymatous organs; 3) a ″mixed form″ of both (Cahn and Line, 2010). Studies have shown that the wet form of FIP is predominant in most field infections (Horhogea et al., 2011; Tsai et al., 2011); however, another study found that the dry form of FIP was presented in numbers almost equal to the wet form in field infections (Norris, 2005). However, it is possible that the more prominent clinical presentation of the wet form may account for the higher reported incidence of the wet form over the dry form. Still, distinct differentiation between these two forms is not always possible since mixed-form infection and transformation between the two forms during infection are not uncommon (Cahn and Line, 2010; Tsai et al., 2011).

The wet form of FIP is typically characterized by a pyogranulomatous effusive exudate in peritoneum, pleura, and/or pericardium (**Fig. 1.3.1**) (Cahn and Line, 2010; Pedersen, 2014). The infected cat often shows clinical signs such as abdominal swelling and masses, enlarged mesenchymal lymph nodes, difficult breathing, and cyanotic mucous membranes (Cahn and Line, 2010; Hartmann et al., 2005; Pedersen, 2014).

Figure 1.3.1. ***Lungs and peritoneal viscera of a cat with FIP (wet form).*** Note the yellow and tan plaques of fibrin throughout the serosal surfaces of the lungs and visceral organs along with typical, straw-colored, frothy effusion. (From Hsieh and Burney, 2014).

On the other hand, cats with the dry form of FIP frequently have granulomatous lesions in kidneys, brains, and eyes (**Fig. 1.3.2**) (Kipar and Meli, 2014).

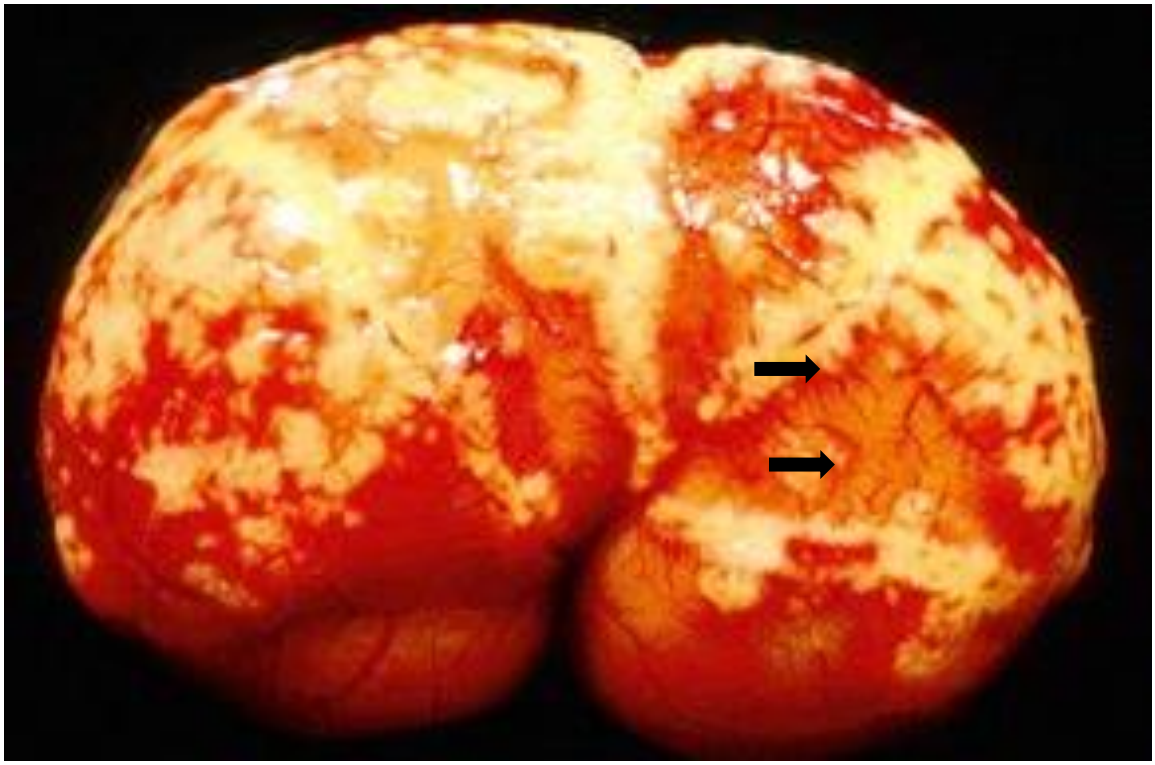

Figure 1.3.2. ***Kidney of a cat with FIP (dry form).*** Note the granulomatous lesions throughout the capsule of the kidney along with granulomatous phlebitis and periphlebitis of capsular veins (arrows). (Courtesy of Prof. Reinacher, Germany).

Clinical signs of neurological lesions are commonly found in FIP field infections (Diaz et al., 2009; Marioni-Henry et al., 2004; Rand et al., 1994; Tamke et al., 1988; Timmann et al., 2008). Hydrocephalus and hydromyelitis have been found in FIP cats with lesions confined to brain and spinal cord (Tamke et al., 1988). One study showed that FIP is one of the most common cause of spinal cord disease in cats (Marioni-Henry et al., 2004). The multifocal clinical signs associated with the central nervous system (CNS) reflect the different regions of CNS involvement, most commonly including ataxia followed by seizures and nystagmus (Cahn and Line, 2010; Tamke et al., 1988). Other signs include

deficits in cranial nerve function, central vestibular signs, hyperesthesia, paresis, and lameness (Cahn and Line, 2010; Tamke et al., 1988; Timmann et al., 2008). Ocular lesions are also commonly seen in cats with FIP, mainly characterized by uveitis, iritis, keratic precipitates, anisocoria, and chorioretinitis (Cahn and Line, 2010; Diaz et al., 2009; Horhogea et al., 2011). Occasional papular cutaneous lesions and skin fragility syndrome were also documented in cats with FIP (Cahn and Line, 2010). Despite the clinical manifestations with either form of FIP, the general clinical presentations associated with FIP are often non-specific (Cahn and Line, 2010; Horhogea et al., 2011; Norris et al., 2005; Tsai et al., 2011), such as inappetence, lethargy, weight loss, vomiting, diarrhea, and relapsing fever. For this reason, FIP diagnosis has remained difficult.

Histological findings. The histological appearance of FIP lesions is often pathognomic and therefore is used as the gold standard for diagnosis of FIP. As reported, the classic histological findings are serosal plaques consisting of considerable amounts of fibrin and inflammatory cells such as macrophages, plasma cells, lymphocytes, with occasional clusters of neutrophils (Cahn and Line, 2010; Kipar and Meli, 2014). Pyogranulomas can be found as large and consolidated lesions, occasionally with varying degrees of focal tissue necrosis (Cahn and Line, 2010) (**Fig. 1.3.3**). Phlebitis and periphlebitis are often found in FIPV infected cats that are mediated and dominated mainly by activated infected monocytes (Kipar and Meli, 2014). In some cases, lymphoid depletion in lymphoid tissues owing to apoptosis of lymphocytes can also be found in FIPV infected cats (Cahn and Line, 2010). The definitive diagnosis of FIP is often made by the classical FIP lesions (**Fig. 1.3.3**) combined with the presence of FCoV in macrophages shown by immunochemistry (**Fig. 1.3.4**).

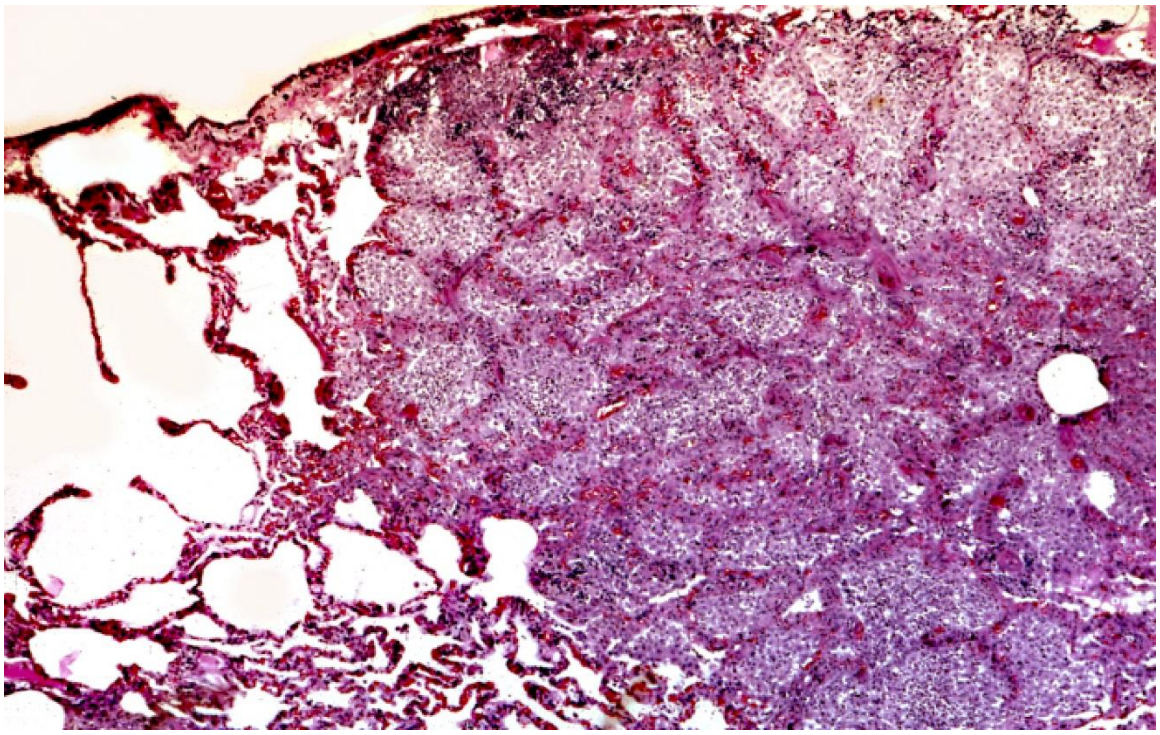

Figure 1.3.3. ***Hematoxylin and eosin (H&E) stain of lung tissue of an FIPV infected cat.*** Vasculitis/perivasculitis and multifocal pyogranulomas with alveolar edema can be observed. Infiltrates of inflammatory cells composed of plasma cells, macrophages, lymphocytes, and neutrophils are seen in the lung tissue. Blood vessel lumens are narrowed by these infiltrates. Thickened alveolar walls due to dilated capillaries and interstitial edema can be found. (Courtesy of Richard Jakowaski, USA).

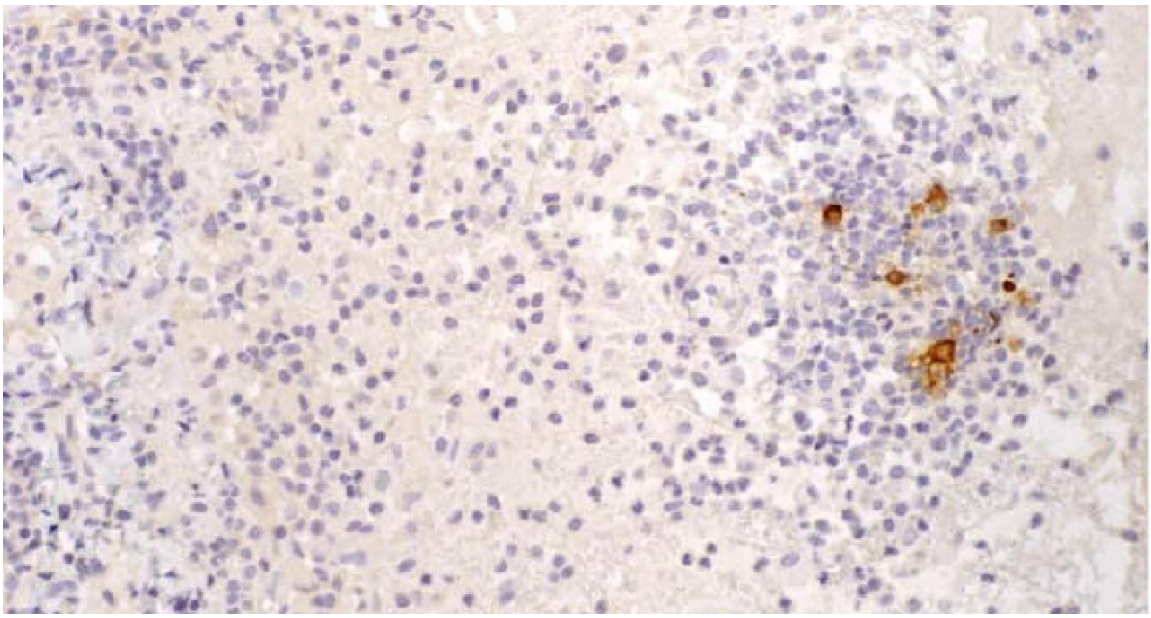

Figure 1.3.4. ***Definitive diagnosis of FIP.*** Feline coronavirus (FCoV) antigen is localized within macrophages along with FIP classic granulomatous lesions in the granulation tissue. Immunohistology (IH), mouse anti-FCoV (clone FCoV3-70). (From Kipar and Meli, 2014).

1.4 DIAGNOSTIC CONUNDRUM OF FELINE INFECTIOUS PERITONITIS

The definitive diagnosis of FIP can be obtained by detection of the presence of FCoV in monocytes/macrophages combined with gross and histological FIP-pathognomonic findings. However, a definitive ante-mortem diagnosis of FIP, in particular, the dry form of FIP, remains intangible. Therefore, a well-rounded diagnostic plan combining clinical manifestations and reliable diagnostic methods, rather than a single diagnostic method, is the preferred approach for an accurate ante-mortem FIP diagnosis. Diagnostic parameters and assays are usually evaluated by their sensitivity (Se), specificity (Sp), positive predictive value (PPV) and negative predictive value (NPV). In the case of FIP, a high PPV is more important than a high NPV because FIP diagnosis often results in euthanasia. Here, both indirect and direct ante-mortem diagnostic tests are discussed.

Circumstantial evidence. The combination of unspecific findings in physical examination, hematological and biochemical laboratory parameters, effusion and cerebral spinal fluid analysis, and serological tests can be very useful in diagnosing FIP in combination with the tests that directly detect virus in the specimens.

Physical examination. Early signs of either the dry or wet form of FIP are often non-specific such as anorexia, weight loss, lethargy, and recurring fever (Cahn and Line, 2010; Horhogea et al., 2011; Norris et al., 2005; Tsai et al., 2011). As the disease progresses, clinical presentations vary dependent on organ involvement. In the wet form of FIP, cats with peritoneal effusion often show abdominal distension with a fluctuation under palpation (Trotman et al., 2007). Occasionally, abdominal masses due to enlarged mesenteric lymph nodes, or omental and visceral adhesions can also be palpated (Cahn and Line, 2010). Cats with pleural effusion associated with FIP may have difficulty of

breathing and cyanotic mucous membranes (Cahn and Line, 2010). In the case of pleural effusions, auscultation of muffled heart sound and manifestation of low-voltage QRS complexes on ECG can be observed (Madias, 2013). Diagnostic imaging can confirm the presence of effusions in either peritoneum or pleura. In cats with the dry form of FIP, clinical presentations vary mainly depending on organ involvement, including ocular lesions, and neurological signs due to CNS or spinal cord involvement. Irregular nodules can be palpated in affected organs such as liver, kidney, or lymph nodes, and occasionally cutaneous lesions can also be found in cats with FIP. Collectively, FIP is often considered a primary differential diagnosis when a young cat develops vague symptoms consistent with FIP. However, to pinpoint the diagnosis of FIP, more information is needed.

Hematology and serum biochemistry. White blood cell counts (WBC) can be decreased or increased in cats with FIP. The most common hematological alterations include lymphopenia, mild to moderate non-regenerative anemia, and increased serum total protein (TP) concentration due to increased γ-globulin. One study indicated that increased serum TP concentration is the most consistent laboratory findings (Sharif et al., 2010), which is presented in nearly 50% of the cats with the wet form of FIP and in 70% with dry form.

Hartmann et al. (2003) compared different diagnostic parameters including TP concentration, γ-globulin concentration, and albumin to globulin ratio in serum. They showed an optimum cutoff value for different parameters: 8.0 g/dL for TP concentration, 2.5 g/dL for γ-globulin concentration, and 0.8 for A/G. There is consensus that among all parameters, A/G has a significantly greater FIP diagnostic value than total protein and γ-globulin concentration (Addie et al., 2009; Cahn and Line, 2010; Hartmann et al., 2003).

Some studies showed that an A/G <0.8 may have a PPV as high as 92%, but ranging also to a low PPV of 60% (Cahn and Line, 2010; Hartmann et al., 2003; Hartmann et al., 2005), but Jeffery et al. (2012) found only 12.5% PPV, in poorly defined FIP-suspect population that displayed only single FIP-consistent clinical symptoms. However, at an A/G >0.8, FIPV infection is highly unlikely (61%-100% NPV) (Cahn and Line, 2010; Jeffery et al., 2012).

As mentioned, diagnostic parameters with high PPVs are preferred in FIP diagnosis. However, PPV and NPV are subject to change depending on the prevalence of the disease. Liver (ALT, ALP) or kidney (BUN, creatinine) enzymes may be elevated depending on organ involvement (Addie et al., 2009), but they not specific enough to establish an etiologic diagnosis (Cahn and Line, 2010). However, FIP should be taken into differential diagnosis when hyperbilirubinemia combined with elevated liver enzymes are found in clinical cases (Cahn and Line, 2010).

Effusion analysis. Since effusion is a typical signature of the wet form of FIP, tests on effusion fluid generally have a much higher diagnostic value than blood tests (Addie et al., 2009; Cahn and Line, 2010; Hartmann et al., 2005). A classical effusion caused by FIP is usually clear straw colored to yellow, and viscous (Addie et al., 2009; Cahn and Line, 2010; Goodson et al., 2009; Hartmann et al., 2005). However, cases with pink and chylous effusions have also been reported. In addition, the effusion may froth when shaken due to the high protein concentration (>3.5g/dL) (Greene, 2013). This high protein content of effusions caused by FIP is classified as a modified transudate, nevertheless, the cellular content is generally low (<5000 nucleated cells/mL), with primarily neutrophils and macrophages (Addie et al., 2009; Cahn and Line, 2010; Goodson

et al., 2009 , Hartmann et al., 2005). Additionally, the Rivalta test can be used to distinguish between effusions caused by FIP and effusions of other causes. This is a simple test in which a drop of 98% glacial acetic acid is mixed with ~8 mL of distilled water in a transparent reagent tube, then one drop of effusion is then added (Addie et al., 2009; Hartmann et al., 2003). The high concentrations of fibrin and inflammatory cells in FIP effusion produce a positive reaction, which the drop retains its shape rather than dissolve in water. On study investigated the diagnostic utility of the Rivalta test in 497 confirmed FIP cases (Fischer et al., 2012). They found the test had a Sp of 65.5%, Se of 91.3%, PPV of 58.4%, and NPV of 93.4% with an FIP prevalence of 34.6% in the study cat population. However, bacterial peritonitis or lymphoma can also generate a positive result.

The collateral parameter of high protein content is a high γ-globulin concentration of the effusion, and therefore a low A/G, typically less than 0.5 is highly suggestive of FIP, whereas a A/G >0.8 has high NPV for FIP (Cahn and Line, 2010). Collectively, a straw-colored viscous effusion with high TP concentration (>3.5g TP/dL) and low cellularity of mainly macrophages and neutrophils, is highly indicative of FIP.

Other than the Rivalta test, some studies have shown that the delta total nucleated cell count (ΔTNCC) is high in effusions caused by FIP (da Cunha et al., 2009; Giordano et al., 2015). The TNCC is a parameter used to differentiate transudates and exudates (da Cunha et al., 2009). The TNCC can be determined by Sysmex XT-2000iV, a veterinary hematology analyzer, which has two laser channels, DIFF and BASO (da Cunha et al., 2009). The DIFF channel differentiates cells depending on nucleic acid content and complexity, whereas the BASO channel differentiates cells depending on volume and the complexity of cellular residues generated after contact with an acidic reagent that collapses

all nucleated cells except basophils (da Cunha et al., 2009). The delta total nucleated cell count (ΔTNCC) is the ratio between DIFF and BASO TNCC. Based on the findings, all the FIP cats in the study had a ΔTNCC >3.0, and only 2 cats out of 20 FIP cats had a ΔTNCC <3.0 (Giordano et al., 2015). They determined that the best cut off value for ΔTNCC was 1.7. Therefore, ΔTNCC can also be considered as an alternative for FIP effusion analysis.

Cerebrospinal fluid (CSF) analysis. Cats with neurological symptoms associated with the dry form of FIP often have increased CSF protein (50-350 mg/dL; reference value: <25 mg/dL) and pleocytosis (100-10,000 nucleated cells/mL) consisting of mainly lymphocytes, macrophages, and neutrophils (Addie et al.,2009; Cahn and Line, 2010). However, due to the viscous nature of the CSF, obtaining the sample is challenging. Brain herniations are seen in some cases when performing a CSF tap, and therefore extra care must be taken when having the procedure (Greene, 2013). However, studies of cats with neurological signs associated with FIP have found normal CSF in many of these animals, rendering CSF analysis a poor diagnostic approach (Addie et al., 2009; Cahn and Line, 2010; Hartman et al., 2005).

Anti-FCoV antibody detection. Current available serological tests can only detect antibody against FCoV, and cannot differentiate antibodies against high-virulence FIPV strains from low-virulence FECV strains. Moreover, a high FCoV antibody titer can be found in most clinically healthy cats in multi-cat environments (>90% seropositive) yet only 5% of the population develops subsequent FIP (Drechsler et al., 2011). Therefore, a positive FCoV antibody titer should be interpreted carefully along with other clinicopathogical findings and diagnostic results. Very high FCoV antibody titers of or

above 1:1600 are highly suggestive an FIPV infection. A false-negative antibody test result can be generated when virus particles in the serum specimen bind to the antibody, making it unavailable to antigen binding in the test (Greene, 2013). However, serological tests can be particularly useful in preventative population screening and subsequent disease management (Cahn and Line, 2010).

Direct FCoV detection. A tentative ante-mortem diagnosis of FIP can be made with signalment and FIP-associated clinical presentations, combined with indirect diagnostic tests such as effusion analysis and/or serological tests. However, not a single indirect diagnostic test per se is able to generate a definitive diagnosis of FIP. A potential definitive ante-mortem diagnosis of FIP can be made via direct virus detection either by 1) detection of viral RNA (RT-PCR), or 2) detection of virus particles in monocytes/macrophages in specimens (IF or IHC).

Polymerase chain reaction (PCR) testing. In 1994, a PCR assay for FIP diagnosis was first reported (Li and Scott, 1994). FCoV viral load can be measured qualitatively and quantitatively via either detecting the actual presence of virus (genomic RNA) or active replication of the virus (mRNA). A PCR detecting genomic RNA provides the quantity of FCoV present in the specimen. However, based on the sequence similarities of FECV and FIPV, PCR testing is unable to differentiate the two FCoV biotypes. In addition, viremia can be detected not only in FIP diseased cat but also in clinically healthy cats th, indicating that a small number of FCoV particles may enter the bloodstream but fail to replicate or cause FIP.

For this reason, Simons et al. (2005) first proposed a PCR detecting the actively replicating virus via detection of FCoV mRNAs. Replicating FCoV outside of the

intestinal tract would represent the pathogenetic principle of FIP, thus an FCoV mRNA PCR assay would definitively diagnose FIP (Simon et al., 2005). By utilizing the unique continuous coronavirus transcription mechanism, they designed a PCR targeting the leader sequence along with a downstream gene-specific primer that allows, via subgenomic mRNA detection, the identification of replicating FCoV. Combined with the leader sequence at the 5' end of the FCoV genome, the highly conserved M gene was used as the target for this PCR.

This PCR assay was applied to detect FCoV mRNAs in 1,075 blood specimens. The results showed that 5% of the clinically healthy cats were positive, whereas 93% of histologically confirmed FIP-positive cats were positive. These results indicated that 1) the PCR that detected mRNAs of FCoV M gene has high PPV and NPV for FIP diagnosis; and 2) the notion that FCoV is capable of replicating outside of the intestinal tract is not the sole determinant of FIP development. A subsequent study investigated the utility of the same PCR platform for quantification of FCoV in blood specimens from cats with or without clinical signs of FIP (Can-Sahna et al., 2007). The results of this study demonstrated that 14 out of 26 (54%) of the cats were positive for FCoV, however, only one of the cats had clinical presentations that were associated with FIP. Moreover, more than half (52%) of the clinically healthy cats in this study were positive by this PCR, demonstrating dramatically different results from those reported by Simons et al. (2005).

Another study investigated the utility of PCRs that detected either M gene mRNA or genomic RNA of the membrane-nucleocapsid junction of the FCoV genome (Dye et al., 2008) in blood specimens and feces from 205 clinically healthy shelter cats (Fish et al., 2017). Nine cats (4.4%) of the cat population were positive for genomic RNA in blood

specimens, and only 1 cat out of these 9 cats was positive for FCoV M gene mRNA, indicating active FCoV replication outside of the intestinal tract. This PCR assay targets the same M gene region reported by Simons et al. (2005) yet with modifications of degenerate primers and probe designed to cover all the known FCoV variants. Also, step-down thermal cycles and optimization of nucleic acid extraction and PCR were applied to maximize the efficiency of the PCR to robust single target copy detection and differentiation by high resolution melting curve analysis (Kaltenboeck, US patent 7252937 B2, 2007). The nucleotide sequence of this PCR amplicon demonstrated a unique upstream 33-bp in frame deletion combined with multi-locus nucleotide polymorphisms (Fish et al., 2017). The cat remained clinically healthy within the 6-month observation period after testing positive.

This study again showed that active FCoV replication outside the intestinal tract does not guarantee subsequent FIP disease. The host genetic background and environmental factors also play roles in FIP development. However, it is possible that the low copy numbers of the FCoV RNAs in the specimen indicated low amount of replicating virus presented in the cat, which may not be sufficient to trigger potent B cell immunity that enhances the uptake and the replication of FCoV in macrophages that result in subsequent clinicopathological changes associated with FIP. In conclusion, PCR has been proven as one of the most reliable tests for FIP diagnosis. However, different laboratory techniques in design and execution of PCRs can vastly influence the accuracy of the tests. These include differences in the pre-PCR step: specimens handling and nucleic acid extraction method; and the PCR design and execution itself: primers and probe design, PCR optimization and data analysis. Additionally, it is more difficult to quantify the target

copy number due to uncertain amount of cDNA templates present after the initial RT step (Bustin and Nolan, 2004). Hence, the resulting varying Sp and Se of the currently available PCR tests for FIP diagnosis suggests that PCR testing should not be the sole diagnostic approach for a definitive FIP diagnosis.

Immunolabeling of FCoV. Immunolabeling of FCoV antigens in effusions or tissues is considered the most specific test for FIP diagnosis since it enables the direct visualization of FCoV viral particles in macrophages, which is the functional characteristic of an FIPV infection (Cahn and Line, 2010). There are four general classes of immunolabeling techniques: direct and indirect detection combined with immunohistochemical (IHC) or immunofluorescent (IF) visualization. Direct detection uses a single Ab that binds the specific target and is also conjugated either to an enzyme (IHC) such as peroxidase or to fluorescent dye (IF). Indirect detection uses two antibodies, the unlabeled primary Ab specifically binds the target molecule, and the secondary Ab, conjugated with an enzyme (IHC) or a fluorophore (IF), binds to the primary Ab. Both techniques therefore allow visualization of the distribution of the target molecules and their association with cells throughout the specimen. However, indirect detection allows better control of the reaction, and therefore has higher specificity than direct detection.

Immunohistochemical (IHC) FCoV labeling. IHC has been mostly applied to tissue specimens from FIP-suspect cats with the dry FIP form (Brown et al., 2009; Hugo et al., 2013; Paltrinieri et al., 2001; Poncelet et al., 2008; Tammer et al., 1995). To obtain optimal pre-mortem tissue specimens, invasive methods such as laparotomy or laparoscopy are usually required (Addie et al., 2009). However, immunohistochemical FCoV labeling can also be applied to effusions or fluids from FIP-suspicious cats. Ives et al. (2013)

reported the first use of IHC in the CSF specimen along with other FIP pathognomonic histological findings in one FIP suspicion cat. The IHC staining showed 5 out of 16 infected cells by the presence of intra-cytoplasmic brown-stained FCoV antigen. However, the study was not able to demonstrate the utility of the test based on a single case. Later, another group (Gruendl et al., 2017) conducted a case-control study to investigate the utility of the same IHC assay that Ives et al. (2013) described in a larger clinical cohort of 41 cats. They reported that this IHC assay had a Se of 85.0%, however, the Sp of this assay was lower in cats with histologically confirmed CNS lesions (77.8%) than in those without (Gruendl et al., 2017). They concluded that the few positively stained macrophages found in the FIP cats without histologically confirmed CNS lesions might not be enough to trigger a robust inflammatory response and thus cause the histological lesions. In addition, non-specific staining and specimen contamination might contribute to the false positive results (Gruendl et al., 2017). However, the literature consensus is that a positive IHC of FCoV within macrophages should still be considered a definitive diagnosis of FIP.

Immunofluorescent FCoV staining. Parodi et al. (1993) performed direct IF (DIF) on pleural and peritoneal effusions from 32 cats with clinical signs of FIP. The study found high Se (95.5%) and high Sp (100%), and thus concluded DIF should be included in routine diagnosis of FIP. A later study (Hartmann et al., 2003) also investigated the diagnostic utility of a DIF method similar to that of Parodi et al. (1993). The study demonstrated a Se of 57% and Sp of 100% for this assay. Despite varying Se and Sp of different DIFs, the PPVs of the test are 100%, suggesting a positive result of DIF confirms a FIPV infection. Another study was conducted by Litster et al. (2013) to examine the high PPV of FIP DIF, but used an anti-FCoV antibody conjugate different from that used by

Parodi et al. (1993). A Se of 100% and Sp of 71.4% were reported (Lister et al., 2013). These studies confirmed a very good diagnostic utility of DIF for detecting FCoV in macrophages, albeit with differences in specificity in dependence of the detection antibody used.

Indirect immunofluorescence (IIF) is preferred because it allows better control of unspecific background signals. However, investigations into the diagnostic utility of IIFs for FIP diagnosis, however, are limited (Amer et al., 2012; Hok, 1989; Tresnan et al., 1996). An early study examined the diagnostic utility of an IIF assay on a cat population of 231 cats from multi-cat households (Hok, 1989). They compared the IIF results to serological tests and virus isolation using blood and various diseased tissue specimens respectively. The results demonstrated an IIF with a Se of 71-100% and Sp of 67-100% for FIP diagnosis (Hok, 1989). A subsequent study investigated the role of feline aminopeptidase N in various coronaviruses including FCoV by using IIF as a tool to demonstrate the successful FCoV transfection of the laboratory cell lines (Tresnan et al., 1996). However, the emphasis of the study was not on the evaluation of diagnostic value of the IIF. Another study successfully demonstrated the demographic distribution of FCoV particle in infected Crandell feline kidney cells by IIF (Amer et al., 2012). The fluorescent signal was only apparent in the cytoplasm of the infected cells, but not the nucleus. This finding was consistent with the life cycle of FCoV in which mature virions are assembled and transported in the cytoplasm of infected cells before exocytosis (Fung and Liu, 2014). In conclusion, IF as an ante-mortem diagnostic approach is promising, however, different antibodies used, assays of low quality, and cumbersome experimental procedures make IF

less of a primary diagnostic tool for FIP diagnosis. However, IF can be a highly reliable confirmatory assay due to its high PPV.

CHAPTER 2 RESEARCH OBJECTIVES

2.1. RESEARCH OBJECTIVES

An accurate ante-mortem diagnosis of FIP is of great importance due to several reasons: 1) to provide a robust basis for further study of FIP pathogenesis; 2) to provide reliable background information for FIP epidemiological studies; 3) to ensure the best clinical descision making between treatment options or euthanasia of the diseased cats; 4) to prepare the owner and/or manager of multi-cat facilities for disease control and prevention. An accurate ante-mortem diagnostic test for FIP diagnosis will be valuable by its ability to: 1) directly detect virus itself by either detection of viral RNA/mRNA or visualization of viral particles within the infected cells; 2) deliver high Se, Sp, PPV, and NPV, with preference for a test of high PPV over one with high NPV; 3) generate a potentially definitive test result by itself, or with only a few confirmatory tests; 4) produce equally accuate results among all specimen types, with preference for tests that require small specimen quantities; 5) generate consistenct results; and 6) offer quick turn-around time favoring clinical decision making.

FIP infection has been intensively studied since its first emergence in the 1950s, however, an accurate ante-mortem diagnosis of FIP is still a substantial challenge. The hindrances are 1) non-specific clinical presentations and laboratory findings of FIP - the clinical signs and laboratory findings associated with FIP lead to a broad spectrum of differential diagnoses; 2) no currently available serological diagnostic assays are able to distinguish FIPV from FECV infections, nor can determine whether the animal is immune or susceptible to FIP infection. In addition, Se and Sp of the tests vary markedly between laboratories, and even personnel in the same laboratory.

Taking these issues into consideration, we hypothesized that 1) FIPV is functionally characterized by its ability to replicate outside the intestinal tract; 2) the membrane (M) and nucleocapsid (N) genes are most conserved among FCoV strains; 3) a PCR assay that detected the mRNAs of the two most conserved M or N gene region of the virus was able to detect the active replication of FIPV outside of the intestinal tract, identifying the functional characteristics of FIP infection; 4) an immunofluorescent (IF) assay that demonstrated the presence of FCoV in monocytes and/or macrophages is considered a definitive diagnostic method of FIP; 5) a well-rounded accurate FIP diagnostic approach would include a careful evaluation of patient history, critical clinicopathological findings, and PCR and IF results; 6) amino acid changes within the R-S/A-R-R-S furin cleavage motif in the region between receptor binding (S1) and fusion (S2) domains of the FCoV spike protein render this protein resistant to furin cleavage and convert FCoV into an FIP virus that is capable of replicating in cells (monocytes/macrophages) other than enterocytes, precipitating FIP disease in susceptible cats. Thus, detection of a mutated furin cleavage S1/S2 (fcS1/S2) motif with one or more amino acid substitutions is highly suggestive, if not indicative of FIP. The purpose of this study was to pinpoint the most accurate diagnostic plan of FIP infection, and the hypotheses on which this study was based determined the research objectives.

The research objectives of this investigation were,

1) Evaluate the diagnostic accuracy (sensitivity & specificity) of an FIP membrane gene mRNA quantitative real-time PCR assay (FIP M gene mRNA qRT-PCR). Achieve this goal in a case-control study by obtaining from submitting veterinarians the clinical and final diagnostic data of positive and negative cases out of the

approximately 1,800 FIP specimens submitted annually to the AU Molecular Diagnostics Laboratory for diagnosis by FIP M gene mRNA.

2) Evaluate the diagnostic accuracy (sensitivity & specificity) of FIP nucleocapsid gene mRNA quantitative real-time PCR assay (FIP N gene mRNA qRT-PCR) and FIP membrane and nucleocapsid quantitative real-time gene PCR assay (FIP MN gene qRT-PCR). Achieve this goal by utilizing cases from objective 1.
3) Establish a FIPV indirect immunofluorescent (IF) assay. Achieve this goal by utilizing primary antibodies against FCoV and macrophages, combined with fluorophore-conjugated secondary antibodies.
4) Evaluate the correlation of mutations in the fcS1/S2 motif of the FCoV spike (S) gene, as determined by fcS1/S2 motif quantitative real-time PCR assay (FIP fcS1/S2 gene qRT-PCR) and DNA sequencing. Achieve this goal by use of nucleic acids isolated from an FIP-biased population of clinically confirmed positive FIP cases obtained for objective 1 and from an FIP-unbiased FCoV sequence population obtained from randomly-sampled FIP fcS1/S2 gene PCR-positive juvenile cats undergoing FCoV herd infection at the Animal Shelter of the Montgomery Humane Society in Montgomery, AL.
5) Establish the most accurate approach to diagnosis of FIP, by finding optimal correlates of FIP disease outcome and combinations of patients' history, critical clinical/clinicopathological parameters, FIP M gene mRNA qRT-PCR, FIP N gene mRNA qRT-PCR, FIP MN gene qRT-PCR results, and IF results.

CHAPTER 3 FIP Membrane gene messenger RNA quantitative reverse transcription PCR (FIP M gene mRNA qRT-PCR)

3.1. INTRODUCTION

Ante-mortem diagnosis of Feline infectious peritonitis (FIP) still remains a challenge since its first recognition in 1963. Circumstantial clinical findings such as physical examination, laboratory parameters, and analysis of effusions and CSF are not specific to FIP diagnosis, which makes the initial differential diagnosis difficult. Serologically, an anti-FCoV titer greater than 1:1600 is highly suggestive of FIP. However, serological tests cannot differentiate FECV and FIPV strains, and therefore a positive result should be interpreted carefully together with other diagnostic findings. Direct FCoV detection including polymerase chain reaction (PCR) and immunofluorescence (IF) seem promising. However, sensitivity and specificity of such reported test are dubious (Doenges et al., 2017; Fish et al., 2017; Li and Scott, 1994; Hartmann et al., 2003; Herrewegh et al., 1995; Simons et al., 2005), and careful examination of details including experimental design and optimization must be addressed to correct shortcomings of current assays.

Polymerase chain reaction, by use of a thermostable DNA polymerase, is a laboratory technique that enables the replication of billions of copies of an original piece of target DNA in a test tube within hours. Since the introduction in 1987, PCR has been refined and extensively used for molecular diagnostics to detect minute target DNA or RNA in the specimens. To detect feline coronavirus (FCoV), a RNA virus, an extra step of reverse transcription (RT) of RNA to complementary DNA (cDNA) is included as the initial step in the PCR. RT-PCR can be carried out in either one-step or two-step methods.

The one-step method combines reverse transcription reaction and PCR operation in one tube, priming cDNA only from the downstream target-specific primer. The two-step method involves a separate step of generating cDNA with random hexa- or deca-mer oligonucleotides, followed by addition of the cDNA to the subsequent PCR. In molecular diagnosis, one-step RT-PCR is preferred over two-step RT-PCR, which generates an abundance of background cDNA that results in non-specific amplicons and inefficient PCRs that are incapable of detecting single target molecules. A RT-PCR can be designed to detect either the actual presence of the virus (genomic RNA) of FCoV or the active replication of the virus (mRNA).

PCR has been described for FCoV detection and FIP diagnosis for more than two decades (Li and Scott et al., 1994). PCR assays that detect genomic RNA of FCoV reported high Sp of 88-100% (Hartmann et al., 2003; Herrewegh et al.,1995) but Se as low as 23.1% (Doenges et al., 2017). However, PCRs that detect FCoV genomic RNA do not necessarily indicate an ongoing FIPV infection since FCoV viremia has also been reported in clinically healthy cats (Cahn and Line, 2010; Fish et al., 2017). The fact that FIPV replicates in macrophages while the low virulence FECV counterpart cannot may provide a functional solution to the FIPV detection conundrum. Simons et al. (2005) developed a novel PCR assay that detects FCoV mRNA rather than genomic RNA. Thus, by detecting active replicating FCoV, this assay detects FIPV by its functional characteristic, the virus replication in extra-intestinal tissue that triggers the subsequent, fatal immune response. The assay demonstrated a Se of 93% and a Sp of 100% detecting FCoVs in blood specimens, representing a profound improvement over previously described FIPV PCR assays (Li et al., 1994; Hartmann et al., 2003; Herrewegh et al., 1995).

In this study, we included the fundamental concept of a functional FIPV PCR assay that Simon et al. (2005) reported to design a FIP M gene mRNA qRT-PCR. The PCR design includes a forward primer of the universal FCoV mRNA leader sequence and a reverse primer from a highly conserved region of FCoV M gene. In this method, the anti-sense reverse primer anneals to FCoV subgenomic M gene mRNA, priming the synthesis of anti-sense cDNA of M gene mRNA. The positive-sense forward primer derived from the leader sequence anneals to full-length cDNA of the FCoV M gene mRNA, as well as to the upstream single leader sequence of the negative sense FCoV genomic RNA template produced during FCoV replication and or cDNA of genomic RNA primed by the reverse M gene primer. Therefore, both primers create single-stranded cDNAs that will recombine to form the double-stranded PCR target, amplifying only the short, partial subgenomic mRNA target of the FCoV M gene. In addition, we used optimal nucleic acid extraction methodology that stabilizes nucleic acids in specimens and concentrates them 10-50 times higher for PCR input than standard methodology, as well as optimized real-time PCR and RT-PCR chemistry and thermal cycling. The use of fluorescence resonance energy (FRET) probes enables this PCR assay to accurately quantify FCoVs in real time. Collectively, these improvements resulted in robust amplification of single PCR targets, thereby maximizing sensitivity at virtually 100% specificity (DeGraves et al., 2003; Kaltenboeck & Wang, 2005; Wang et al., 2004; US Patent 7,252,937 B2). More importantly, while using FCoV genomic RNA and cDNA templates in addition to the M gene mRNA template, the FIP M gene mRNA qRT-PCR eventually detects only FCoV M gene mRNA, the functional equivalent of FIPV.

3.2. MATERIALS AND METHODS

Design of primers and probes. This PCR design exploited the fact that coronaviruses have unique transcription mechanism. All coronaviruses mRNAs share identical leader RNAs derived from the 5' end of the genomic RNA. Upon transcription, this leader sequence is spliced onto the transcript encoding every gene, producing the final subgenomic mRNA (Jeong et al., 1994). Thus PCR-targeting the leader sequence along with a downstream gene-specific primer would allow, via subgenomic mRNA detection, the identification of replicating FCoV. Combined with the leader sequence at the 5' end of the FCoV genome, the highly conserved M gene is the target for the FIP M gene mRNA qRT-PCR. A complete set of FCoV M gene sequences was aligned as nucleotide as well as translated amino acid sequences for identification of maximally conserved regions of the FCoV M gene. Long (32-35 bp) degenerate primers were designed that cover all known variants of the leader sequence and a highly conserved region of the M gene to produce a 282 bp amplification product. Fluorescence resonance energy transfer (FRET) probes for an intervening conserved region were also designed as long degenerate oligonucleotides that could hybridize to all known sequence variants and produce a fluorescent signal even from sequences with multiple mismatches. The final primer and probe sequences (**Table 3.2.1**) were designed for maximum statistical fit based on the polymorphism of FCoV M gene. All oligonucleotides were designed by use of the Vector NTI software (Invitrogen Corportation, Carsbad, CA). The fluorescein probe was 3' modified with a donor fluorophore (6-carboxyfluorescein, 6-FAM) and combined with the LCRed 640 acceptor probe (5' labeled with LightCycler Red 640, 3' phosphorylated, and HPLC-purified). All probes were synthesized by Integrated DNA Technologies (Coralville, IA).

Table 3.2.1. Oligonucleotide primers and probes used in FIP M gene mRNA qRT-PCR

Primer/probe	Sequence (5'→3')[a]
Upstream primer	GCCTTGTGCTAGATTTGTCTTCGGACA
Downstream primer	AGCCAGCTAAATTGHGGTCTDCCATATTG
Fluorescein probe	CGTGGTGATCTTATYTGGCATCTYGCWAACTGGA-6FAM
LCRed640 probe	LCR640-CTTCAGCTGGTCTGTAATATTGATYGTTTTTATAACAGT-P

[a] Degenerate bases are marked in red. D represents A or G or T, H represents A or C or T, W represents A or T, Y represents C or T. 6-FAM indicates 6-carboxyfluorescein. P indicates phosphate.

Specimen sources and handling. Between 2014-2016, three thousand and eight hundred ninety one specimens were analyzed. These specimens were collected by veterinarians nationwide from cats, for which there was a clinical suspicion of FIP, and submitted for PCR diagnosis to the Auburn University Molecular Diagnostics Laboratory. The specimens were shipped at ambient temperature without prior refrigeration or frozen storage. Four hundred microliter of each specimen were mixed with an equal amount of binding buffer [6 M guanidine-HCl, 10 mM urea, 20% (v/v) Triton X-100, 10 mM Tris-HCl, pH 4.4] per manufacturer's instructions in a 2 ml vial upon receiving by the laboratory.

Nucleic acid extraction. To maximize the accuracy of this assay, an optimal nucleic acid extraction method was developed to stabilize nucleic acid in specimens and to concentrate them 10-50 times for PCR input (DeGraves et al., 2003). Total nucleic acids were extracted from the specimens by use of glass fiber matrix binding and elution with the High-Pure PCR Template Preparation Kit (Roche Diagnostic, Indianapolis, IN, USA). To the binding buffer and specimen mixture, 80 µl of Proteinase K digestion enzyme was added (Roche Diagnostics, IN) and vortexed in a Precellys 24 homogenization shaker (Bertin Technologies, France) at 3,000×g, three times for 60 seconds with 60 second intervals between shaking cycles. After homogenization, the vials were centrifuged at 8,000 rpm for 1 min to remove the foam. Then the vials were incubated at 72°C for 20

min. Following the incubation, 200 µl of isopropanol (Fischer Scientific) was added to the contents of the 2 ml vial and vortexed. In the next step, DNA was bound to a spin column glass filter that was inserted in a 1.5 ml collection tube. The filter was centrifuged at 3,000×g for 1 min to remove the original sample mixture, then centrifuged each time again after addition of inhibitor removal buffer (500 µl, once) and wash buffer (500 µl each, twice). Subsequently, residual fluid in the filters was removed by centrifugation in a new collection tube at high speed (14,000×g) for 20 sec, then filters were transferred again to a new collection tube. Nucleic acids were eluted in a final volume of 40 µl (2×20 µl), following incubation at 72°C for 5 min with addition of 20 µl elution buffer each time. An extraction blank was included in each extraction set to be used as negative control for surveillance of contamination and/or non-specific amplification.

Optimization and validation of the PCR. The quantification standard was commercially synthesized as target DNA cloned into an expression plasmid. The assay is performed as one-step RT-PCR modeled on the proprietary RT-PCR thermal design (Wang et al., 2004). The PCR was optimized by fine-tuning the annealing and fluorescent signal acquisition temperature, extension time and temperature. The sensitivity of the FIP M gene mRNA PCR was validated by serial limiting dilution of positive specimens. The limit of detection was a single mRNA copy per reaction, based on the Poisson distribution of positive and negative reactions at the limiting dilution (Kaltenboeck and Wang, 2005). High resolution melting curves were generated at the end of thermal cycling by increasing reaction temperature from 35°C to 80°C over 4 minutes while fluorescence was continuously acquired. Verification of reverse transcription was initially achieved by amplification of RNA produced *in vitro* from this vector, and later routinely by re-

amplification of known FCoV-positive specimens in the presence and absence of reverse transcriptase. Validation of specificity was performed by sequence determination of positive amplifications in this study. These data established that the PCR was equally effective at single copy input and verified the robust ability of the PCR to detect single target copies.

Operation of the FIP M gene mRNA qRT-PCR. All PCRs were performed as single-step reverse transcriptase PCRs in volumes of 10 µl of reaction master mixture and 10 µl sample aliquot in a LightCycler Real-Time Thermal Cycler 1.5 (Roche Diagnostic, IN). All Lightcycler Red 640 probes were used at a concentration of 0.2 µM, the carboxyfluorescein probes were used at 0.1 µM, and per 20 µl qPCR 0.0075 U ThermoScript™ reverse transcriptase and 1.5 U hot start Platinum® *Taq* DNA polymerase (Invitrogen, Carlsbad, CA) were used (Wang et al., 2004). For each real-time PCR, the reaction master mixture was freshly assembled from separate stocks of double-distilled water, 5× PCR buffer, 5× oligonucleotides (primers and probes) in TE buffer, 50× PCR Nucleotide Mix® (Roche Diagnostic, IN), ThermoScript™ reverse transcriptase, and Platinum *Taq* DNA polymerase. For convenient pipetting, ThermoScript™ reverse transcriptase was used at a 1:140 dilution in storage buffer. The PCR buffer consisted of 4.5mM $MgCl_2$, 50 mM KCl, 20 mM Tris-HCl, pH 8.4, supplemented with 0.05% each Tween® 20 and Non-idet P-40™, and 0.03% acetylated BSA (Roche Diagnostics, IN). Nucleotides were used at 0.2 mM (dATP, dCTP, dGTP, dTTP). The thermal cycling profile (**Fig. 3.2.1**) consisted of a reverse transcription step at 55° for 10 min before the initial 2 min denaturation at 95°C, followed by 18 high-stringency step-down thermal cycles: 6 cycles of 15 sec at 95°C, 30 sec at 70°C, and 30 sec at 72°C; 9 cycles of 15 sec

at 95°C, 30 sec at 68°C, and 30 sec at 72°C; 3 cycles of 15 sec at 95°C, 30 sec at 66°C, and 30 sec at 72°C. The high-stringency cyles were followed by 30 low-stringency fluorescence acquisition cycles of 8 sec at 58°C with fluorescence acquisition, 30 sec at 72°C, and for 0 sec at 95°C. The melting curve was determined by continuous fluorescence acquisition over 4 minutes in 0.2°C steps between 35° C and 80°C (**Fig. 3.2.1**).

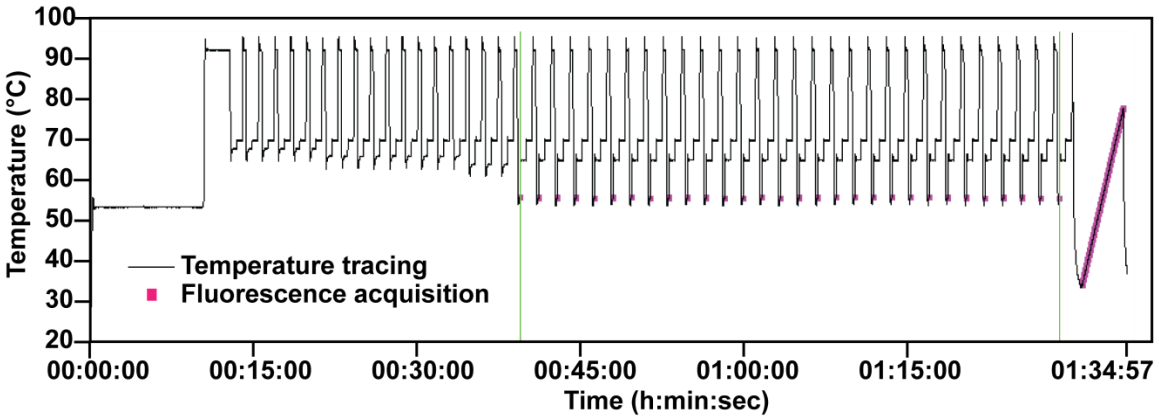

Figure 3.2.1. ***Thermal cycling profile of the FIP M gene mRNA qRT-PCR.*** The first step, reverse transcription, is perfomed at 55° for 10 min, followed by a 2 min denaturation step at 95°C. Subsequently, 18 high-stringency step-down cycles are performed, each consisting of 15 sec at 95°C, followed by 30 sec annealing and 30 sec extension at 72°C. The annealing temperature is 70°C for 6 cycles, 68°C for 9 cycles, and 66°C for 3 cycles. The step-down cycles are followed by 30 low-stringency fluorescence acquisition cycles of 8 sec at 58°C with fluorescence acquisition, 30 sec at 72°C, and 0 sec at 95°C. Finally, the high-resolution melting curve is determined by continuous fluorescence acquisition over ~4 minutes in 0.2°C steps between 35° C and 80°C.

Standard reactions containing four positive standards, 10,000, 1,000, 100, and 10 copies of FCoV DNA templates, were performed without reverse transcription and used for absolute quantification of the concentration of FCoV mRNA template copies in the specimens. In routine diagnostic assays with limited requirement for highest quantitative accuracy, only the 1,000 and 10 template copy standards were used. As control for transcription, a positive specimen from a previous batch was included in each batch. Two

negative controls, 1× standard diluent and the extraction blank of each batch of extracted specimens, were also included.

Analysis of PCR results. Data were analyzed using the LightCycler software version 3.5 (Roche Diagnostic, IN). As initial step, melting curve analysis was used to separate positive from negative amplification reactions. Data were analyzed as 640 nm:530 nm (F2/F1) fluorescence ratios. The melting peak of positive reactions was identified in the first derivative of fluorescence intensity over temperature (-d(F2/F1)/dt) in the final segment of continuous signal acquisition from 35-80°C. In this analysis, the most rapidly changing fluorescence intensity results in a "melting peak" curve at the temperature where 50% of the hybridization probe is bound to the target and 50% is free in solution. Presence or absence of a melting peak allows unambiguous discrimination of positive amplification reactions from negative ones.

For subsequent quantitative analysis, background noise was delineated by setting a noise band between positive and negative reactions. Amplification threshold cycle numbers (crossing points) were derived from the intersection of the best fit line through the log-linear portion of the amplification curve of each reaction and the signal threshold line set after background elimination. Based on the crossing points and copy number of the standard templates, a linear regression was calculated that related crossing points to standard copy numbers. Based on this equation, target copy numbers in unknown specimens were determined by their crossing points.

DNA sequence analysis. Ten high copy number (>500 copies/μl) amplification products (AUMD1-10) were sequenced in both directions, using upstream and down-stream PCR primers. The GenBank accession numbers used for comparative analysis

were: isolate 26M, KP143512; UCD13, FJ94376.4; UCD17, FJ917527.1; 79-1146, DQ010921.1; UU22, GU553361.1; FECV-M, AB086904.1; C1Je, DQ010921.1. Sequence alignment was determined in the Vector NTI software package by use of the ClustalW algorithm (Thompson et al., 1994), and phylogram construction was performed by neighbor-joining algorithm (Saitou and Nei, 1987).

3.3. RESULTS

Single target copy detection by the FIP M gene mRNA RT-PCR. To validate the sensitivity of single target copy detection by the assay, a limiting dilution series of positive specimens in 20 ng of unrelated background nucleic acids was performed (**Fig. 3.3.1**). Positive reactions were identified by high-resolution melting curve analysis that confirmed a melting peak for positive, but not for negative amplifications.

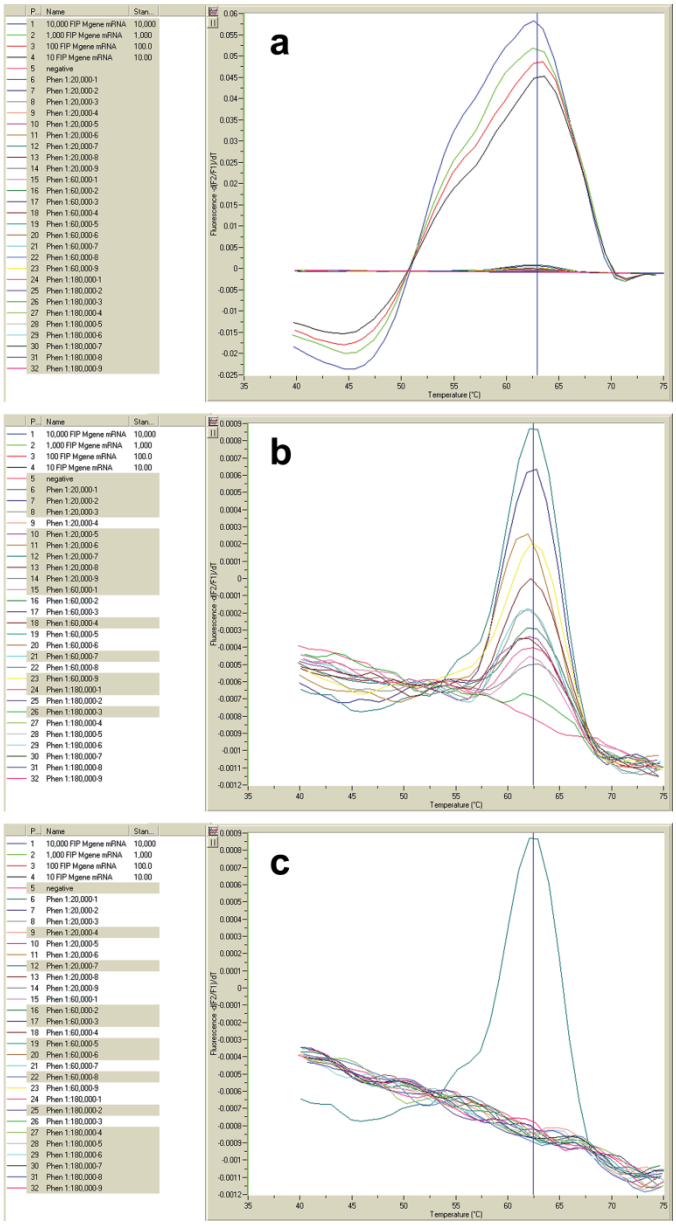

Figure 3.3.1. ***Identification of positive and negative reactions by high-resolution melting curve analysis at limiting dilution of a positive specimen.*** Total nucleic acids extracted from the highly positive peritoneal effusion specimen "Phen" were diluted 1:20,000 to 1:180,000 in standard diluent (2 µg gGEM plasmid DNA/µl in 10 mM Tris-HCl, 0.1 mM EDTA, pH 8.5) and amplified in the FIP M gene mRNA RT-PCR. At these dilutions, reactions became either positive at very low copy numbers or remained negative. a) Positive specimens at the limiting dilution show much lower copies in amplification, and consequently much lower melting peaks and areas under the melting curve than the reactions standards. b) Identification of positive specimens without signal suppression by positive standards. Positive reactions (gray background) can be unambiguously identified by their distinct melting peaks relative to the negative control (red line). c) Negative reactions are indistinguishable from the negative control relative to a positive calibration reaction.

The results in **Fig. 3.3.1** indicate unambiguous identification of positive amplifications. Positive as well as negative amplifications can be observed in different aliquots of each of the limiting dilutions. These data imply Poisson distribution of target copies at the limiting dilution range, such that some aliquots of the limiting dilution contain one or more target molecules, while others contain none (**Fig. 3.3.2**).

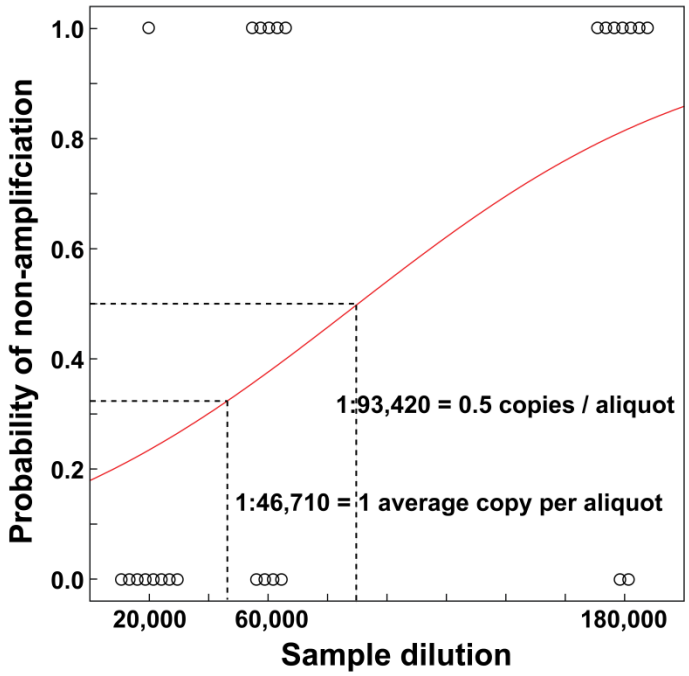

Figure 3.3.2. ***Logistic regression determines target copies at the limiting dilution range of a positive specimen.*** Positive (1.0) and negative (0.0) reactions of diluted specimen aliquots were plotted against the respective dilution, and the maximum likelihood fit for probability of non-amplification at the limiting dilution range was determined by logistic regression analysis.

From plotted positive and negative amplifications of each dilution, logistic regression allowed the determination of the probability of amplification (= 1-probability of non-amplification) at each dilution (**Fig. 3.3.2**). For the highly positive peritoneal effusion specimen "Phen", the point where 50% of amplification reactions are positive and 50% negative is a 1:93,420-fold dilution of the original specimen. At this dilution, each 10 µl PCR input aliquot contains on average 0.5 copies of the FCoV amplification target RNA. Thus, an aliquot of the 1:46,710-fold dilution contains on average one target copy, and the undiluted original extracted nucleic acid specimen of "Phen" therefore contains 46,710

target RNA copies per 10 µl. These results ascertain that the FIP M gene mRNA PCR is capable of detecting a single copy of the target molecule in a reaction.

Analysis of FIP M gene mRNA RT-PCR. The PCR results of a testing batch of 16 specimens are shown to demonstrate the performance of the PCR (**Figs. 3.3.3, 3.3.4**). These specimens include 2 positive standards, 2 negative controls, and 12 FIP diagnostic specimens. The positive standards were 1,000 and 10 copies of FCoV DNA templates; two negative controls were 1× standard diluent (and the extraction blank of each batch of extracted specimens.

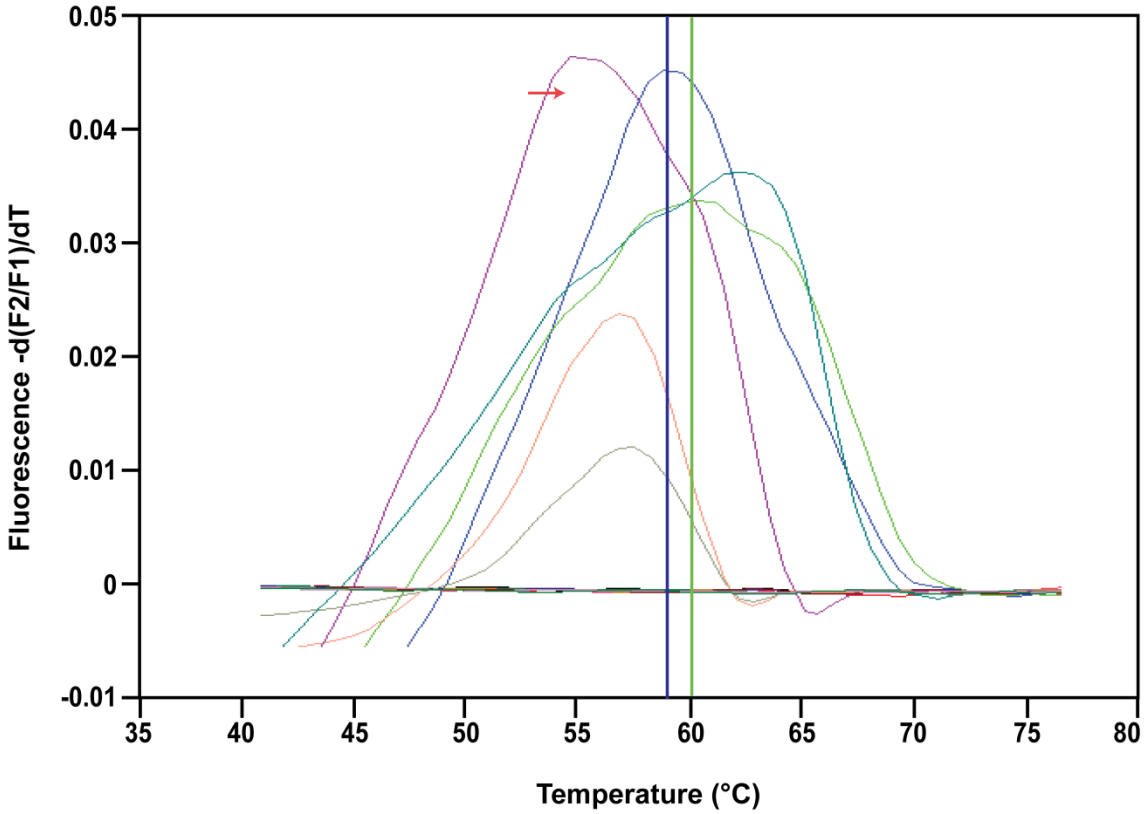

Figure 3.3.3. ***Melting curves of FCoV diagnostic specimens*****.** Melting curve and lines indicating melting peak ($\boldsymbol{T}_m$) of 1000 and 10 copy standard FCoV templates are shown in blue and green, respectively. Four positive FIP diagnostic specimens show distinct melting curves and $\boldsymbol{T}_m$. Area under the curve (AUC) of the first derivative of the melting curve represents the total fluorescence that the amplification product generates. Fluorescence detected in the PCR is directly proportional to the amount of DNA template present in the specimens. High copy number specimens generate more fluorescence hence manifest larger AUC (red arrow) than low-copy specimens.

Results were first evaluated by high-resolution melting curve analysis for unambiguous identification of positive specimens by distinct melting peaks (**Fig. 3.3.3**). The melting peaks of the curve of first derivative of fluorescence intensity over temperatures (melting curve) indicated different melting temperatures ($\boldsymbol{T}_m$) of the positive diagnostic specimens. These different $\boldsymbol{T}_m$ of the specimens are the result of different degrees of mismatch of the probes to the sequences. The area under the curve (AUC) of the melting curve reflects the intensity of fluorescence detected in the specimen and is directly proportional to the amount of FCoV DNA template present in a specimen. Single base polymorphisms in the probe region often result in 2-3°C lower melting temperatures, which allow identification of target specificity. For negative controls and specimens, the first derivative of fluorescence intensity over temperatures showed no change of fluorescent intensity, and thus displayed no melting peaks (**Fig. 3.3.3**).

From the original data on fluorescence intensity of each specimen at each amplification cycle, the LightCycler software generated amplification curves, and background noise was manually delineated by setting a noise band between negative and positive control samples (**Fig. 3.3.4a and 3.3.4b**). The positive specimens showed low numerical values for the points where the fluorescent signal crossed the manually set green threshold line (crossing points) due to the few amplification cycles required to produce a fluorescent signal from the high numbers of FCoV templates present in the specimens (**Fig. 3.3.4c**). This indicates that the exponential amplification phase occurs earlier in high copy specimens as compared to low positive specimens with higher values for crossing points.

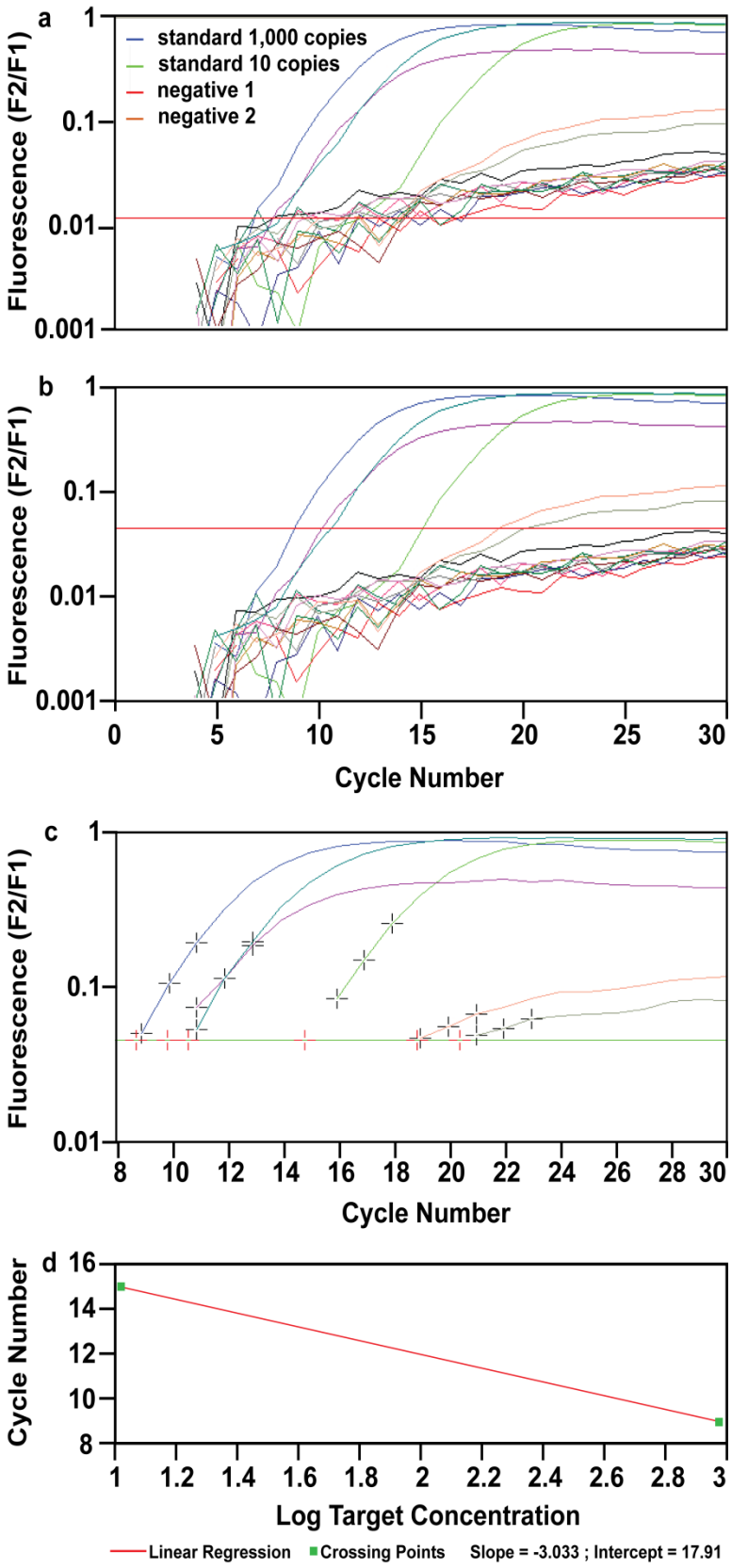

Figure 3.3.4. ***PCR amplification curves of FCoV diagnostic specimens.*** Each amplification curve represents the accumulation of amplification products generated from individual specimens over the duration of thermal cycling. The amplification curves are shown before (a) and after (b) the adjustment of the noise cutoff band (red line) between negative and positive control specimens. (c) Crossing points (red cross) at the manually set fluorescence threshold line (green) indicate the cycle number at which the signal from each specimen crosses an arbitrary detection threshold. (d) Linear regression between the logarithm of input target copies and crossing point of the positive standard templates. This equation allows determination of input target copies of unknown specimens from their crossing point.

Based on the known template concentrations of the two positive standard templates, a linear regression between the logarithm of target copies and the respective crossing point can be established. The negative slope of the regression line characterizes the efficiency of the PCR, with a slope of -3.322 indicating 100% efficiency, i.e. doubling of the target copies at every cycle ($2^{3.322} = 10$). In this PCR, the slope was -3.033 (**Fig. 3.3.4d**), indicating 81.85% efficiency of the PCR, a very high efficiency of target amplification for a reverse transcription PCR with total nucleic acid input. Total nucleic acids contain among RNA more than 80% of highly folded, thus self-priming, ribosomal RNAs that are notorious for producing high amounts of non-specific background PCR products that are strongly inhibitory on specific target amplification.

To further confirm the results of the PCR, gel electrophoresis of positive amplification products was performed. Lanes 1-4 in **Fig. 3.3.5** show different length of amplification products, hence confirm the polymorphic amplifications of targets.

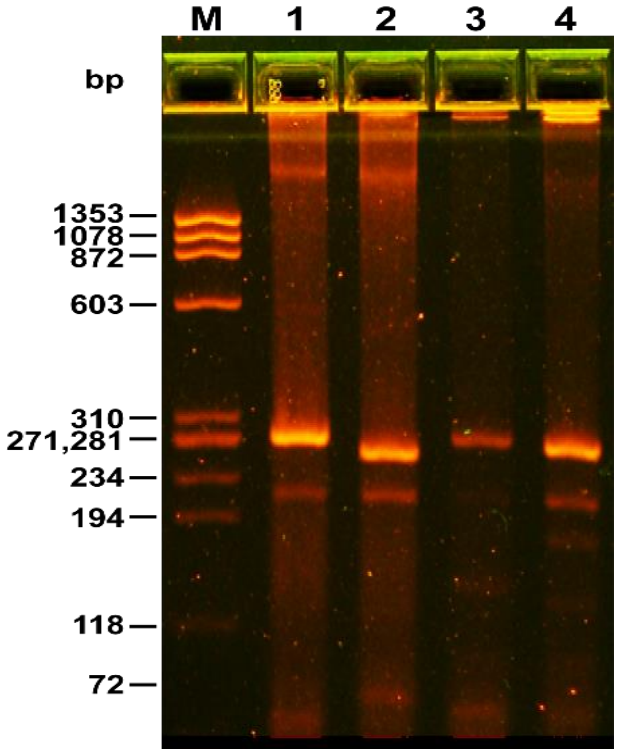

Figure 3.3.5. ***PCR amplification products of four positive FCoV diagnostic specimens.*** Products of the FIP M gene mRNA RT-PCR separated in a 2% low-melting-point agarose gel stained with ethidium bromide. Lane M, φX174 RF DNA/HaeIII marker DNA fragments ranging from 72 - 1353 base pairs (bp); Lanes 1-4 show different lengths of the PCR amplification products as the top bands, with shorter aberrant products and primer dimers below.

Polymorphism of FIP M gene mRNA amplification product. To further confirm the correct amplification and investigate the polymorphism of the M gene mRNA PCR amplification products, 10 high copy number PCR amplification products (AUMD-1 to -10) were chosen and Sanger DNA sequenced on both strands. Deduced amino acid (AA) sequences were first aligned by Clustal W software against an intermixture of published FECV and FIPV M deduced AA sequences (**Fig. 3.3.6a**). Based on the AA alignment, gaps were introduced into the nucleotide (NT) sequences for accurate and functionally correct alignment (**Fig. 3.3.6b**). The sequence alignments show that the upstream and downstream portion of the sequences including the probe regions were highly conserved, especially from AA position 41 to the C-terminus of the sequences. However, the region from AA position 25-39 demonstrated high polymorphism in AUMD PCR amplification products as well as published FECV/FIPV M gene sequences, reflected at the nucleotide level in positions 75-117 (**Fig. 3.3.6b**). Notably, in the AA alignment, 5 AUMD PCR amplification products and 1 published FIPV isolate demonstrated an in frame deletion in position 38.

The polymorphism of the FCoV M genes is also evident in the phylogram derived from the amino acid sequence alignment (**Fig. 3.3.7**). The complete intermixture of published FECV sequences with published FIPV sequences and AUMD amplification products suggests that polymorphisms in the amplified portion of the FCoV M gene do not separate between FECV and FIPV isolates, and therefore do not associate with FIPV conversion of FECV.

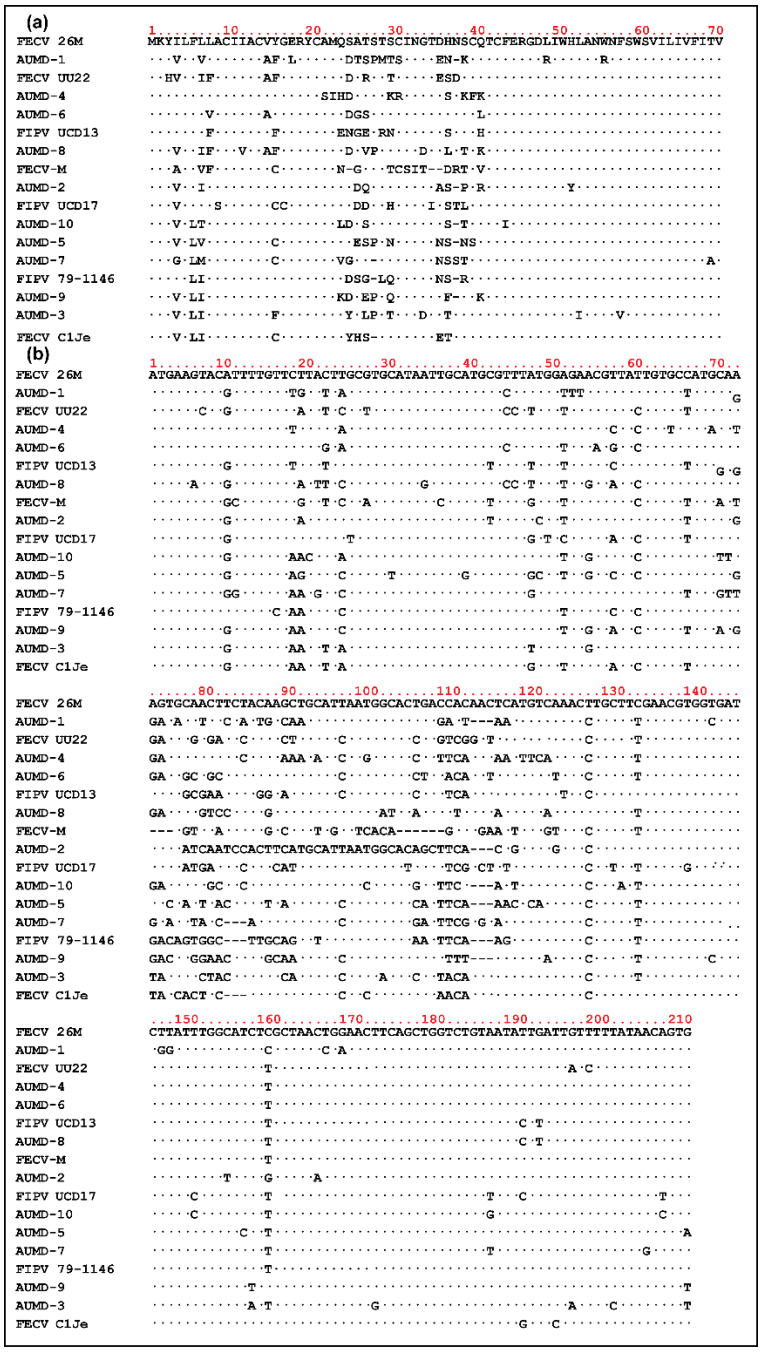

Figure 3.3.6. ***Investigation of polymorphism of the partial M gene mRNA sequence of 10 high copy number PCR amplification products (AUMD-1 to -10).*** Alignments of the partial FCoV M gene mRNA sequences of the PCR products and a selection of published FECV and FIPV isolates are shown at both deduced amino acid (a) and nucleotide level (b). Dots indicate residues identical to the FECV 26M reference sequence, and dashes indicate deletions. (a) The alignment shows that the most polymorphic region extends from position 25-39, whereas the downstream sequences from position 41 to the C-terminus is highly conserved. In addition, 5 PCR products (AUMD-1, 2, 5, 9, 10) and the published FIPV 79-1146 isolate show an in frame deletion at position 38. (b) Nucleotide sequences after introduction of gaps based on the AA sequences show highest polymorphism from position 75 through 117, and maximum conservation downstream. The in frame deletion at AA position 38 corresponds to nucleotides 112-114.

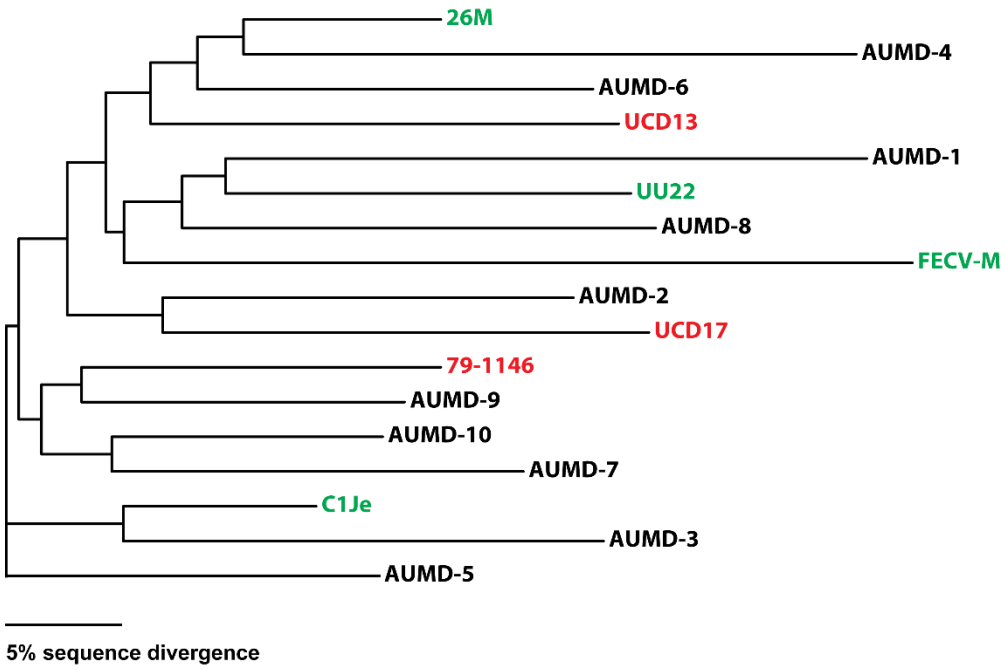

Figure 3.3.7. ***Phylogram of the partial FCoV M gene mRNA sequences.*** AUMD amplification products (AUMD-1 to 10) are shown in black font. An intermixture of FECV and FIPV isolates is shown in green and red fonts, respectively. FECV, FIPV, and AUMD sequences are completely interspersed and occur in the major clades in the phylogram, confirming the high polymorphism, but non-association with FECV to FIPV conversion, of the FCoV M gene sequence.

Overview of specimens received for FIP diagnosis by the FIP M gene mRNA qRT-PCR assay. After establishment and validation, this PCR was offered beginning in 2007 to veterinarians for FIP diagnosis. Since that time, the Auburn University Molecular Diagnostics Laboratory receives annually approximately 1,300 specimens for FIP diagnosis, mostly peritoneal effusions, submitted by veterinarians and diagnostic services nationwide. In 2014-2016, on average 1,297 specimens were received annually (**Table 3.3.1**), and approximately one third tested positive in the PCR (**Table 3.3.1**). Specimens encompassed body fluids (60.0%), whole blood (33.6%), tissue (3.3%), feces (1.1%), cerebrospinal fluid (0.8%), and urine (0.7%) (**Table 3.3.2**). Of all specimen types received, body fluid was dominant, followed by whole blood specimens. The highest PCR positive

percentage was for body fluid specimens followed by urine, tissue, and CSF specimens (**Table 3.3.2**). The FIP PCR positive percentage of whole blood specimens was the lowest of all specimen types.

Table 3.3.1. 2014-2016 total number of specimens received for FIP M gene qRT-PCR.

Year	Total specimens received	Positive specimens	Positive percentage (%)
2014	1,239	353	28.5
2015	1,282	371	28.9
2016	1,370	401	29.3
Average	1,297	375	28.9

Table 3.3.2. 2014-2016 annual average number of specimens received and PCR positive percentage by specimen type.

Specimen type	Ave. annual received (%)	PCR positive (%)
Body fluid	60.0	43.1
Whole blood	33.6	4.1
CSF	0.8	26.1
Tissue	3.3	27.5
Feces	1.1	13.6
Urine	0.7	36.0

3.4. DISCUSSION

To overcome the difficulty to differentiate FECV from FIPV strains, we have established a highly sensitive and specific real-time PCR assay (FIP M gene mRNA qRT-PCR) for detection of subgenomic FCoV mRNA, indicating replicating virus in extra-intestinal specimens, i.e. detection of FIPV based on the functional characteristics of FIPV. In addition, the specific signal obtained by use of fluorescence resonance energy (FRET) probes in the PCR allows accurate quantification of viral load, which further aids in FIP diagnosis.

To validate the sensitivity of the FIP M gene mRNA qRT-PCR, we performed the PCR on a limiting dilution series of positive specimens. Distinct high-resolution melting peaks clearly discriminated positive individual PCRs from negative ones, and allowed unambiguous determination of positive amplifications at the PCRs of the multiple sample aliquots at each dilution step (**Fig. 3.3.1**). This indicates that the PCR detects single copies of the FCoV M gene mRNA target, and that the frequency of negative amplifications increases at high sample dilutions (**Fig. 3.3.2**). The results also showed that the amplification by the FIP M gene mRNA qRT-PCR is 100% specific, with no evidence of contamination or product carry over. Thus, the Poisson distribution derived from the serial limiting dilution demonstrates that this PCR is able to specifically detect single target mRNA copies in clinical specimens. This is accomplished against a high background of unrelated nucleic acids that are derived from the large 0.1 mL specimen aliquot that is the input in every PCR.

We then tested the PCR on randomly selected FIP-suspicious field specimens. As expected, the high-resolution melting curves unambiguously distinguished positive

specimens from negative ones. Positive specimens showed distinct melting peaks, typically different from the reactions standards, indicating different degrees of mismatch of the probes to the target sequences (**Fig. 3.3.3**). The corollary is that even single mismatches between probes and amplification target can be determined. Thus the detection of a melting peak by itself, derived from a continuous 71-nucleotide sequence to which the probes hybridize, indicates with essentially 100% accuracy the amplification of the specific FCoV M gene mRNA target. Positive amplifications generated fluorescent signals, which crossed an arbitrary detection threshold at different cycle numbers. Based on the different crossing points and known concentrations of the standard templates, a linear regression accurately calculated the target copy numbers of the specimens tested (**Fig. 3.3.4**). Subsequently, the positive PCR amplification products were validated by gel electrophoresis showing positive amplicons of minor variations in length (**Fig. 3.3.5**).

Since FCoV, as an RNA virus, is prone to mutate at high frequency, we also investigated the polymorphism of FIP M gene mRNA qRT-PCR products by DNA sequencing. The deduced amino acid sequences as well as the nucleotide sequences of the PCR amplicons (AUMD 1-10) were then compared to the sequences of an intermixture of published FECV and FIPV isolates (**Fig. 3.3.6**). The sequence alignments identified highly polymorphic regions of the partial M gene mRNA sequences. However, sequences of the PCR amplicons do not separate between that of the published FECV and FIPV isolates (**Fig. 3.3.7**). This result indicates that there is not a single prototype sequence among the highly polymorphic FCoV strains that represents either FECV or FIPV strains.

After successful validation and application of the FIP M gene mRNA qRT-PCR on the field FIP-suspicion specimens, this assay was offered for FIP diagnosis since 2007.

Since then, Auburn University Molecular Diagnostics Laboratory receives annually approximately 1,300 specimens for FIP diagnosis nationwide by veterinarians and diagnostic services. From 2014 to 2016, an annual average of 1,297 specimens of all types were received for FIPV diagnosis (**Table 3.3.1**), and nearly 30% of the specimens were positive by this PCR. Among all specimen types received, body fluid, mainly from the peritoneum, was primary, followed by whole blood (**Table 3.3.2**). The positive rate was the highest in body fluid specimens, which can be expected since body fluid is the usually closet to the FIP lesions containing the highest concentration of the FCoVs. The positive rate in whole blood specimens was the lowest among all specimen types. This is probably due to that fact that FIPV usually aggregates in tissues, triggering severe localized inflammatory responses. Only a portion of FIP viruses would actually circulate in the bloodstream, and therefore high viremia is not expected. Overall, this PCR is able to detect FCoVs in various types of specimen and has been a primary PCR assay offered for FIP diagnosis on the market.

In summary, we developed a PCR assay that detects FIPV based on its functional characteristics. The virtually 100% specificity of this assay is achieved by the use of FRET probes. This PCR amplifies single target molecules, and thereby maximizes assay sensitivity by its combination with a nucleic acid extraction method that provides high target recovery and real-time PCR and RT-PCR chemistry and thermal cycling optimized for robust assay characteristics. The value of this FIPV PCR has been proven by years of application to thousands of clinical specimens. While the 100% positive predictive value (PPV) of this assay is assured by high-resolution melting curve analysis of every single test, we still do not know its detection sensitivity relative to a gold standard test for FIP

diagnosis, i.e. the direct immunohistological detection of the virus in clinical specimens. Therefore, in a continuation study, we will aim to evaluate sensitivity and negative predictive value (NPV) of the FIP M gene mRNA qRT-PCR.

CHAPTER 4 Immunofluorescence Assay for Detection of FCoV

4.1. INTRODUCTION

Immunofluorescence (IF) assay is histochemical labeling technique that exploits the exquisite specificity of antibody-antigen interaction with a fluorophore-conjugated antibody to detect the presence and distribution of a target antigen in tissue (Mohan et al., 2008). Visualization of FCoV in infected macrophages by immunofluorescence (IF) is the gold standard for FIP diagnosis (Pedersen et al., 2014). Application of IF to effusion specimens is particularly essential for ante-mortem diagnosis of FIP. A true positive result by IF is 100% predictive of FIP (Paltrinieri et al., 1999; Parodi et al., 1993; Hartmann et al., 2003). Therefore, it can be used to compare and assess the diagnostic utility of other diagnostic tests of FIP.

There are two detection methods in immunofluorescence: direct and indirect. Direct immunofluorescence (DIF) is a one-step process that uses a single fluorescently-labeled antibody that binds and illuminates the target antigen. Indirect immunofluorescence (IIF) is a two-step process involving two antibodies. First, the unlabeled primary antibody is applied to bind to the specific target antigen, followed by a fluorescently-labeled secondary antibody that binds the primary antibody. DIF is often used in research due to its ease. However, when using IIF, analysis of a control specimen without primary antibody allows fine-tuning of assay parameters for optimal elimination of background signals. In addition, multiple primary antibodies from different host species allow simultaneous detection of several targets by use of secondary antibodies labeled with different fluorophores. Finally, multiple secondary antibodies can bind to a single primary antibody, thereby intensifying the fluorescent signal from the target antigen.

Due to simple experiment protocols, more FIP diagnostic studies used DIF rather than IIF (Hartmann et al., 2003; Horhogea et al., 2011; Litster et al., 2013; Parodi et al., 1993; Paltrinieri et al., 1999). However, the Se and Sp of these DIF assays were variable. Some of the studies found many false positive DIF results indicating a poor PPV (Parodi et al., 1993; Litster et al., 2013), while another study found many false negative DIF results, indicating a poor NPV (Hartmann et al., 2003). These data suggest high operator dependence of DIF assays, and therefore a lack of robustness and general applicability. On the other hand, fewer studies used the IIF method for FIP study (Amer et al., 2012; Hök, 1989; Tresnan et al., 1996). Only Hök (1989) investigated the diagnostic utility of IIF assay for FIP diagnosis, whereas the other two studies used IIF as a confirmatory test for demonstrating successful infection of FCoVs in cell culture (Amer et al., 2012; Tresnan et al., 1996). Hök (1989) examined the diagnostic utility of an IIF on epithelial cells from the membrana nictitans of 231 cats in a mixed population of clinically healthy and FIP-suspicious cats. She showed an image of a typical positive IIF result demonstrating the vivid presence of FCoV in infected cells. The study first compared anti-FCoV IIF results to anti-FCoV antibody levels, and found a concordance of 85% between the tests (Hök, 1989). She then compared the IIF results to viral isolation results from different FIP-affected tissues. The comparison generated a Se of 71-100% and a Sp of 67-100% for the IIF assay. In particular, Sps of the assay were 100% in 4 out of 6 types of diseased tissue specimens. Based on the findings, she concluded that IIF is an adequate diagnostic method for FIP (Hök, 1989).

To confidently evaluate the diagnostic utility of an assay for ante-mortem FIP diagnosis, a reliable diagnostic gold standard such as an IF assay is required. However, the currently available DIF assays have inconsistent Sps and Ses, and the knowledge about reliable IIF assays is limited. In addition, none of the studies demonstrated the use of simultaneous

differential fluorescent labeling of FCoV and macrophages, respectively, a method that can provide even better proof of FIP diagnosis than immunofluorescent detection of FCoV alone (Amer et al., 2012; Hartmann et al., 2003; Horhogea et al., 2011; Hök, 1989; Litster et al., 2013; Parodi et al., 1993; Paltrinieri et al., 1999; Tresnan et al., 1996). In this study, we developed a high quality IIF assay that 1) simultaneously labeled FCoV and macrophages in green and red fluorescence, respectively, allowing unambiguous detection of FCoV-infected macrophages while identifying any cell nucleus by blue fluorescence; 2) eliminated background fluorescence by fine-tuning reaction and image analysis parameters; and 3) provided assurance of test results by including a negative control for each specimen. This method can be used with confidence as a gold standard to investigate the diagnostic utility of the FCoV M gene mRNA qRT-PCR, or of any other FIP diagnostic assay.

4.2. MATERIALS AND METHODS

Preparation of microscope slides with fixed effusion cells. Effusion specimens that were positive or negative in the FIP M gene mRNA qRT-PCR were randomly selected for testing by the FCoV immunofluorescence (IF) assay. A 0.5 mL aliquot of effusion specimen was diluted 1:1 with phosphate-buffered saline (PBS), 10 µl of hyaluronidase, 100 mg/ml, was added and incubated for 10 min at room temperature (Litster et al., 2013). Cells were sedimented at 750×g for 10 min, and resuspended with a wide-bore pipette in 1 mL PBS. This washing step was repeated twice until the supernatant was clear. The cells were finally resuspended in 100 µl PBS, 40 µl were added into the Cytofunnel™ chamber of a Shandon Cytospin™ 3 Cytocentrifuge (ThermoFisher Scientific, Inc.), and 4 drops of buffered zinc formalin fixative (Z-Fix, Anatech, Inc.) were added. The zink formalin fixative was used because it preserves the antigen structure in formalin fixed tissue specimens, allowing effective immunostaining (Wester et al., 2003). To deposit the cells on the two 113 mm^2 encircled areas of the cytospin microscope slides, the specimen was spun at 72×g for 5 min. The slides were then air-dried for 5-10 min and stored in a humid chamber at 4°C until further processing. Each experiment included specimen slides with a negative control without primary antibodies, and a method control slide with a negative and one positive control specimen.

Immunfluorescent labeling. Prior to addition of blocking buffer, specimen slides were examined by dark-field microscopy, and only specimens with 40 or more cells per encircled area were further processed. The specimen slides were blocked in a humid chamber at room temperature for 1 hr by dropping 30 µl of blocking buffer (5% BSA and 10% donkey serum in PBS) onto the encircled areas of the slides (Kroeber et al., 1998).

Specimen slides were drained and briefly blotted, followed by addition to the encircled spots of 30 µl of the mixed primary antibodies, diluted appropriately in blocking buffer. Subsequently, the slides were incubated overnight at 4°C in a humid chamber (Donaldson et al., 2001). The primary antibodies were then gently rinsed off with PBS and immersion-washed for 5 min each in three changes of fresh PBS. After brief blotting, 30 µl of the mixed secondary antibodies, appropriately diluted in blocking buffer, were applied to the encircled spots, and slides were incubated for 45 min in the dark at room temperature in a humid chamber (Chakraborty et al., 2013). This incubation was followed with three wash steps as described after primary antibody incubation. Immediately after air-drying, a drop of SlowFade Diamond Antifade Mountant with DAPI (ThermoFisher Scientific, Inc.) was added to each encircled area, and a single cover slip was placed on top that covered both encircled areas. To secure and seal the cover slips, nail polish was applied around the edges. The positive and negative controls were specimens that had previously tested positive and negative, respectively. The specific negative control of each specimen slide was the second encircled area in which only secondary, but not primary, antibodies were used.

Primary and secondary antibodies. In signal optimization, the concentration of primary antibodies was determined first, followed by the concentration of secondary antibodies (Hoffman et al., 2008).

For primary labeling of feline coronavirus, pan-coronavirus mouse IgG2a monoclonal antibody FIPV3-70 (Fisher Cat. #MA1-82189) was used (Litster et al., 2013) at 1:400 dilution. Bound anti-coronavirus antibody was detected by 1:500 diluted donkey anti-mouse IgG polyclonal antibody conjugated to Alexa Fluor 488 (Fisher Cat. # R37114).

For primary labeling of macrophages, goat anti-mouse Allograft Inflammatory Factor 1 (A1F1) polyclonal antibody (Fisher Cat. #ABIN184738; Utans et al., 1995) was used at 1:800 dilution. This antibody targets the C-terminal peptide TGPPAKKAISELP of the murine A1F1 protein, which is 83% homologous at amino acids 2-13 of the feline homolog sequence GPPAKRNISELP. In comparative analyses, the anti-mouse A1F1 antibody also bound to the feline homolog. Bound anti-A1F1 antibody was detected by 1:500 diluted donkey anti-goat IgG (H+L) polyclonal antibody conjugated to Alexa Fluor 594 (Fisher Cat. # A11058).

Microscopic observation and image processing. The slides were then examined under oil immersion with a Plan Apochromat 60× objective in a confocal laser scanning Nikon Eclipse TE2000 inverted microscope. Images were saved as TIFF format in NIS-Elements Viewer 4.20 software, and then processed by use of Photoshop CS3 software. Cell nuclei were visualized with 350 nm excitation in the blue 405 nm emission of 4', 6-diamidino-2-phenylindole (DAPI), FCoV at 490 nm excitation in the green 525 nm emission channel of fluorescein isothiocyanate (FITC), and macrophages at 557 nm excitation in the red 576 nm emission channel of tetramethyl rhodamine isothiocyanate (TRITC). Brightness and contrast were separately adjusted for each blue, green, and red channel across each entire image.

4.3. RESULTS

Differential immunofluorescent labeling. We used three different fluorophores to label cell nuclei (blue), macrophages (red), and feline coronavirus (green; FCoV) respectively. One FCoV-positive and -negative peritoneal effusion specimen each were labeled in series with either DAPI only (**Figures 4.3.1a and d**), DAPI and anti-A1F1 primary mouse monoclonal antibody and anti-mouse Alexa Fluor 594 conjugate (**Figures 4.3.1b and e**), or DAPI, anti-A1F1, and anti-pan coronavirus primary goat ploYclonal antibody and anti-goat Alexa Fluor 488 conjugate (**Figures 4.3.1c and f**).

Figures 4.3.1a and **d** show only cell nuclei of FCoV-positive and -negative peritoneal effusion specimens labeled blue by DAPI. There are two shapes of nuclei: a single round nucleus of macrophages or lymphocytes, or a lobed nucleus of polymorphonucleated granulocytes, mostly neutrophils. **Figures 4.3.1b** and **e** show that macrophages are labeled as single round nuclei in blue with a surrounding red cytoplasm (Alexa 594). **Figure 4.3.1c** shows FCoV-infected macrophages in the FCoV-positive specimen with single nuclei in blue, along with red cytoplasm, and green vesicles containing FCoV antigen (Alexa 488). In contrast, the FCoV-negative specimen in **Figure 4.3.1f** does not show any green-stained vesicles, despite incubation with the complete set of primary antibodies and fluorescent conjugates. Non-uninfected cells in both Figures **4.3.1c** and **f** were either non-macrophage cells (labeled in blue) or macrophages (labeled in blue and red).

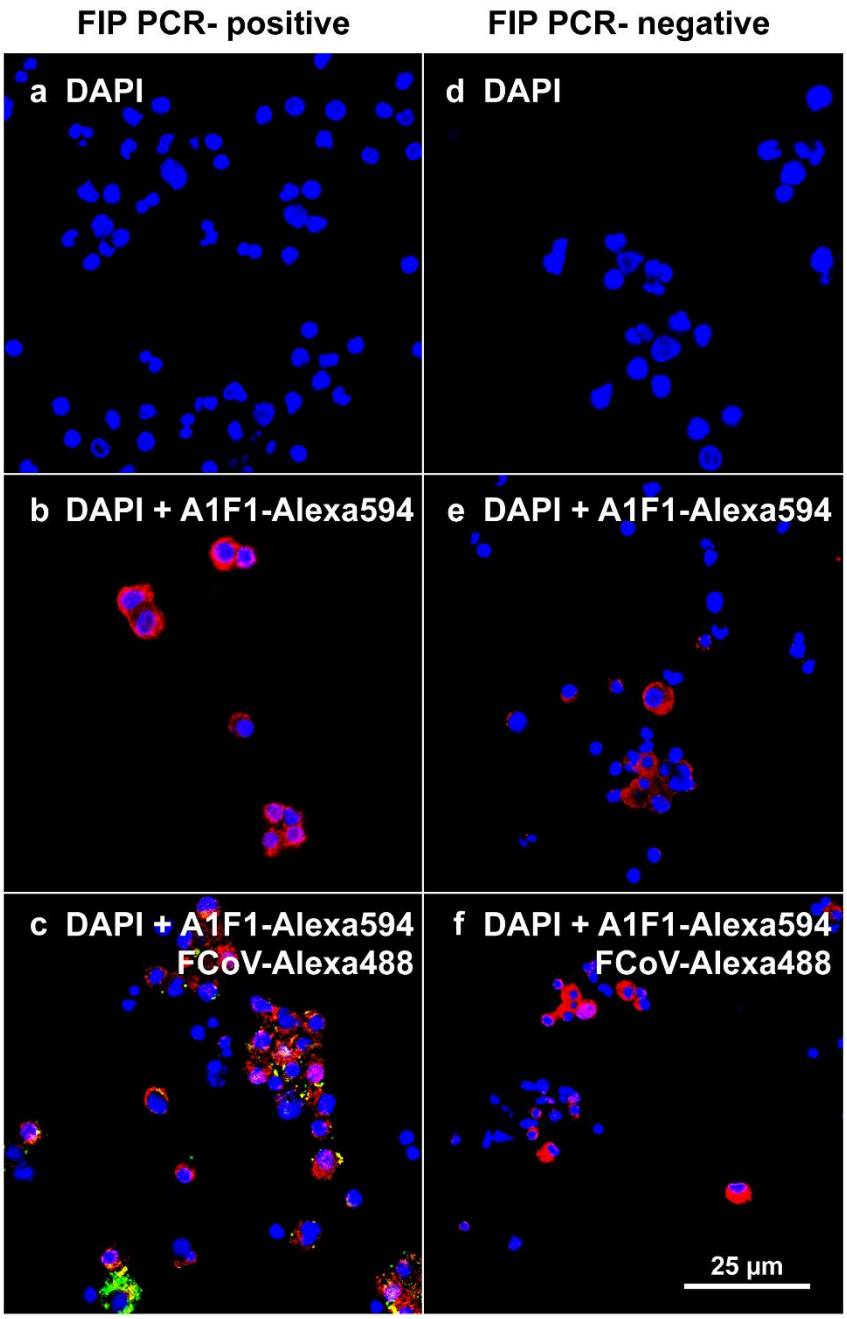

Figure 4.3.1 ***Immunofluorescent labeling of macrophages and feline coronavirus*.** Show is differential labeling of cells from a FIP PCR-positive (left panel) and -negative (right panel) effusion specimen. (a) and (d) Cell nuclei are labeled in blue by DAPI. Cell nuclei are either shaped as a single round nucleus (macrophage or lymphocyte), or a lobed nucleus (neutrophil). (b) and (e) Macrophages are labeled as single round nuclei in blue with surrounding cytoplasm in red. (c) FCoV-infected macrophages in the FIP PCR-positive specimen with FCoV particles labeled in green, in addition to the single round nuclei in blue along with the cytoplasm in red. (d) Green-stained FCoV is not present in macrophages of the FIP PCR-negative specimen.

4.4. DISCUSSION

We have established a high quality immunofluorescence (IF) assay that unambiguously identifies even single intracellular vesicles containing feline coronavirus antigen. This assay can be used as a reliable gold standard to evaluate the diagnostic utility of the FIP M gene mRNA qRT-PCR. For maximum information and control of signal to noise ratio, we developed this IF assay as a dual FCoV/macrophage target indirect immunofluorescence assay rather than the direct immunofluorescence that Litster et al. (2013) described.

To establish the assay, we applied the differential fluorescent labeling on FIP PCR-positive and negative peritoneal effusion specimens either only with DAPI (**Figures 4.3.1a and d**), DAPI and anti-A1F1 primary mouse monoclonal antibody and anti-mouse Alexa Fluor 594 conjugate (**Figures 4.3.1b and e**), or DAPI, anti-A1F1, and anti-pan coronavirus primary goat polyclonal antibody and anti-goat Alexa Fluor 488 conjugate (**Figures 4.3.1c and f**). The results demonstrated that this differential fluorescent labeling unambiguously stained cell nuclei in blue (**Figures 4.3.1a and d**), and macrophages of nuclei in blue and surrounding cytoplasm in red (**Figures 4.3.1b and e**). In FIP PCR-positive specimen, FCoV particles were labeled in green within the infected macrophages (**Figure 4.3.1c**). Conversely, the FIP PCR-negative specimen did not show any green-labeled viral particles.

Collectively, this IF assay is able to demonstrate the co-localization of FCoV in macrophages, thereby virtually eliminating false positive results. Combined with other assays of suitable cellular effusion specimens, it allows the determination of the specificity, sensitivity, NPV, and PPV of the FIP M gene mRNA qRT-PCR. Furthermore, the

visualization of viral distribution, and spatial correlation of infected and non-infected cells may provide additional insight into FIP pathogenetic mechanisms.

CHAPTER 5 Diagnostic accuracy of the FIP membrane gene messenger RNA quantitative reverse transcription PCR (FIP M gene mRNA qRT-PCR)

5.1. INTRODUCTION

The significance of the FIP IF assay as described in chapter 3 is the excellent diagnostic accuracy achieved by simultaneous antibody-mediated detection of FCoV and macrophages in abdominal effusion specimens, that provides the physical evidence of the FIP infection by demonstrating the co-localization of FCoV and macrophages. Pedersen et al. (2014) FCoV IF detection in macrophages the gold standard for FIP diagnosis. As for any assay, determination of specificity and sensitivity of the FIP M gene mRNA qRT-PCR is essential for confident diagnostic use. The dual-labeling IF assay enables us now to do this.

Parallel to the IF assay, known clinical and hematological diagnostic criteria for FIP can also be used to establish the validity of PCR FIP diagnosis by achieving separation between positive and negative cases in accordance to their clinical/hematological characteristics. While clinical signs tend to non-specifically associate with FIP, some hematological and serum biochemical parameters strongly correlate with verified FIP diagnosis (Cahn and Line, 2010; Horhogea et al., 2011; Norris et al., 2005; Tsai et al., 2011). Based on this known correlation with FIP, we selected a set of widely determined hematological parameters (red blood cell, neutrophil, and lymphocyte counts) as well as serum biochemical parameters (albumin and globulin) for comparative evaluation in cases diagnosed positive and negative by the FIP M gene mRNA qRT-PCR.

Therefore, to evaluate the diagnostic accuracy of the FIP M gene mRNA qRT-PCR, we examined both the comparative consistency of PCR diagnosis of FIP with

immunofluorescent and clinical/hematological FIP diagnosis. Subsequent to the development of an immunofluorescent assay for detection of FCoV in macrophages in peritoneal effusion specimens, we determined specificity, sensitivity, NPV, PPV, and accuracy of the FIP M gene mRNA qRT-PCR relative to the gold standard of immunofluorescent detection. We also evaluated the consistency of FIP PCR detection with known clinical symptoms and deviations in hematological parameters. Collectively, the analyses obtained from both IF assay and clinical/hematological parameters would serve as a robust approach to evaluate the diagnostic accuracy of the FIP M gene mRNA qRT-PCR assay. Moreover, information observed in this process may enable further understanding of the molecular and clinical aspects of FIP.

5.2. MATERIALS AND METHODS

Specimen enrollment. FIP M gene mRNA qRT-PCR-positive and -negative effusion specimens were randomly chosen for testing by the FIP immunofluorescence (IF) assay. The clinical information of a different set of -positive and -negative PCR effusion specimens was obtained from the submitting veterinarians.

Nucleic acid extraction and FIP M gene mRNA qRT-PCR. Total nucleic acid extraction of the effusion specimens as well as the PCR design and execution were performed by using the methodology described in chapter 2. Copy numbers of FIP M gene mRNA per mL original effusion specimen were derived from the 0.1 mL effusion specimen aliquot in the 10 µl extracted total nucleic acids used per PCR.

Immunofluorescent (IF) labeling analysis. Handling and testing of the effusion specimens by the IF assay followed the description in chapter 3. Based on this protocol, the cells of a 0.2 mL aliquot of the original specimen were sedimented onto a microscope slide. Only specimens with 40 or more cells per encircled area after cytospin centrifugation were further processed. The total number of cells, macrophages, and FCoV-infected macrophages was recorded, and the distribution pattern of the FCoV labeling was differentiated into punctuated/localized versus diffuse.

Determination of FIP M gene mRNA qRT-PCR assay performance as sensitivity (Se), specificity (Sp), positive predictive values (PPV), negative predictive value (NPV), and accuracy. True positive/negative and false positive/negative results must be determined prior the calculation of Se, Sp, NPV, PPV, and accuracy (di Ruffano et al, 2012). These test outcome values of the PCR were to be determined against the gold-standard test, the FIP IF assay (**Table 5.2.1**). The positive results of the IF assay represent

the diseased population, whereas the negative results represent the non-disease population. Based on that notion, true positive (TP) or true negative (TN) values of the PCR are the ones that are consistent with the results of the IF assay (**Table 5.2.1**). In contrast, false positive (FP) or false negative (FN) values of the PCR are the ones that are inconsistent with the results of the IF assay (**Table 5.2.1**).

Table 5.2.1. Determination of test outcome values

PCR test results	IF-positive (Diseased)	IF-negative (Non-diseased)
Positive	TP	FP
Negative	FN	TN

The assay performance characteristics, i.e. Se, Sp, NPV, PPV, and accuracy can then be derived as follows based on these test outcome values (di Ruffano et al, 2012).

Sensitivity = TP/(TP+FN)

Specificity = TN/(FP+TN)

PPV = TP/(TP+FP)

NPV = TN/(TN+FN)

Accuracy = (TP+TN)/(TP+FP+TN+FN)

Determination FIP M gene mRNA qRT-PCR performance relative to IF labeling analysis. By establishing the IF assay as the gold standard, sensitivity, specificity, NPV, and PPV as well as the diagnostic accuracy of the corresponding FIP M gene mRNA qRT-PCR assay were derived. In discrepant analysis (McAdam et al., 2000), borderline cases were identified that were minimally positive in either one assay (single IF-positive cell, <2 target copies in the PCR assay). Poisson distribution of very low target numbers may result in discordant results because aliquots of either assay input may or may not

contain a target. Following elimination of these discordant cases, the corrected performance characteristics were re-determined.

Clinical diagnostic criteria analysis. The study was performed as a matched case-control study. Equal numbers of PCR-negative and -positive patients matched by sex and age were selected. Signalement, history and clinical symptoms of the enrolled patients were reported by the submitting veterinarian. Based on relevant literature (Addie et al., 2009; Cahn and Line, 2010; Hartmann et al., 2003), a set of blood parameters including RBC, neutrophil and lymphocyte count and biochemical parameters including total plasma protein (TP) and plasma albumin, as well as the derived parameters plasma globulin and albumin to globulin ratio (A/G) were also recorded.

Statistical analysis: Data were evaluated by use of the STATISTICA 7.0 software. Pearson's correlation coefficient analysis was performed to determine the associative strength between the log-transformed PCR copy numbers and the numbers of infected macrophages detected by IF labeling. Differences in hematological/serum biochemical parameters between the PCR-positive and -negative matched pair populations were evaluated by Wilcoxon matched pairs test.

5.3. RESULTS

Overview of the IF results of the FIP M gene mRNA qRT-PCR. **Table 5.3.1** shows the M gene mRNA copy numbers of the effusion specimens and the corresponding IF labeling results. The FCoV immunofluorescence (IF) assay was performed on a total of 132 submitted FIP-diagnostic specimens. Only 63 specimens (47.7%) fulfilled the requirement of the minimum number of 40 detectable cells per cytospin microscopic area and were included in the analysis (**Table 5.3.1**).

The 63 analyzed specimens are ranked in descending order by PCR copy numbers. The PCR copy number ranges from 27 to 56,834 copies of M gene mRNA per milliliter of positive effusion fluid specimens (**Table 5.3.1**). The numbers of FCoV IF-positive macrophages ranges from 1 to 86 (**Table 5.3.1**). Pearson's correlation coefficient analysis showed no significant correlation of the log-transformed PCR copy numbers and the numbers of IF-positive macrophages ($r^2 = 0.06$, p=0.16; Case #25 eliminated as outlier).

Table 5.3.1. IF results of FIP M gene mRNA qRT-PCR-positive and -negative specimens.

Specimen #	M gene mRNA/mL	IF-positive macrophages
1	56,834	26
2	21,053	1
3	19,259	1
4	13,874	29
5	3,326	2
6	2,585	13
7	2,417	39
8	2,151	7
9	1,705	22
10	1,444	10
11	1,383	1
12	1,280	11
13	1,081	6
14	622	1
15	585	15
16	422	1
17	375	23
18	300	22
19	290	5
20	238	2
21	232	1
22	206	3
23	206	2
24	178	2
25	163	86
26	144	27
27	135	1
28	116	14
29	74	1
30	64	4
31	56	14
32	40	2
33	27	15
34	33	4
35	0	18
36	0	12
37	0	14
38	0	31
39	0	17
40	0	3
41	0	3
42	0	5
43	0	2
44	0	1
45	0	1
46	0	1
47	0	1
48	0	1
49	0	1
50	0	1
51	0	1
52	0	0
53	0	0
54	0	0
55	0	0
56	0	0
57	0	0
58	0	0
59	0	0
60	0	0
61	0	0
62	0	0
63	0	0

As evident in **Table 5.3.2**, a total of 34 specimens were true positive (TP) by FIP M gene mRNA qRT-PCR because they were also FIP-positive in the IF assay (#1-34). Twelve specimens were true negative (TN) because they were negative in both assays (#52-63), and 17 cases were false negative (FN) because they were negative by FIP M gene mRNA qRT-PCR but FIP-positive in the IF assay (#35-51). Zero cases were false positive (FP) because all cases positive in the FIP M gene mRNA qRT-PCR were also positive in the IF assay.

Table 5.3.2. Performance of the FIP M gene mRNA qRT-PCR.

PCR test result	IF-positive (Diseased)	IF-negative (Non-diseased)
Positive	34	0
Negative	17	12

These data resulted in the following performance characteristics of the FIP M gene mRNA qRT-PCR as shown in **Table 5.3.3.** Zero FP cases of the PCR assay generates a 100% of specificity (Sp) and positive predictive value (PPV), respectively. The high FN rate contributes to a Se of 66.7% and a NPV of 41.4% (**Table 5.3.3**). The overall accuracy of the assay is 73.0% (**Table 5.3.3**).

Table 5.3.3. Se, Sp, PPV, NPV, and accuracy of FIP M gene mRNA qRT-PCR

	Se	Sp	PPV	NPV	Accuracy
FIP M gene mRNA PCR	66.7%	100%	100%	41.4%	73.0%

IF labeling of positive and negative PCR specimens. Figure 5.3.1a demonstrates typical IF labeling of TP cases, showing FCoV-laden vesicles labeled in bright green within infected macrophages labeled in red (**Fig. 5.3.1a**). **Figure 5.3.1d** demonstrates the contrast of TN to TP cases, showing no FCoV vesicles in an abundance of non-infected cells,

largely macrophages (**Fig. 5.3.1b**). The non-macrophage mono-nuclear cells in this panel d may be either lymphocytes or plasma cells (Cahn and Line, 2010; Kipar and Meli, 2014), whereas the cells with multi-nucleated nuclei typically are neutrophils (Cahn and Line, 2010; Kipar and Meli, 2014).

In FCoV-positive IF labeling, the viral distribution can be distinguished into either diffuse (**Fig. 5.3.1b**) or punctuated (**Fig. 5.3.1e**) patterns. In the diffuse pattern, the green FCoV vesicles diffusely occupy the cytoplasm of infected macrophages (**Fig. 5.3.1b**). In contrast, in the punctuated pattern there are only few consolidated FCoV clumps within the infected macrophages (**Fig. 5.3.1e**). Interestingly, we found that the diffuse pattern tends to associate with higher M gene mRNA copy numbers than the punctuated pattern.

Borderline cases in IF labeling demonstrate only a single FCoV-infected macrophage (**Fig. 5.3.1c** and **f**) in the cells of a 0.2 mL aliquot of the original specimen that had been sedimented onto the encircled area of the cytospin microscope slide. Given this low density of FCoV-positive cells, in examination of more 0.2 mL aliquots, some may be also be negative. Similarly, if a borderline M gene mRNA PCR detected two or less target copies, some aliquots of 0.1 mL of the original effusion specimen analyzed by PCR may be positive while others are negative. Because of this Poisson diagnostic uncertainty, borderline cases were excluded after discrepant analysis of performance evaluation of the FIP M gene mRNA qRT-PCR.

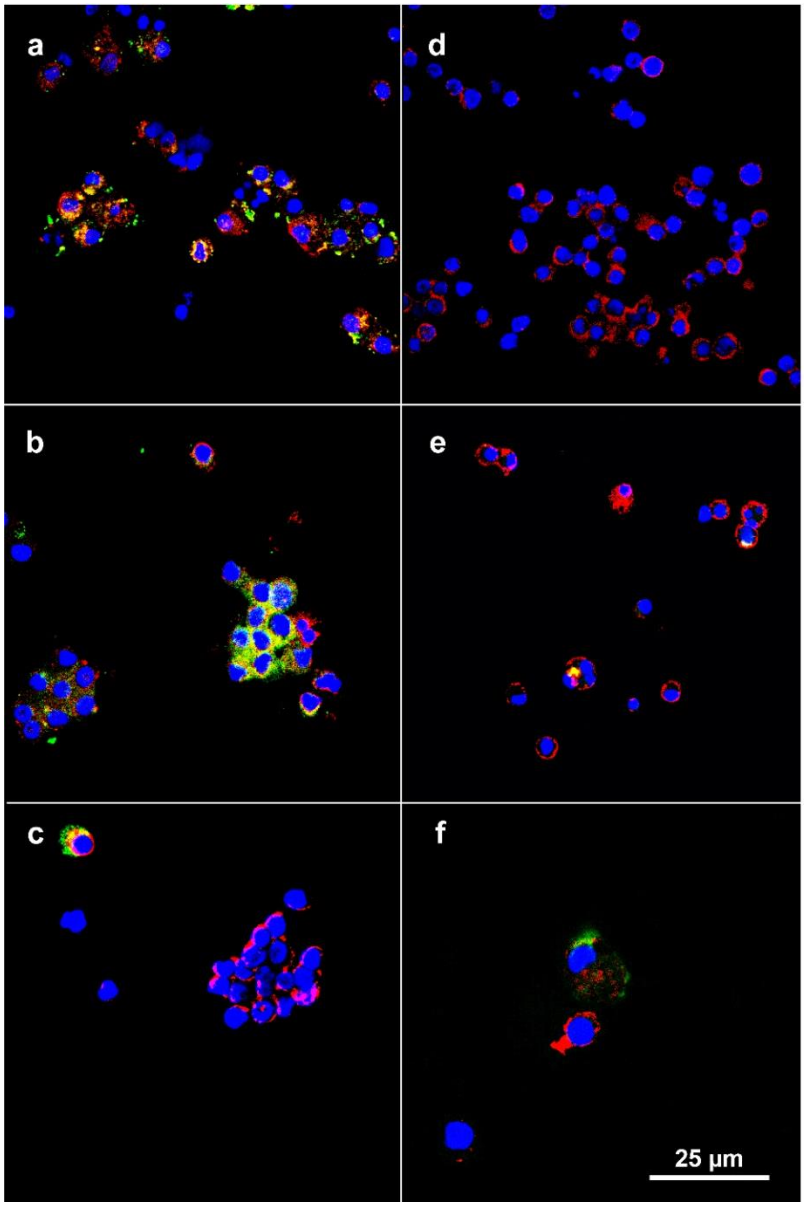

Figure 5.3.1 ***Immunofluorescent labeling of peritoneal effusion cells specimens for FCoV- and macrophage-specific proteins.*** All panels show full differential labeling with DAPI for cellular nuclei, A1F1-Alexa 594 for macrophages, and FCoV-Alexa 488 for FCoVs. Panels (a) and (d) show typical labeling of true positive (TP) and true negative (TF) specimens, respectively, with the same result in both M gene mRNA PCR and IF assay. The vibrant green disseminated FCoV vesicles in (a) genuinely reflect the active ongoing FIP infection in the specimen, whereas there is no FCoV detected by IF in the TN specimen (d). Panels (b) and (e) show the diffuse and punctuated distribution pattern of FCoV vesicles, respectively. In the diffuse pattern, FCoV vesicles of variable labeling intensity occupy the cytoplasm of numerous cells (b), in the punctuated pattern while only a single FCoV vesicle can be observed in two cells (e). Panels (c) and (f) demonstrate two examples of borderline cases found in IF labeling. The single FCoV-infected macrophage in the complete labeled specimen can be observed associated with cell clumps (c) or solitary (f).

Following this initial performance analysis, discordant cases were identified in discrepant analysis (McAdam et al., 2000). Cases 44 to 51 are negative in the PCR assay but show only a single IF-labeled infected macrophage (**Table 5.3.1**). For this reason they were ruled as borderline cases that may show Poisson distribution in analyses of specimen aliquots and therefore may show discordant results in PCR and IF assays. Following elimination of these discordant cases, the corrected performance characteristics were re-determined and shown in **Table 5.3.4** and **5.3.5**.

Table 5.3.4. Re-evaluation of FIP M gene mRNA qRT-PCR performance after correction by discrepant analysis.

PCR test result	IF-positive (Diseased)	IF-negative (Non-diseased)
Positive	34	0
Negative	9	12

After the removal of 8 borderline cases, we obtain increases of Se from 66.7% to 79.1%, NPV from 41.4% to 57.1%, and accuracy from 73.0% to 83.6%, respectively. The Sp and PPV remain 100% (**Table 5.3.5**).

Table 5.3.5. Re-evaluation of Se, Sp, PPV, NPV, and accuracy of the FIP M gene mRNA qRT-PCR after discrepant analysis.

	Se	Sp	PPV	NPV	Accuracy
FIP M gene mRNA PCR	79.1%	100%	100%	57.1%	83.6%

Statistical analysis of clinical data collected from PCR-positive and -negative patients. **Table 5.3.6** shows the dataset collected from 24 matched PCR-positive and -negative cases. In addition to sex, age, and target copy numbers in FIP M gene mRNA qRT-PCR, **Table 5.3.6** shows the dataset of FIP-relevant hematological and serum

biochemical parameters of the population. The positive cases are highlighted, and each positive case is paired with a negative case matched by sex and age. It was not possible to collect sufficient signalement and history data from the patients for statistical analyses.

Table 5.3.6. Clinical data of 24 matched pairs of PCR -positive and -negative patients.[a]

Case #	PCR copy #/mL	Sex	Age (yr)	RBC (M/ µl)	MCV (fL)	MCHC (g/dL)	Neutrophils (cells/µl)	Lymphocytes (cells/µl)	Total Plasma Protein (g/dL)	Plasma Albumin (g/dL)	Plasma Globulin (g/dL)	Plasma A/G	Total Plasma Bilirubin (mg/dL)
1	760	F	0.92	5.30	46.0	31.8	9,200	2,900	11.0	2.4	8.6	0.28	0.20
1'	0	F	0.92	8.31	46.8	33.2	2,000	3,700	8.1	3.7	4.4	0.84	0.30
2	520	F	8.00	5.59	45.6	32.3	4,092	419	5.9	1.5	4.4	0.34	2.30
2'	0	F	8.00	4.51	44.0	37.8	4,725	1,890	5.8	3.1	2.7	1.15	1.20
3	640	F	12.00	3.94	53.6	35.7	82,800	7,300	8.3	2.5	5.8	0.43	0.30
3'	0	F	12.00	9.61	44.0	32.5	16,340	2,451					
4	582	F	1.00	6.52	34.4	36.2	11,160	810	10.1	2.2	7.9	0.28	0.90
4'	0	F	0.33	7.96	39.0	32.7	14,680	2,720	6.8	3.3	3.5	0.94	2.90
5	240	F	3.00	6.30	40.0	33.2			7.8	2.3	5.5	0.42	0.20
5'	0	F	7.00	7.50	51.3	32.1	11,139	2,397	5.1	2.2	2.9	0.76	0.20
6	168	F	0.83	5.59	44.8	32.2	3,650	320	9.3	1.9	7.4	0.26	4.10
6'	0	F	1.00	5.56	60.9	31.6	13,400	2,600	9.1	3.3	5.8	0.57	1.30
7	117	F	0.50	5.80	43.0	31.6		696	6.6	2.3	4.3	0.53	0.20
7'	0	F	0.33	7.96	39.0	32.7	14,680	2,720	6.8	3.3	3.5	0.94	2.90
8	30	F	0.58	4.77	34.0	37.4	1,813	2,244	8.1				
8'	0	F	0.58	7.90	40.2	33.9	14,900	1,000	9.0	3.2	5.8	0.55	0.20
9	255	F	4.00	5.41	50.2	31.5	14,875	1,225	7.3	2.2	5.1	0.43	0.80
9'	0	F	2.00	8.97	46.7	29.6	9,042	3,151	8.2	2.7	5.5	0.49	0.10
10	120	F	10.00	4.78	27.0	33.6	30,868	1,844	8.1	2.0	6.1	0.33	1.40
10'	0	F	13.00	6.72	51.5	32.9	30,430	320	8.8	3.7	5.1	0.73	0.10
11	6,500	F	6.00	6.04	39.1	36.0			7.7	2.4	5.3	0.45	1.30
11'	0	F	4.00				9,500	740	6.4	1.6	4.8	0.33	0.52
12	1,812	M	4.00	6.81	47.0	34.2	11,280	870	7.3	2.5	4.8	0.52	0.60
12'	0	M	3.00	9.68	47.6	31.5	4,100	2,200	6.9	3.9	3.0	1.30	0.05
13	1,550	M	14.00	4.86	42.0	29.9	25,415	3,588	6.6	1.7	4.9	0.35	0.60
13'	0	M	11.00	5.68	55.7	32.4	10,509	452	6.5	2.9	3.6	0.81	0.20
14	1,422	M	0.33	7.70	38.0	30.7	26,663	2,051	7.4	2.1	5.3	0.40	0.30
14'	0	M	0.25	7.67	39.7	33.9	28,200	1,600	7.3	3.6	3.7	0.97	0.05
15	630	M	0.50	5.50	47.0	29.8	12,144	4,400	8.1	2.5	5.6	0.45	0.20
15'	0	M	0.50	8.00	50.4	33.0	21,663	2,088	6.4	2.7	3.7	0.73	0.10
16	420	M	1.50	7.12	46.3	31.1	7,677	427	8.8	2.1	6.7	0.31	1.40
16'	0	M	2.00	2.62	59.3	32.9	5,370	1,990	7.7	2.6	5.1	0.51	0.10
17	290	M	8.00	8.81	47.0	30.2	32,414	652	8.8	2.4	6.4	0.38	0.10
17'	0	M	7.00	7.96	46.9	34.6	12,604	822	5.1	3.2	1.9	1.68	0.20
18	180	M	0.50	6.48	33.0	34.9			8.2	2.1	6.1	0.34	0.90
18'	0	M	0.50						7.2	2.0	5.2	0.38	7.40
19	20	M	12.80	7.30	38.0	34.3	18,890	1,210	7.7	2.6	5.1	0.51	1.30
19'	0	M	11.00	5.32	41.9	33.2	900	600	10.4	3.1	7.3	0.42	1.20
20	167	M	8.00	5.43	49.2	58.2	14,420	2,750	7.5	2.3	5.2	0.44	0.30
20'	0	M	8.00	7.95	37.2	33.8	748	500	10.4	2.8	7.6	0.37	0.50
21	180	M	0.75	7.71	39.4	37.1	10,000	5,400	7.4	2.3	5.1	0.45	0.10
21'	0	M	0.83	8.05	48.7	30.9	4,240	1,770	6.6				
22	20	M	0.50	7.20	42.9	33.1	16,400	2,100	8.7	2.9	5.8	0.50	0.05
22'	0	M	0.92	8.14	35.0	30.5	11,937	1,201	12.6	1.9	10.7	0.18	0.10
23	20,000	M	2.00	6.98	46.7	31.9	13,590	2,090	8.6	2.9	5.7	0.51	0.30
23'	0	M	1.00	6.00	46.5	33.8	13,450	2,430	12.4	2.5	9.9	0.25	0.90
24	100	M	2.50	8.78	34.0	34.8	11,868	1,366	10.0	2.5	7.5	0.33	4.00
24'	0	M	1.00				43,400	4,491	10.5	2.5	8.0	0.31	0.10

[a] RBC- red blood cell; MCV- mean corpuscular volume; MCHC- mean corpuscular hemoglobin concentration; A/G – ratio of plasma albumin to plasma globulin; blank cells indicate missing data.

Table 5.3.7 shows the mean and standard deviation of the hematological and serum biochemical parameters between PCR-positive and -negative populations. Compared to the normal reference range, the means of red blood cell concentration, plasma albumin, and albumin to globulin ratio (A/G) are low in the PCR -positive population. Neutrophil count and total plasma bilirubin exceed the reference range in both populations. Of note, the standard deviation is particularly high in the neutrophil count of both populations, and in plasma albumin and globulin of the PCR -negative population. The Wilcoxon matched pair test reveals that out of the 9 clinical parameters, only red blood cell concentration, plasma albumin, and plasma A/G are significantly different between the two populations (**Table 5.3.8**).

Table 5.3.7. Hematological and serum biochemical parameters in PCR -positive and -negative populations.

Variables	N (+)[a]	N (-)	Mean (+)	Mean (-)	Reference Values[b]
RBC (M/ µl)	24	21	6.28 ± 1.73	7.24 ± 1.89	6.90-10.10
MCV (fL)	24	21	42.01 ± 6.98	46.30 ± 1.18	40.00-52.00
MCHC (g/dL)	24	21	34.24 ± 5.58	32.83 ± 1.67	32.00-35.00
Neutrophils (cells/µl)	20	23	17,961 ± 17,503	12,955 ± 10,211	2,300-10,700
Lymphocytes (cells/µl)	21	23	2,127 ± 1,799	1906 ± 1,097	1,200-6,800
Plasma Albumin (g/dL)	24	23	2.29 ± 0.33	2.90 ± 0.62	2.80-4.20
Plasma Globulin (g/dL)	23	22	5.85 ± 1.12	5.17 ± 2.31	2.70-4.90
Plasma A/G	23	22	0.40 ± 0.08	0.69 ± 0.37	0.60-1.60
Total Plasma Bilirubin (mg/dL)	23	22	0.95 ± 1.13	0.94 ± 1.67	0-0.20

[a] (+) indicates FIP-positive population; (-) indicates FIP-negative population; unequal numbers are due to missing data.

[b] Reference values as indicated by the Cornell University Veterinary Clinical Pathology Laboratory.

Table 5.3.8. Analysis of differences between PCR -positive and -negative populations by Wilcoxon matched pair test.

Parameter	N	p^a
RBC (M/µL)	21	0.035
MCV (fL)	21	0.122
MCHC (g/dL)	21	0.578
Neutrophils (cells/ µL)	20	0.204
Lymphocytes (cells/ µL)	21	0.821
Plasma Albumin (g/dL)	21	0.004
Plasma Globulin (g/dL)	21	0.126
Plasma A/G	21	0.011
Total Plasma Bilirubin (mg/dL)	21	0.271

[a] Significant at $p < 0.05$

5.4. DISCUSSION

In this study, we successfully used the IF assay as the gold-standard test to determine the diagnostic performance of the FIP M gene mRNA qRT-PCR assay. However, only 63 specimens (47.7%) in a total of 132 submitted FIP-diagnostic specimens produced IF results and were subsequently included in the analysis (**Table 5.3.1**). Due to the general low cellular content (<5000 nucleated cells/mL) of the FIP effusion (Goodson et al., 2009), it is difficult to isolate sufficient cells in the first place. The fact that FIPV-infected macrophages only account for an even smaller portion of the isolated cells further complicates the IF assay. An adequate number of cells deposited on the encircled area of the slides is critical for acceptable assay sensitivity, and therefore specimens with insufficient cells (<40 cells per encircled area) were excluded. Specimens with multiple layers of cells were also excluded due to the high fluorescence background resulting from overlapping cells.

A total of 63 specimens was analyzed, consisting of 34 positive and 29 negative specimens by PCR analysis. The PCR copy numbers and the corresponding numbers of FCoV IF-positive macrophages encompass wide ranges (**Table 5.3.1**), and there was no correlation between log-transformed PCR copy numbers and the numbers of IF-positive macrophages ($r^2 = 0.06$, p=0.16).

To investigate the diagnostic performance of the FIP M gene mRNA qRT-PCR assay, we first identified the TP, TN, FP, and FN results by the use of a two-by-two contingency table (**Table 5.3.2**). The TP and TN cases of the PCR were the consistent results obtained from both assays, whereas the FP and FN cases were the inconsistent results (**Table 5.3.2**). We then derived the Se, Sp, PPV, NPV, and accuracy of the PCR

assay. The Se and PPV of the assay were 100% due to the zero FP cases identified by the PCR assay (**Table 5.3.3**). However, a relatively large number of FN cases generated disappointing Se and NPV of 66.7 and 41.4%, respectively. Upon closer inspection by discrepant analysis, we removed eight borderline cases that were negative in the PCR , but positive in IF by only a single FCoV infected macrophage (**Table 5.3.1**), and thus may have been negative in the PCR due to Poisson distribution of the very low number of PCR target molecules (**Table 5.3.1**). In re-evaluation after correction, we re-evaluated the diagnostic performance of the PCR assay (**Table 5.3.4 and 5.3.5**), and observed now Se and NPV of 79.1 and 57.1%, respectively, at 100% Sp and PPV (**Table 5.3.5**).

Along with the examination of the diagnostic performance of the PCR assay, we show the IF labeling results to compare TP and TN cases (**Fig. 5.3.1a** and **d**). By use of differential IF labeling, the TP specimen demonstrated widely disseminated FCoV vesicles in green within the red macrophages. In contrast, the TN specimen demonstrated no presence of green FCoV vesicles. On a side note, the IF labeling also reveals additional information about FIP infection. In **Fig. 5.3.1a**, multiple macrophages were FCoV-infected, but staining for FCoV was located not only in the cytoplasm of the macrophages but also outside of the cytoplasm, which indicates viral exocytosis *in situ*. In addition, we also found that the FCoV vesicles distributed in two patterns, diffuse and punctuated, which tended to associate with high and low PCR-positive specimens, but we were not able to demonstrate significance for this observation due to the insufficient number of specimens (**Fig. 5.3.1b** and **e**). Lastly, the IF labeling results of the borderline cases showed only a single infected macrophage among either multiple cells or only a few cells (**Fig. 5.3.1c** and **f**). These actual images of single infected macrophages in IF labeling visualize the

potential for random Poisson distribution of these cells. The examined 0.1 mL (PCR) or 0.2 mL (IF) aliquots of such low-density FCoV-infected specimens may or may not contain these scarce infected macrophages, creating ample opportunity for FN results in either IF labeling or PCR testing, or both.

Although the Se, NPV, and accuracy of the PCR assay increased after the removal of the discordant cases, the assay still suffered from unsatisfactory sensitivity due to high numbers of FN cases. Fortunately, in the case of FIP, a high Sp and PPV is of utmost importance due to the high euthanasia rate for FIP-confirmed patients. In FIP, the number of infected macrophages is generally low. This represents a difficult-to-solve diagnostic conundrum of maximizing sample size versus sensitivity that is reduced by the PCR-inhibitory high nucleic acid background of large samples. A factor contributing to low sensitivity may be directly related to the PCR principle of FCoV mRNA amplification. The M gene-specific downstream primer anneals to positive-sense mRNA and directs production of cDNA from M gene mRNA during the initial reverse transcription step of the single-step PCR. However, the leader sequence-derived universal FCoV mRNA upstream primer anneals to the negative-sense intermediates of FCoV mRNAs (Fehr and Perlman, 2016; Wu and Brian, 2010). These negative sense intermediates are only about 1% as abundant as the positive-sense mRNA counterparts (Sethna et al., 1991), creating a huge disparity in overlapping cDNAs directed by the PCR primers. In addition, the M gene intermediate represents only one of many FCoV mRNA intermediates, further aggravating the disparity in positive and negative strand cDNAs of the FCoV M gene.

Another contributing factor to unsatisfactory sensitivity of may be nucleic acid fragmentation of specimens for PCR diagnostics, resulting in incomplete cDNAs. In that

case, overlapping sense and anti-sense fragments of the PCR target must first recombine to a full-length target before effective amplification can commence. Yet another factor confounding the PCR sensitivity may be mutant M gene target sequences that bind the downstream primer poorly or not at all. This possibility is strongly suggested by the nine false negative cases #35-43 that are negative in the FIP M gene mRNA qRT-PCR, but highly positive in the IF assay.

Parallel to the IF assay, we also evaluated the diagnostic accuracy of the FIP M gene mRNA qRT-PCR assay via a case-control study of a dataset collected from 24 age- and sex-matched PCR -positive and -negative cases (**Table 5.3.6**). Since age and sex are the matching criteria, we did not compare the mean differences of these two parameters between the PCR -positive and -negative cases. We did not include breed as one of the parameters because most diagnostic specimens that we received were from mixed-breed cats.

While the mean age of the presented FIP cases in this study is 4.26 years, the median age of 2.25 years is substantially lower. These data are not entirely consistent with the young age range for FIP-diseased cats (3 months - 3 years old) mentioned in most studies (Kipar and Meli, 2014; Pedersen et al., 2014; Pesteanu-Somogyi et al., 2005). However, some studies indicate that geriatric cats (> 10 years old) are also vulnerable to FIP infection (Goodson et al., 2009; Rohrbach et al., 2001). In fact, the ages of the FIP in this study showed a skewed distribution, with 12 cats younger than 2.25 years, 4 cats of 2.25-4 years, 4 cats of 6-8 years, and 4 cats 10-14 years of age. This supports a concept of bimodal age distribution of FIP cases, either young or geriatric.

We were able to obtain data from most cases on well-described critical hematological and serum biochemical parameters of the two populations (**Table 5.3.7**). Red blood cell (RBC) concentration, plasma albumin, and albumin to globulin ratio (A/G ratio) were lower in the PCR -positive population, and blood neutrophil counts were higher (**Table 5.3.7**). Wilcoxon matched pair testing confirmed the reduced RBC and plasma albumin concentration, and the lower A/G ratio, but not the elevated neutrophil counts. The findings clearly defined the most critical laboratory parameters that are associated with FIP, and are in complete agreement with those reported by others (Norris et al., 2005; Paltrinieri et al., 2001; Riemer et al., 2016; Tsai et al., 2011). The anemia associated with FIP is a result of chronic infection. The chronic infection compromises the release of iron by the reticulo-endothelial system, which contributes to ensuing anemia (Viana, 2011). In FIP, the anemia is generally normochromic-normocytic, which is consistent with our data shown in **Table 5.3.7**.

We also analyzed albumin and globulin as global plasma markers of inflammation (Gabay and Kushner, 1999). Albumin is exclusively produced by hepatocytes, and inflammation reduces its synthesis, thus albumin is an inverse marker of the acute-phase response (Fleck, 1989). Globulin encompasses all remaining plasma proteins that include hepatocyte-produced proteins such as haptoglobin, but also immunoglobulins, and is a direct marker of the acute-phase response due to its increase during inflammation (Cray et al., 2009). The low albumin plasma concentration in FIP cats may be in part the result of extravasation triggered by vasculitis in cats with abdominal effusions, but more likely is it that the severe systemic inflammatory status associated with FIP downregulates liver synthesis of albumin. Thus albumin, as inverse marker of the acute-phase response, is an

clinical excellent marker for FIP, and its low level in combination with specific detection of FIPV virtually ensures correct diagnosis. Although several studies emphasize hyperglobulinaemia as a diagnostic FIP marker (Diaz and Poma, 2009; Hsieh and Burney, 2014; Paltrinieri et al., 2001; Riemer et al., 2016), we found that plasma globulin is only weakly elevated in FIP cases, and therefore cannot recommend it as clinical diagnostic marker.

In addition to serum albumin, the serum albumin to globulin ratio is arguably one of the best clinical chemical FIP markers due to its objective value, which, as ratio, is resistant to fluctuations of absolute values such as plasma albumin and globulin. Studies have shown that an A/G less than 0.8 (Cahn and Line, 2010; Hartmann et al., 2003; Hartmann et al., 2005) is highly suggestive of FIP, some even suggested an A/G less than 0.6 is exclusively diagnostic for FIP (Jeffery et al., 2012). In our data, we produced a cut-off value of 0.5 of A/G for FIP diagnosis (**Table 5.3.7**). Of note, the mean A/G in the PCR-negative population was also lower than the reference range (**Table 5.3.7**), which might be the result of potential FN cases in the matched negative population. This may also explain the high standard deviation of A/G found in this population.

However, in our study, we did not find neutrophilia, lymphopenia, and hyperbilirubinaemia frequently associated with FIP PCR detection (**Table 5.3.7** and **Table 5.3.8**). We found elevated neutrophil counts in both PCR-positive and -negative cases in our study, but substantially more elevated in the FIP-positive population. Nevertheless, the high standard deviation compromises the viability of neutrophil counts as FIP marker. We found the lymphocyte count in our study within the normal range in both matched groups, whereas the bilirubin concentration strongly exceeded the reference range in both

PCR-positive and-negative populations, but did not differ between them. Some studies found that these two parameters are some of the most common laboratory findings associated with FIP (Addie et al., 2009; Hartmann, 2005; Paltrinieri et al., 2001; Tsai et al., 2011). These differences may be attributable to different stages of the FIP disease course, with early stage cases as examined in this study differing from the terminal cases with histopathologial confirmed FIP typically examined in most studies.

Collectively, we were able to develop a reliable FIP IF labeling assay and by its use successfully determine the diagnostic performance of the FIP M gene mRNA qRT-PCR. Additionally, we were able to identify the critical laboratory parameters associated with FIP that are consistent with literature findings. However, it is evident that the FIP M gene mRNA qRT-PCR assay, while 100% specific, is compromised by a substantial number of false negative results. The relatively high number of cases negative in the PCR, but strongly positive by FCoV IF assay suggests that the PCR may not be able to detect every FCoV M gene variant despite its ability to detect single copies of the target mRNA. Thus, critical re-examination of the PCR target region and overall design is warranted.

CHAPTER 6 Diagnostic accuracy of the FIP nucleocapsid (N) gene messenger RNA and MN gene PCRs

6.1. INTRODUCTION

Previously, we have successfully evaluated the diagnostic performance of the FIP M gene qRT-PCR by the use of the FIP IF labeling assay as the gold standard. The initial performance assessment showed that the PCR assay demonstrated a 100% specificity and positive predictive value, however unsatisfactory sensitivity and negative predictive value of 66.1% and 41.4%, respectively (**Table 5.3.3**). After elimination of eight borderline specimens that showed a single FIP-positive macrophage in the IF assay, thus were prone to false negative results due to Poisson distribution of targets, we were able to increase Se and NPV to 79.1% and 57.1%, respectively (**Table 5.4.5**). However, this diagnostic performance of the PCR assay is still deficient. We attribute the disappointing performance mainly to polymorphisms of as yet unknown target M gene sequence for the upstream primer, because the remaining false negative specimens were highly positive by IF labeling. This could lead to substantial mismatches between the downstream PCR primer and the M gene target, jeopardizing the annealing step of the PCR. Another reason may be the principally inefficient amplification of coronavirus mRNA. The downstream M gene specific primer anneals to the abundant positive sense FCoV mRNAs, whereas the upstream primer containing the universal FCoV leader sequence anneals to the far less abundant negative sense intermediates of FCoV mRNAs (Sethna et al., 1991). This creates the disparity in overlapping cDNAs generated by the both primers, resulting in a delay in recombination to a full-length PCR target. Moreover, the notion that M gene intermediates only account for a portion of the total FCoV mRNA intermediates further exacerbates the

disparity in leader sequence-primed positive and M gene-primed negative strands of cDNA of the FCoV M gene mRNA. Another reason, exacerbating the inefficient amplification from mRNA, may be that most target sequences will be contained within fragmented rather than full-length mRNA and intermediates, due to the fragile nature of single-stranded nucleic acids. This fragmentation results in generation of incomplete cDNAs for subsequent PCR amplifications.

Collectively, we believe to have pinpointed the possible shortcomings of the FIP M gene mRNA qRT-PCR. In the current study, we developed two novel PCRs aimed to solve the mentioned diagnostic conundrum of the FIP M gene mRNA qRT-PCR. In one PCR, we still choose to amplify an FCoV mRNA and corresponding intermediate, but target a more conserved 5' segment of the nucleocapsid (N) gene (FIP N gene mRNA qRT-PCR) with the downstream primer. This should minimize mismatches between PCR primers and target templates. In another PCR, the FCoV genomic RNA of the highly conserved 3' end of the M gene along with the 5' portion of the N gene is targeted instead of mRNA. It is worth mentioning that any PCR that detects genomic coronavirus RNA will inevitably also rely on viral replication due to the abundant production of the full-length negative-sense genomic RNA template by the viral replication-transcription complex (Sawicki, 2007). After establishing these PCRs, we then would cross-examine their diagnostic performance using the set of specimens for which we know the M gene mRNA PCR and IF data.

6.2. MATERIALS AND METHODS

Design of primers and probes. Like the FIP M gene mRNA qRT-PCR, the FIP N gene mRNA qRT-PCR targets the universal FCoV mRNA leader sequence, therefore the same upstream primer as the FIP M gene mRNA qRT-PCR. Together with the highly conserved downstream nucleocapsid (N) gene primer, the N gene mRNA qRT-PCR amplifies a 250 bp amplification product. Both donor and acceptor FRET probes of the FIP N gene mRNA qRT-PCR are non-degenerate and follow a design strategy similar to the M gene mRNA qRT-PCR. Different from the M gene PCR with the LightCycler Red 640 acceptor probe with 640 nm emission read in the F2 channel, the TYE705 acceptor probe maximally emits fluorescence at 705 in the F3 channel. Due to the lower spillover at 705 nm from the F1 emission by the fluorescein donor probe, the background signal is reduced, resulting in a higher signal-to noise ratio in the F3 channel. Primers and probes for the FIP N gene mRNA qRT-PCR were synthesized by Integrated DNA Technologies (Coralville, IA), and are shown in **Table 6.2.1**.

Table 6.2.1. Oligonucleotide primers and probes used in FIP N gene mRNA qRT-PCR

Primer/probe	Sequence (5'→3')[a]
Upstream primer	GCCTTGTGCTAGATTTGTCTTCGGACA
Downstream primer	CCAATTTGTTGATCYTTATTACCTATTCCYTTGGGAAC
Fluorescein probe	ACGTCTTTTGGAAGGTTCATCTCCCCAGT-6FAM
TYE705 probe	TYE705-GACGCGTTGTCCCTGTGTGGCCAT-P

[a] Degenerate bases are marked in red. Y represents C or T. 6-FAM indicates 6-carboxyfluorescein. P indicates phosphate.

The FIP MN gene qRT-PCR assay amplifies a 281 bp target region spanning the membrane-nucleocapside (MN) gene junction on the FCoV genome. The target region covers the exact N gene amplification region in the FIP N gene mRNA qRT-PCR (250 bp), and therefore shares the same downstream primer and probes with the FIP N gene mRNA

qRT-PCR. The upstream primer is derived from a highly conserved 3' region of the FCoV M gene. The primers and probes for the FIP MN gene qRT-PCR are shown in **Table 6.2.2**.

Table 6.2.2. Oligonucleotide primers and probes used in FIP MN gene qRT-PCR

Primer/probe	Sequence (5'→3')[a]
Upstream primer	GCYGGTGATTACTCAACAGAAGCACGTACTGA
Downstream primer	CCAATTTGTTGATCYTTATTACCTATTCCYTTGGGAAC
Fluorescein probe	ACGTCTTTTGGAAGGTTCATCTCCCCAGT-6FAM
TYE705 probe	TYE705-GACGCGTTGTCCCTGTGTGGCCAT-P

[a] Degenerate bases are marked in red. Y represents C or T. 6-FAM indicates 6-carboxyfluorescein. P indicates phosphate.

Nucleic acid extraction and PCR operation. Total nucleic acid extraction of the effusion specimens as well as PCR thermal cycling were performed by using the methodology described in Chapter 3. Standard templates were created from linearized plasmids containing the synthetically produced target nucleic acid sequences of both PCRs. Copy numbers of FIP N gene mRNA and FIP M-N genomic RNA per mL original effusion specimen were derived from the 0.1 mL effusion specimen aliquot in the 10 µl extracted total nucleic acids used per PCR.

6.3. RESULTS

Overview of the IF results of the FIP PCRs. Table 5.3.1 demonstrates the PCR copy numbers of the FIP N gene mRNA qRT-PCR and FIP MN gene qRT-PCR and their corresponding IF labeling results using the set of effusion specimens that were also analyzed by the FIP M gene mRNA qRT-PCR (**Table 5.3.1)**. The N gene mRNA copy numbers range from 7 to 61,383 copies per milliliter in positive effusion specimens, whereas the copy numbers of MN gene genomic RNA target range from 11 to 71,863 copies per milliliter in positive effusion specimens (**Table 6.3.1**). Pearson's correlation analysis showed no significant correlation of the log-transformed PCR copy numbers of both PCRs with the numbers of IF-positive macrophages ($r^2 = 0.0006$, p=0.89 for the FIP N gene mRNA qRT-PCR; $r^2 = 0.0042$, p=0.67 for the FIP MN gene qRT-PCR).

Table 6.3.1. N gene mRNA and MN gene PCR results of previously tested effusion specimens.

Specimen #	M gene mRNA/mL	IF-positive macrophages	N gene mRNA/mL	MN gene/mL
1	56,834	26	61,383	71,863
2	21,053	1	8,443	33,589
3	19,259	1	367	5,471
4	13,874	29	9,641	20,014
5	3,326	2	108	4,961
6	2,585	13	374	487
7	2,417	39	354	928
8	2,151	7	15	45
9	1,705	22	3,319	14,095
10	1,444	10	6,091	29,644
11	1,383	1	677	2,922
12	1,280	11	874	3,141
13	1,081	6	12,000	56,422
14	622	1	8,923	37,286
15	585	15	265	158
16	422	1	1,336	11,362
17	375	23	187	3,278
18	300	22	523	1,442
19	290	5	585	2,350
20	238	2	771	357
21	232	1	403	2,277
22	206	3	836	14,411
23	206	2	85	415
24	178	2	633	5,284
25	163	86	104	255
26	144	27	338	623
27	135	1	53	306
28	116	14	202	1,517
29	74	1	41	227
30	64	4	9	601
31	56	14	507	2,109
32	40	2	481	3,626
33	33	4	44	58
34	27	15	0	135
35	0	18	152	2,205
36	0	12	40	467
37	0	14	7	11
38	0	31	0	111
39	0	17	0	0
40	0	3	0	0
41	0	3	0	0
42	0	5	0	0
43	0	2	0	0
44	0	1	210	1,817
45	0	1	40	627
46	0	1	0	964
47	0	1	0	30
48	0	1	0	0
49	0	1	0	0
50	0	1	0	0
51	0	1	0	0
52	0	0	463	618
53	0	0	0	4,883
54	0	0	0	231
55	0	0	0	69
56	0	0	0	0
57	0	0	0	0
58	0	0	0	0
59	0	0	0	0
60	0	0	0	0
61	0	0	0	0
62	0	0	0	0
63	0	0	0	0

As shown in **Table 6.3.2**, a total of 38 true positive (TP) and 11 true negative (TN) cases were identified in the FIP N gene mRNA qRT-PCR. One false positive (FP) and 13 false negative (FN) cases were identified in the same PCR assay.

Table 6.3.2. Performance of the FIP N gene mRNA qRT-PCR.

PCR test result	IF-positive (Diseased)	IF-negative (Non-diseased)
Positive	38	1
Negative	13	11

These data resulted in the following performance characteristics of the FIP N gene mRNA qRT-PCR as shown in **Table 6.3.3.** A single FP case of the PCR assay generates 91.7% specificity (Sp) and 97.4% positive predictive value (PPV). The high FN rate contributes to a Se of 74.5% and a NPV of 45.8%. The overall accuracy of the assay is 77.8%.

Table 6.3.3. Se, Sp, PPV, NPV, and accuracy of FIP N gene mRNA qRT-PCR.

	Se	Sp	PPV	NPV	Accuracy
FIP N gene mRNA PCR	74.5%	91.7%	97.4%	45.8%	77.8%

According to the discrepant analysis (McAdams et al., 2000), a total of 6 cases (case 46-51) were identified as borderline cases that are negative in the PCR but show only a single IF-labeled infected macrophage (**Table 6.3.1**). These discordant results may show Poisson distribution in analyses, thereby were removed from the performance re-evaluation of the N gene mRNA qRT-PCR. This results in a decrease of FN cases from 13 to 7, while the other performance values remain the same. After removal of these 6 borderline cases, we obtain increases of Se from 74.5% to 84.4%, NPV from 45.8% to 61.1%, and accuracy from 77.8% to 86.0%, respectively. The Sp and PPV remain the same (**Table 6.3.4**).

Table 6.3.4. Performance re-evaluation of the FIP N gene mRNA qRT-PCR after removal of borderline cases.

	Se	Sp	PPV	NPV	Accuracy
FIP N gene mRNA PCR	84.4%	91.7%	97.4%	61.1%	86.0%

In the FIP MN gene qRT-PCR, as shown in **Table 6.3.1**, a total of 42 TP and 8 TN cases were identified (**Table 6.3.5**). Four FP and 9 FN cases were identified in the same PCR assay.

Table 6.3.5. Performance of the FIP MN gene qRT-PCR.

PCR test result	IF-positive (Diseased)	IF-negative (Non-diseased)
Positive	42	4
Negative	9	8

The derived performance characteristics of the FIP MN gene qRT-PCR is shown in **Table 6.3.6.** Relatively high FP cases of this PCR assay generates a 66.7% of Sp and 91.3% of PPV, respectively. The lower FN rate contributes to a Se of 91.3% and a NPV of 47.1%. The overall accuracy of the assay is 79.4%.

Table 6.3.6. Se, Sp, PPV, NPV, and accuracy of the FIP MN gene qRT-PCR.

	Se	Sp	PPV	NPV	Accuracy
FIP MN gene PCR	82.4%	66.7%	91.3%	47.1%	79.4%

We identified a total of 4 cases (case 48-51) as borderline cases in discrepant analysis that are negative in the PCR but show only a single IF-labeled infected macrophage (**Table 6.3.1**). These discordant results were removed from the performance re-evaluation of the MN gene qRT-PCR. This change causes a decrease of FN cases from 9 to 5, while the other performance values remain the same. After the removal of the four

borderline cases, we obtain increases of Se from 74.5% to 89.4%, NPV from 45.8% to 61.5%, and accuracy from 77.8% to 84.7%, respectively. Sp and PPV remain the same (**Table 6.3.7**).

Table 6.3.7. Performance re-evaluation of the FIP MN gene qRT-PCR after removal of borderline cases.

	Se	Sp	PPV	NPV	Accuracy
FIP MN gene PCR	89.4%	66.7%	91.3%	61.5%	84.7%

Given the near symmetrical distribution for the IF and MN gene PCR assays of cases that can be can be considered either false positive or negative in either assay, one may argue that either assay could be considered gold-standard. For neither assay do we have evidence that it becomes falsely positive due to high background and an inability to discriminate a true from a false signal. That leaves only the possibility of spuriously false positive/negative cases due to Poisson distribution of FIP virus in specimen aliquots. Thus with the inherent nature of FIP as a low-level chronic progressive disease, it will for either assay, assuming 100% specificity, be inevitable that in certain cases the presence of FIP virus will remain undetected. Under this consideration, we evaluated the performance of the IF assay in comparison to the FIP MN gene qRT-PCR, the most sensitive of the PCR assays, as gold standard. Under this aspect, cases 1-38 and 44-47 were positive by both assays, thus represent 42 true positives (**Table 6.3.8**). Cases 56-63 were negative by both assays, that are 8 true negatives. Cases 52-55 were positive by PCR, but negative by IF, thus represent 4 false negative cases. And finally cases 39-43 and 48-51were negative by PCR, but positive by IF, thus false positive (9). Of these, the latter 4 cases were single-cell positive in the IF assay, thus representing borderline cases.

Table 6.3.8. Performance of the FIP IF assay using the FIP MN gene qRT-PCR as the gold standard.

IF test result	PCR-positive (Diseased)	PCR-negative (Non-diseased)
Positive	42	9
Negative	4	8

The derived performance characteristics of the IF assay versus the FIP MN gene qRT-PCR as gold standard is shown in **Table 6.3.9.** Relatively high numbers of FP cases of this PCR assay generates a Sp of 47.1% and a PPV of 82.4%. The lower FN rate contributes to a Se of 91.3% and a NPV of 66.7%. The overall accuracy of the assay is 79.4%.

Table 6.3.9. Se, Sp, PPV, NPV, and accuracy of the FIP IF assay.

	Se	Sp	PPV	NPV	Accuracy
FIP IF assay	91.3%	47.1%	82.4%	66.7%	79.4%

We identified a total of 4 cases (case 48-51) as borderline cases in discrepant analysis that show only a single IF-labeled infected macrophage but are negative in the PCR (**Table 6.3.1**). These FP discordant results were removed from the performance re-evaluation of the FIP IF assay. This change causes a decrease of FP cases from 9 to 5, while the other performance values remain the same. After the removal of the four discordant cases, we obtain increases of Sp from 47.1% to 61.5%, and of PPV from 82.4% to 89.4%, and accuracy from 79.4% to 84.7%, respectively. Se and NPV remain the same (**Table 6.3.10**).

Table 6.3.10. Performance re-evaluation of the FIP IF assay after removal of borderline cases.

	Se	Sp	PPV	NPV	Accuracy
FIP IF assay	91.3%	61.5%	89.4%	66.7%	84.7%

6.4. DISCUSSION

In this study, we first successfully developed two novel PCR assays, the FIP N gene mRNA qRT-PCR (N gene mRNA PCR) and the FIP MN gene qRT-PCR (MN gene PCR), aimed to overcome the high false negative cases identified by FIP M gene mRNA qRT-PCR (M gene mRNA PCR). We then performed these PCR assays on the same set of 63 effusion specimens previously used by the M gene mRNA PCR performance analysis. We show in **Table 6.3.1** the PCR copy numbers of the two novel PCRs and their corresponding IF labeling results in addition to the previously shown results of M gene mRNA PCR (**Table 5.3.1)**. **Table 6.4.1** demonstrates the total numbers of PCR-positive and -negative results of the three PCR assays. Compared to the M gene mRNA PCR, the N gene mRNA PCR generated 5 additional positive results. The MN gene PCR generated the most positive results (46 specimens). It generated 12 more positive results than the M gene mRNA PCR, and additional 7 positive results when compared to N gene mRNA PCR.

Table 6.4.1. Total number of positive and negative PCR results of the PCRs.

PCRs	Positive	Negative
M gene mRNA PCR	34	29
N gene mRNA PCR	39	24
MN gene PCR	46	17

Upon closer inspection of PCR positive cases, the MN gene PCR generates more copy numbers than the other two PCRs in most cases (**Table 6.3.1**). This indicates that the PCR may detect more FCoV variants than the other two PCRs, since its amplification region covers sections of two of the most conserved gene segments (of the M and N gene) in the FCoV genome. In addition, the MN gene PCR, by detecting genomic RNA also inevitably detects FCoV replication since the negative genome template created by the

FCoV replication-transcription complex serves as target for the upstream M gene primer of this PCR. In this manner, the MN gene PCR detects not only the genomic FCoV RNA but also detects FCoV replication. This notion is also in agreement with the functional characteristics of FIP that the FCoVs, which replicate outside of the intestinal tract, may potentially cause FIP. Thereby, detecting FCoV replication outside of the intestinal tract is a diagnosis of FIP.

To investigate the diagnostic performance of the N gene mRNA PCR and MN gene PCR assays, we first identified the TP, TN, FP, and FN results of the two PCRs by the use of a two-by-two contingency table (**Table 6.3.2 and 6.3.5**). We then derived the Se, Sp, PPV, NPV, and accuracy of the PCR assays (**Table 6.3.3 and 6.3.6**). In Table 5.4.2, we show the performance of the three PCRs.

Table 6.4.2. Initial evaluation of PCR performance.

	Se	Sp	PPV	NPV	Accuracy
FIP M gene mRNA PCR	66.7%	100%	100%	41.4%	73.0%
FIP N gene mRNA PCR	74.5%	91.7%	97.4%	45.8%	77.8%
FIP MN gene PCR	82.4%	66.7%	91.3%	47.1%	79.4%

The low false positive cases, due to low sensitivity, identified by the M gene and N gene mRNA PCRs contribute to high specificity (Sp) and positive predictive value (PPV) relative to the FIP immunofluorescent assay (**Table 5.3.2 and 6.4.2**). In contrast, there were four positive results identified by the MN gene PCR results that were negative in IF labeling (**Table 6.3.1**). These four FP cases compromised the Sp and PPV of the MN gene PCR (**Table 6.3.6 and 6.4.2**). Nevertheless, the lower false negative cases of the MN gene PCR produced the highest sensitivity (Se) and negative predictive value (NPV) of the three PCRs (**Table 6.3.5 and 6.4.2**). The MN gene PCR also produced the highest diagnostic

accuracy of the PCRs owing to its capability to identify more true positive and true negative cases (**Table 6.3.5**).

To eliminate the effect of Poisson distribution at low target concentrations, that might compromise the performance analysis of the PCRs, we identified cases that were negative in the PCRs, but positive in the IF labeling by only a single FCoV infected macrophage as discordant cases (**Table 6.3.1**). We then re-evaluated the performance of the PCRs after the removal of the discordant cases (**Table 6.3.4 and 6.3.7**). The re-evaluation of the performance of the PCRs are shown in **Table 6.4.3**. After the correction, we observed increases of Se and NPV of the three PCRs. The M gene mRNA PCR showed the most drastic changes of Se and NPV among the PCRs due to the removal of the most discordant cases (8 cases). However, the MN gene PCR still demonstrates the highest of both Se and NPV among the PCRs.

Table 6.4.3. Re-evaluation of PCR performance after correction by discrepant analysis.

	Se	Sp	PPV	NPV	Accuracy
FIP M gene mRNA PCR	79.1%	100%	100%	57.1%	83.6%
FIP N gene mRNA PCR	84.4%	91.7%	97.4%	61.1%	86.0%
FIP MN gene PCR	89.4%	66.7%	91.3%	61.5%	84.7%

Upon closer inspection, we found that the MN gene was able to detect 5 more true positive cases (case 34, 38, and 46-47) that were also positive in the IF labeling than the N gene mRNA PCR (**Table 6.3.1**). In these 5 TP cases, 2 (case 46 and 47) cases showed only a single positive FCoV-infected macrophage in the IF labeling (**Table 6.3.1**). In addition, the MN gene PCR detected 3 positive cases (case 53-55) that were both negative in the IF labeling and the M and N gene mRNA PCRs. These findings suggest that the MN gene PCR is the not only the most sensitive PCR among the three assays but also potentially

captures FIP positive specimens that IF labeling and the two other PCRs cannot capture. Given that high-resolution melting curve analysis ensures 100% specificity of the assay with regard to target identification, the false positive cases identified by the MN gene PCR are in fact true positive cases despite the negative findings in the IF assay. Thereby, the Se and PPV of the MN gene PCR should also be 100% after removing all the FP cases.

On the same notion, we also found nearly symmetrical distribution of the cases that were positive or negative in either IF assay or MN gene PCR assay. We did not find evidence that neither assay would generate false positive results due to high background or inability to distinguish a true from a false signal. In consideration of the fact that that FIP is a chronic progressive infection characterized by low numbers of FIP virus, it is likely that any one assay, though 100% specific, is destined to miss detection of some cases of low-level FIP infection. Therefore, we reversed our FIP diagnostic performance analysis and evaluated the performance of the IF assay using the most sensitive MN gene PCR as the gold standard test. We first identified the performance of the IF assay in **Table 6.3.8**, followed by calculating Se, Sp, PPV, NPV, and accuracy of the IF assay (**Table 6.3.9 and 6.3.6**). In this case, we obtained relatively high sensitivity (91.3%) and positive predictive value (82.4%), along with low specificity (47.1%), driven by high numbers of false positive cases, and negative predictive value (66.7%). The accuracy of the IF assay is the same as the MN gene PCR assay (79.4%) (**Table 6.3.9**).

Subsequently, we re-evaluated the performance of the FIP IF assay (**Table 6.3.10**) by eliminating the 4 discordant cases (case 48-51) that showed only a single infected macrophage in the IF labeling but negative in the MN gene PCR in the discrepant analysis. After the correction, we obtained increases of Sp from 47.1% to 61.5%, PPV from 82.4%

to 89.4%, and accuracy from 79.4% to 84.7% (**Table 6.3.10**). This accuracy of the IF assay is the same as the MN gene PCR after the correction (**Table 6.3.7 and 6.3.10**).

Collectively, we developed two novel FIP PCRs that successfully improved the sensitivity and negative predictive value of the FIP M gene mRNA qRT-PCR. The new PCRs have improved sensitivity and negative predictive value, in particular, the FIP MN gene qRT-PCR demonstrated at nearly 90% the highest sensitivity among the three PCR assays (**Table 6.4.2 and 6.4.3**). Although Sp and PPV appeared compromised due to the higher FP cases identified by this assay, upon closer inspection, the FP cases (case 52-55) are actually true positive cases by the criterion of high-resolution melting curve analysis. The high MN gene copy numbers in these specimens further support this notion (**Table 6.3.1**). In addition, we also found that the IF assay and the MN gene PCR mirrored each other, with almost identical results (**Table 6.3.1, 6.3.7, and 6.3.10**). This intriguing finding led us to overturn the performance analysis by using the MN gene PCR as the gold standard for IF assay performance evaluation (**Table 6.3.8, 6.3.9, and 6.3.10**). Interestingly, the five FP cases (case 39-43) in the IF assay compared to the MN gene PCR showed more than one FIP-infected macrophage, which indicates these specimens were true positive rather than false positive or borderline cases. Under this consideration, we eliminated the FP cases in both assays, aiming to generate a genuine performance re-assessment of the two assays (**Table 6.4.4 and 6.4.5**).

Table 6.4.4. Re-evaluation of the MN gene PCR and the IF assay performance after reassignment of FP cases to TP cases.

MN gene PCR	IF-positive (Diseased)	IF-negative (Non-diseased)
Positive	46	0
Negative	5	8
IF assay	**PCR-positive (Diseased)**	**PCR-negative (Non-diseased)**
Positive	47	0
Negative	4	8

Table 6.4.5. Se, Sp, PPV, NPV, and accuracy of the MN gene PCR and the IF assay after reassignment of FP cases to TP cases.

	Se	Sp	PPV	NPV	Accuracy
MN gene PCR	90.2%	100%	100%	61.5%	91.5%
IF assay	92.2%	100%	100%	66.7%	93.2%

After the removal of the FP cases, the two assays demonstrate noticeable increases of Se, Sp, PPV, and accuracy, while the NPV remain unchanged. Both assays deliver 100% Sp and PPV. Although the negative predictive value remains unsatisfactory, we believe that it may be improved by simply repeating the PCR assays for multiple aliquots of a specimen. However, these two assays as well as the other two PCR assays still demonstrate high sensitivity and high specificity when compared to the currently available FIP diagnostic assays (Dye et al., 2008; Hartmann et al., 2003; Hornyák Á et al., 2012; Sharif et al., 2010; Simon et al., 2005;Soma et al., 2013). More importantly, when combining the MN gene PCR and IF assay, the two assays were able to confidently detect 51 positive and 8 negative specimens among all 63 specimens enrolled in this study except for the 4 borderline cases (case 48-51). The excellent diagnostic utility of this combination of the two assays leads us to strongly believe that the most accurate FIP diagnostic regimen is to

first test specimens with the more convenient FIP MN gene qRT-PCR, followed by an IF confirmatory test of the specimens that were negative in the FIP MN gene qRT-PCR.

CHAPTER 7 Role of mutation in the spike protein cleavage site and pathogenesis of FIP

7.1. INTRODUCTION

The functional characteristics of feline infectious peritonitis (FIP) is the acquisition of macrophage tropism of the FCoVs that leads to fatal systemic infection. Spike (S) protein mediates cell entry by initiating cellular receptor binding (S1 domain) and triggering the subsequent viral and host cell membrane fusion (S2 domain) (Ruch and Machamer, 2012), thereby is considered to have an important role in the change of cell tropism of feline coronavirus (FCoV) associated with FIP pathogenicity.

Several studies have investigated whether the mutation within the S protein lead to the macrophage tropism of FCoV seen in FIP infection (Chang et al., 2012; Felten et al., 2017; Licitra et al, 2013; Porter et al., 2014; Rottier et al., 2005). Rottier et al. (2005) was the first to pinpoint that the S protein is the determinant that contributes to the efficacy of macrophage infection. Rottier et al. (2005) constructed different recombinant viruses using an FIP virus isolate as the genome frame modified by either 1) replacing the FIPV 3a-N or S gene with the FECV homologs, or 2) knocking out the FIPV ORF 3abc or the FIPV 7ab gene clusters. They then tested the replication of these viruses in macrophages, and found that only the recombinant FIP virus with the FECV S gene demonstrated significantly reduced macrophage infectivity and limited spread of the infection. For this reason, they concluded that the macrophage cell tropism of FCoV was determined solely by its S protein (Rottier et al., 2005).

While Chang et al. (2012) and Porter et al. (2014) further identified non-synonymous mutations within the S gene that may be responsible for FECV to FIPV

conversion, Licitra et al. (2013) adopted an alternative approach by investigating the role of mutation(s) of the furin cleavage site at the S1/S2 domain boundary (fcS1/S2 motif) in FIP pathogenesis. They identified a well-conserved canonical furin cleavage site motif of R-S/A-R-R-S in the FECV isolates, but not in the FIPV isolates. A fluorogenic peptide furin cleavage assay confirmed that substitutions of amino acid in the S1/S2 motif did alter furin cleavage efficiency. In addition, they examined at two different time points the S1/S2 motifs of two field specimens from cats that harbored FCoV. One cat diagnosed clinically with FIP had a mutated S1/S2 motif at the later time point, while the other clinically healthy cat still harbored the canonical motif. Therefore, they concluded that mutation(s) within the furin cleavage site motif are functionally relevant and are highly correlated to FIP development.

In this study, we aimed to investigate whether the mutation(s) of the furin cleavage site within the S1/S2 gene region (fcS1/S2 motif) are associated to FIP infection. We developed an FCoV fcS1/S2 gene qRT-PCR assay, which amplifies the S1/S2 gene region that harbors the furin cleavage site motif identified by Licitra et al (2013). We approached this aim by performing the PCR on two independent populations: 1) FIP M gene qRT-PCR positive specimens from the Molecular Diagnostic Laboratory FIP diagnostic specimen submissions (the FIP-biased population); and 2) FECV-positive fecal specimens collected from young shelter cats that are frequently FECV-infected (the FIP-unbiased population). After DNA sequencing and translation, we compared mutation frequencies of the fcS1/S2 motif in the two populations. Using this approach, we could establish whether mutations of the fcS1/S2 motif are functionally relevant to FIP infection and may be used as a diagnostic marker for FIP.

7.2. MATERIALS AND METHODS

Design of primers and probe. Regions for primers and probes were chosen based on nucleotide alignment of numerous FECV and FIPV isolates with maximum similarity upstream and downstream of the FCoV S1/S2 domain boundary (S1/S2 motif). This FCoV fcS1/S2 gene qRT-PCR assay amplifies the fcS1/S2 motif region using long degenerate primers that hybridize to conserved sequences adjacent upstream and downstream to the FCoV fcS1/S2 motif, thereby producing an amplification product of typically 211 bp. The fluorescein probe was placed within the fcS1/S2 motif as FRET donor probe, whereas the LCRed 640 FRET acceptor probe was placed one nucleotide upstream of the fluorescein probe in the most highly conserved spike protein sequence (**Table 7.2.1**).

Table 7.2.1. Oligonucleotide primers and probes used in FIP S1/S2 gene qRT-PCR

Primer/probe	Sequence (5'→3')
Upstream primer	GGKGARATTTTCACYGTAGTGCCATGTGATYTAACAG
Downstream primer	CATTATTCCACTTTGTYAYGTAATARAATTGYGGCATAGT
Fluorescein probe	ACACAGTCGAGAAGATCACGTAGGTC-6FAM
LCRed640 probe	LCR640-CAGCYGTYAATCAAACTGATCTRTTTGMKTTTGTAAATCA-P

[a] Degenerate bases are marked in red. K represents G or T, R represents A or G, Y represents C or T, M represents A or C. 6-FAM indicates 6-carboxyfluorescein. P indicates phosphate.

Nucleic acid extraction and PCR operation. Fecal specimens from the FIP-unbiased shelter cat population were collected by rectal insertion of a cytobrush swab which were stored in guanidinium isothiocyanate Triton X-100-based RNA/DNA stabilization reagent in 2 mL vials. After stripping and removal of the swab, the specimens were homogenized in a Precellys 24 shaker (Bertin Technologies, France) at 3,000 RPM, with 3 cycles of 60 seconds shaking followed by 60 seconds rest, using six 3 mm High Wear Resistant Zirconia Grinding Beads (Glen Mills Inc, NJ) per tube. Total nucleic acid extraction of the fecal specimens, as well as PCR thermal cycling of the FCoV S1/S2 gene qRT-PCR were performed by using the methodology described in Chapter 2. FIP M gene

mRNA-positive total nucleic acids originally extracted from submitted effusion specimens were used as templates for the FIP-biased cat population. Two standard templates were created from linearized plasmids containing the synthetically produced nucleic acid sequences of a standard FECV and mutated FIPV target. For convenience, the fecal samples obtained from the FIP-unbiased shelter cat population were only subjected to the FCoV S1/S2 gene qRT-PCR. For that reason, M gene mRNA copy number data were not obtained from this population.

DNA sequencing. Amplification products from specimens with at least 10 fcS1/S1 region starting copies per PCR were subjected to DNA sequencing. Size of the PCR amplification products was first verified by gel electrophoresis of 2 µl of the PCR prior to DNA sequencing. For DNA sequencing, we first treated the remaining 18 µl PCR reaction with 5 µl ExoSAP-IT (Fisher Cat. #78201.1) alkaline phosphatase to dephosphorylate unincorporated nucleotides and primers. This process involved adding 5 µl of the enzyme solution, followed by two 30 min incubations at 37°C and then 80°C. The first low temperature incubation dephosphorylated nucleotides and digested the excess primers. The subsequent high temperature incubation inactivated the enzyme. We then prepared two sequencing reactions for each amplification product with either the upstream or downstream primer. Ten microliters of the ExoSAP-IT treated PCR were first filled up with $T_{10}E_{0.1}$ to 14.25 µl, followed by addition of 0.75 µl of 1:10 diluted (20 µM) primer stock. The pre-mixed sequencing reaction containing ~30 ng of the 231 bp PCR template and 15 pmol primer in 15 µl $T_{10}E_{0.1}$ were shipped to ELIM BIOPHARM for Sanger DNA sequencing.

DNA sequencing result analysis. The DNA nucleotide sequences of the PCR amplification products that were first viewed and edited by Chromas version 2.1.1 software. The sequences were then translated to amino acid sequences by Vector NTI Advance 11 software. The presence or absence of the mutated S1/S2 motifs of the PCR amplification products were then determined by the comparison to the canonical FCoV S1/S2 motif (R-A/S-R-R-S). The mutation frequency between FIP-biased and un-biased population was evaluated by two-tailed Fisher's Exact test. The melting temperature ($\boldsymbol{T}_m$) difference between the two populations was analyzed by Student's t test and logistic regression.

7.3. RESULTS

Overview of DNA sequencing results and probe high-resolution T_m of the FIP S1/S2 gene PCR amplification products. A total of 107 effusion specimens of the FIP-biased population (**Table 7.3.1**) and 114 fecal specimens of the -unbiased population (**Table 7.3.2**) were collected. For ease of analysis, the results of both populations are first separated by standard versus mutated fcS1/S2 motif), and then ranked from the lowest to highest probe melting temperature (T_m) (**Table 7.3.1 and 7.3.2**). In the FIP-biased population, a total of 62 sequences harbor the mutated fcS1/S2 motif versus 45 sequences the canonical fcS1/S2 motif (**Table 7.3.1**). In contrast, in the FIP-unbiased population, only 3 sequences harbor the mutated fcS1/S2 motif versus 111 sequences the canonical fcS1/S2 motif (**Table 7.3.2**).

Table 7.3.1. FIP S1/S2 gene PCR products of the FIP-biased population.

FIP-biased specimen #	M gene mRNA/mL	Probe T_m	Mutated fcS1/S2 motif	Peptide sequence	Nucleotide sequence
1	975	39.98	yes	TRSRTAGRSVQDSVPTY	ACACGGTCCCGAACAGCAGGCAGGTCAGTACAAGATTCAGTACAAACCTAC
2	160	40.83	yes	TQAKRSRSSATGSVTTY	ACACAGGCGAAAAGATCACGTAGTTCAGCAACAGGCTCAGTAAAAACCTAC
3	305	41.32	yes	TPQRRARMSTSDVTKTY	ACTCAGCCTAGAAGAGCACGTATGTCAACCTCCGACACAGTAAAAACCTAT
4	4,748	41.49	yes	TQPRRSRISTSDTVKTY	ACACAGCCGAGAAGGTCACGTATATCAACGTCAGACACAGTAAAAACCTAT
5	35,290	41.78	yes	TQPRRARRPVSKSVQTY	ACACAGCCTAGAAGAGCGCGTAGGCCAGTATCAAAGTCAGTACAAACATAT
6	380	41.86	yes	TQPRRARRPVPDSVQTY	ACACAGCCTAGAAGAGCACGTAGGCCAGTACCAGATTCCGTACAAACCTAT
7	30,000	43.14	yes	THSRRSRRLVSE-VTTY	ACCCATTCTCGAAGATCACGTAGGTTAGTATCAGAA---GTAACCACCTAT
8	670	43.35	yes	TQVRRSLRSAYSPVSTY	ACACAAGTGAGGAGATCCCTTAGGTCAGCATACAGCCCAGTAAGTACATAC
9	390	43.81	yes	TRSRRSFMSTPEPVTTY	ACACGTTCAAGAAGATCACCTATGTCAACACCAGAACCAGTAACTACCTAT
10	3,350	44.48	yes	TQPRGARRSAPESVQTY	ACACAGCCTAGAGGAGCACGTAGGTCAGCACCAGAGTCAGTACAAACCTAT
11	259	44.97	yes	TQTRRSRSSTSNPVTTY	ACACAGACGAGAAGATCACGTAGTTCAACATCAAACCCAGTGACTACCTAC
12	305	45.68	yes	THPRRSRMSTPETVHTY	ACACATCCAAGAAGATCGCGTATGTCAACACCTGAGACTGTACATACCTAC
13	8,460	46.02	yes	TQNRRSRRPVPGKVTTY	ACACAGAATAGAAGATCACGTAGGCCAGTCCCTGGAAAGGTAACAACATAT
14	1,532	46.02	yes	TRSRRASSSTYETVYTY	ACACGTTCAAGAAGAGCAAGTAGCTCGACCATAGAAACAGTATACACCTAC
15	371	46.38	yes	PHSRRTRRSAPEPVRTY	CCACATTCTAGAAGAACACGTAGGTCAGCACCGGAGCCAGTAAGAACCTAT
16	4,590	46.78	yes	TQTRRSRRPASETLETY	ACACAGACAAGGAGATCACGTAGGCCGGCCTCTGAAACACTAGAAACTTAT
17	460	46.79	yes	TQSRRTRSSTSYSVNTY	ACACAGTCTAGAAGAACACGTAGTTCAACATCGTACTCAGTAAACACCTAC
18	760	46.98	yes	THSRRTRRSASDPVKTY	ACACATTCTAGAAGAACAGCTAGGTCAGCATCAGATCCTGTAAAAACTTAT
19	1,100	47.20	yes	TQSRRSLRPAPYTVTTY	ACACAGTCTAGAAGGTCACTTAGACCAGCACCATACACGGTAACCACCTAC
20	830	47.32	yes	TQSRRSRTFTPSTVTTY	ACACAATCGAGGAGGTCACGTACGTTCACACCAAGTACGGTGACCACCTAT
21	3,527	47.63	yes	TQPRGARRSVSESVNTY	ACACAGCCYAGAGGAGCACGCAGGTCAGTGTCAGAGTCAGTAAACACCTAT
22	163	48.42	yes	TQPRRARGSAPESVQTY	ACACAGCCTAGAAGAGCACGTGGGTCAGCACCAGAGTCAGTACAAACCTAT
23	213	48.69	yes	TQSRRSRSSTPESVQTY	ACACAGTCTAGAAGATCACGTAGTTCAACACCAGAGTCAGTACAAACTTAT
24	160	49.18	yes	TQQRRSRRLTSELTITH	ACACAGCAGAGGAGATCACGCAGGTTAACATCAGAGCTAACCCTCACCCAT
25	2,630	49.32	yes	THSRRALRSTNESVQTY	ACACATTCAAGAAGAGCACTCAGGTCGACAAACGAATCAGTGCAAACTTAC
26	90	49.38	yes	TQSKSSRRATPGIVKTY	ACACAATCGAAAAGTTCACGCAGGGCAACACCTGGCATAGTAAATACCTAC
27	1,237	49.39	yes	--PKGSRRSTAETVTTY	------CCAAAAGGATCACGTAGGTCAACCGCAGAAACAGTAACAACCTAC
28	605	49.42	yes	TQARISRRSTSEAVTTY	ACACAGGCAAGAATATCACGTAGGTCGACCTCTGAAGCAGTAACCACCTAT
29	240	50.23	yes	TSSRSSRRSTSEPVQTY	ACAAGTTCAAGAAGTTCACGTAGGTCAACCTCAGAACCAGTACAAACCTAT
30	1,670	50.43	yes	TQSERSRGSTQEPVNTY	ACACAGTCGGAAAGGTCACGTGGTTCTACACAAGAACCAGTAAACACCTAT
31	3,500	50.59	yes	TQSRRSHWSTPETVTTY	ACACAGTCGAGAAGGTCACATTGGTCAACACCAGAAACAGTAACGACCTAT
32	360	51.14	yes	AQPRRALRSASESVTTY	GCTCAGCCTAGAAGAGCACTTAGGTCAGCATCAGAATCGGTAACCACCTAC
33	320	51.55	yes	THARRSRSTTSESVQIY	ACACATGCAAGAAGATCACGCAGTACAACATCTGAAAGTGTACAAATTTAT
34	175	51.64	yes	TQSRSSRRSPSEPVKIY	ACACAGTCAAGAAGTTCACGTAGGTCACCATCAGAACCAGTAAAAATCTAT
35	120	51.76	yes	TQSRRAPSSLPDSVKTY	ACACAGTCGAGAAGGGCACCTAGTTCGTTATCAGACTCTGTAAAAACCTAC
36	7,638	51.90	yes	TQPRSSRRLVQTSVTTY	ACACAGCCTAGAAGTTCACGTAGGTTAGTACAAACCTCAGTAACAACTTAT
37	1,339	52.25	yes	TQSRRSLRSTSSSVTTY	ACACAGTCGAGGAGATCACTTAGGTCAACTTCAAGTTCAGTAACTACCTAC
38	154	52.39	yes	TQSRRSRKAVSNSVNTY	ACACAGTCTAGAAGGTCACGTAAGGCAGTATCAAACTCAGTAAATACCTAC
39	100	52.70	yes	TQSRRARNATVESVTTY	ACACAGTCAAGAAGAGCACGTAATGCAACTGTAGAATCAGTAACCACCTAC
40	626	52.82	yes	TQSGRSRRPTPETVTTY	ACACAATCAGGAAGATCACGTAGGCCAACACCTGAGACTGTAACAACCTAT
41	560	52.90	yes	TQPRRSRSSTSNSVTTY	ACACAGCCGAGAAGATCACGCAGTTCAACGTCAAACTCTGTAACAACCTAT
42	1,600	52.92	yes	TDAGRSLKSRGKAVKTY	ACAGACGCGGGAAGGTCACTTAAGTCAACAGGCAAAGCAGTAAAAACCTAT
43	1,118	53.06	yes	THSRRSLRSTPESVKTY	ACACATTCAAGAAGATCACTTAGGTCAACACCTGAATCAGTAAAAACCTAT
44	372	53.18	yes	TQSRRARRPTPDSVKTY	ACACAGTCAAGAAGAGCACGCAGGCCGACACCTGACTCAGTAAAGACCTAC
45	334	53.23	yes	THSRGSRRSAVESVQTY	ACACATTCCAGAGGATCACGCAGGTCAGCAGTTGAATCAGTACAAACTTAT
46	160	53.27	yes	TQSRRSRGSTPDSVKPY	ACACAATCAAGAAGATCACGTGGGTCAACACCTGACTCAGTAAAACCCTAT
47	43,000	53.69	yes	TQSRRARMSTSELVQTY	ACACAGTCTAGAAGAGCACGTATGTCAACCTCAGAGTTAGTACAAACCTAT
48	220	53.79	yes	TQSRRSRRGSISNQVTY	ACACAATCGAGAAGGTCACGTGGGTCTATATCAAACCAGGTAACTGCTTAT
49	6,230	53.87	yes	TQPRSARRSVSESVQIY	ACACAGCCTAGAAGTGCACGTAGGTCAGTGTCAGAGTCAGTACAAATTTAT
50	290	54.08	yes	TQPRSARKSTSSSVTTY	ACACAGCCGAGAAGTGCACGTAAGTCAACATCAAGCTCTGTAACAACCTAT
51	130	54.85	yes	TQSRKSRRSTPESVKTY	ACACAATCAAGAAAATCACGTAGGTCAACACCTGAATCAGTAAAAACCTAT
52	360	54.85	yes	TQPIRSRMSTSEAVKTY	ACACAGCCAATAAGATCACGTATGTCGACCTCTGAAGCAGTAACCACCTAC
53	1,550	55.04	yes	KSSRRPRRSPSNSVHTY	AAATCGTCGAGAAGACCACGTAGGTCACCATCAAATTCAGTACATACCTAC
54	742	55.48	yes	THSRRSRMSTSETVNIY	ACACATTCGCGAAGATCACGTATGTCAACGTCCGAAACAGTAAACATCTAT

Table 7.3.1.cont. FIP S1/S2 gene PCR products of the FIP-biased population.

FIP-biased specimen #	M gene mRNA/mL	Probe T_m	Mutated fcS1/S2 motif	Peptide sequence	Nucleotide sequence
55	750	56.21	yes	TQSKISRRSTPDTVRTY	ACACAATCGAAAATATCACGTAGGTCAACACCTGACACAGTACGTACATAC
56	1,216	56.74	yes	THSRRSRMSTSETVTTY	ACACACTCAAGAAGGTCACGTATGTCAACTTCTGAAACCGTAACAACCTAT
57	1,467	57.38	yes	THSRRSRGSTSDSVTTY	ACACATTCGAGAAGATCCCGTGGGTCAACTTCGGATTCAGTAACTACCTAT
58	530	57.73	yes	TQTRSSRSSVSETVSTY	ACACAGACGAGAAGCTCACGTACGTCCGTATCAGAAACAGTAAGTACTTAC
59	3,000	59.20	yes	TQSRIARRSTPTPVKTY	ACACAGTCGAGAATAGCACGTAGGTCAACACCAACTCCTGTAAAAACCTAC
60	4,500	59.80	yes	TQPRISRRSTSNSLTTY	ACACAGCCGAGAATATCACGTAGATCTACTTCAAACTCATTAACCACCTAC
61	750	61.09	yes	THSRSSRVSRSGTVKTY	ACACATTCGAGAAGTTCCCGTGTGTCCAGGAGTGGAACAGTGAAGACCTAT
62	1,800	61.87	yes	THSRRSRMSTSNSVTTY	ACACATTCAAGAAGATCACGTATGTCAACATCAAACTCTGTAACAACCTAT
63	112	42.17	no	TGARRSRRST-PEVKTY	ACAGGTGCAAGGAGATCACGTAGGTCAACC---CCTGAAGTAAAAACCTAC
64	210	43.07	no	TQTRRSRRSASETVQTY	ACACAAACGAGGAGATCACGTAGGTCAGCTTCTGAAACAGTACAAACCTAT
65	6,001	44.06	no	TQSRRSRRSTSNSVKTY	ACACAGTCGAGAAGATCACGTAGGTCAACATCAAACTCTGTAAAAACCTAT
66	885	44.66	no	TQARRARRSISESVTTY	ACACAGGCTAGAAGAGCACGTCGTTCAATATCAGAATCAGTAACTACTTAT
67	670	46.38	no	TACRRARRSTLDSLNTY	ACAGCCTGTAGAAGAGCACGTAGGTCAACACTAGACTCCCTAAACACCTAC
68	3,800	46.72	no	TQSRRARRSTPSSVNTY	ACACAGTCTAGGAGAGCACGTAGGTCAACACCAAGTTCAGTAAACACCTAT
69	1,138	49.11	no	TQTRRSRRSAPVAVHTY	ACACAGACGAGAAGATCACGTAGGTCAGCACCAGTTGCAGTACATACTTAT
70	100	49.11	no	TYTRRSRRS--DSVHTY	ACATATACGAGAAGATCGCGTAGATCA------GATTCAGTACACACTTAT
71	1,500	49.42	no	TRSRRARRS-VETVQIY	ACACGGTCTAGAAGAGCACGCAGGTCA---GTAGAGACAGTACAAATCTAT
72	467	49.74	no	THSRRSRRSTSDTVKTY	ACAAGTTCGAGAAGATCACGTATGTCAGCACCAACTACAGTACAAACTTAT
73	117	50.12	no	TQSKRSRRSTSDSVKTY	ACACAGTCAAAAAGGTCACGTAGGTCAACATCTGACTCTGTAAAAACCTAC
74	450	50.43	no	TQTRRSRRSSSSSVTTY	ACACAGACGAGAAGATCGCGCCGGTCATCATCAAGCTCAGTAACCACCTAT
75	140	50.51	no	TQLKRARRSTPNSVRTY	ACACAGTTGAAAAGAGCACGTAGGTCTACACCAAACTCAGTAAGGACTTAC
76	2,437	50.59	no	TSSRRSRRSTPTTVQSY	ACATCGTCAAGAAGATCACGTAGGTCAACCCCTACAACAGTACAAAGCTAC
77	2,950	50.75	no	TQPRRARRSAPESVQTY	ACACAGCCTAGAAGAGCACGTAGGTCAGCACCAGAGTCAGTACAGACCTAT
78	880	50.94	no	TQSRRARRSAPESVRTY	ACACAGTCTAGAAGAGCACGTAGGTCAGCACCAGAGTCAGTAAGAACCTAT
79	10,000	50.94	no	THSRRARRSAPESVRTY	ACACATTCGAGAAGAGCACGTAGGTCAGCACCAGAGTCAGTAAGAACCTAT
80	141	51.29	no	THSRRARRSVSDTVKTY	ACACAGTCCAGAAGAGCACGCATTTCAGTACAAGAGTCAGTACGAACCTAT
81	835	51.33	no	TPSRRSRRSTSNSVKTY	ACACCGTCAAGAAGATCACGTAGGTCAACATCAAACTCTGTAAAAACCTAT
82	200	51.41	no	TQPRRSRRSTANSVTTY	ACACAGCCGAGAAGATCGCGTAGGTCAACCGCAAACTCAGTAACCACCTAC
83	10,000	51.54	no	THSRRSRRSTSNSVTIH	ACACATTCCAGAAGATCACGTAGGTCAACATCAAATTCTGTAACAATCCAT
84	450	51.90	no	THSRRSRRSIPETVHTY	ACACATTCAAGAAGGTCACGTAGGTCAATCCCAGAAACAGTCCATACCTAT
85	310	52.08	no	TQSRRARRSVSEAVQTY	ACACAGTCTAGAAGAGCACGTCGGTCAGTATCAGAGGCAGTACAAACCTAT
86	170,000	52.39	no	TQPRRSRRST-DAVSTVKTY	ACACAACCGAGAAGATCACGTAGGTCAACA---GACGCGGTCAGCACAGTAAAACCTAT
87	270	52.78	no	TQTRRARRSTPQSVTTY	ACACAGACGAGAAGAGCACGTAGGTCAACACCACAATCAGTAACCACCTAC
88	3,100	53.24	no	THSRRARRSTPVTVTTY	ACACATTCTAGAAGAGCACGTAGGTCAACCCCTGTTACAGTAACAACCTAC
89	570	54.08	no	THSRRSRRSTSDT-KTY	ACACATTCAAGAAGATCACGTATATCAACCTCTGAAATT---AAAACCTAT
90	2,962	54.18	no	TQSRRARRSVSESVQTY	ACACAGTCTAGAAGAGCGCGTAGGTCAGTATCAGAGTCAGTACAAACCTAT
91	880	54.22	no	TQSRRSRRSTPDSVKTY	ACACAGTCGAGAAGATCACGTAGGTCAACACCAGACTCTGTAAAAACCTAC
92	2,177	54.45	no	PQPRRSRRSTSNSVTTY	CCACAGCCGAGAAGATCACGCAGTTCAACATCAAATTCAGTAACCACCTAT
93	430	54.78	no	TQPRRARRSTPSLVKTY	ACACAGCCGAGAAGAGCACGTAGGTCAACACCAAGTTTAGTAAAAACCTAC
94	2,650	55.04	no	TQSRRARRSPPESVKTY	ACACAGTCTAGAAGAGCACGTAGGTCACCACCAGAGTCAGTAAAAACCTAT
95	27,000	55.66	no	TQSRRSRRSAPQTAQVY	ACTCAGTCGAGAAGATCACGCAGGTCAGCGCCTCAAGCAGTAAAAGTATAC
96	103	55.66	no	TQSRRSRRSMLESVTTY	ACACAGTCTAGAAGATCACGTAGGTCAATGCTAGAATCAGTAACTACCTAT
97	4,700	55.90	no	TQSRRARRSTTEPVKTY	ACACAGTCAAGAAGAGCACGCAGGTCAACCACTGAACCAGTAAAAACCTAC
98	1,320	56.19	no	TRPRRSRRSTLTSVNTY	ACACGTCCAAGAAGATCACGTAGGTCAACCTTGACCTCAGTAAATACCTAT
99	232	57.31	no	THERRSRRSAPKTVNTY	ACACATGAGAGAAGATCACGTAGGTCAGCACCGAAAACAGTAAACACCTAC
100	1,900	57.39	no	TQSRRSRRSTADSVQLY	ACACAGTCAAGAAGATCACGTAGGTCAACAGCTGACTCTGTACAACTCTAT
101	620	57.68	no	TQSRRSRRSTTDTVKTY	ACACAGTCAAGAAGATCACGTAGTTCAACATCAGACTCTGTAACTATTCAC
102	286	57.81	no	TRSRRSRRSTISTVQTY	ACACGGTCAAGAAGATCACGTAGGTCAACCATCAGTACAGTACAAACCTAT
103	1,300	57.85	no	TQPKRSRRSISRQVTTY	ACACAGCCGAAAAGGTCACGTAGGTCTATATCAAGGCAAGTAACCACCTAT
104	831	58.22	no	TQSRRARRSTSDSVKTY	ACACAGTCGAGAAGAGCACGCAGGTCAACATCAGATTCTGTAAAAACATAT
105	18,000	60.40	no	THSRRSRRSTTETVKTY	ACACATTCAAGAAGATCACGTAGGTCAACCACTGAAACTGTAACAACCTAT
106	1,444	60.61	no	TQPRRSRRSI-SPVNTY	ACACAGCCTAGAAGATCACGTAGGTCAATA---AGTCCTGTGAACACCTAC
107	10,000	64.68	no	TQSRRSRRSTSNSLTTY	ACACAGTCGAGAAGATCACGCAGGTCAACCTCAAACTCACTAACCACCTAT

Table 7.3.2. FIP S1/S2 gene PCR products of the FIP-unbiased population.

FIP-unbiased specimen #	Probe T_m	Mutated fcS1/S2 motif	Peptide sequence	Nucleotide sequence
1	44.30	yes	TTSRRTRRSTSDSVNTY	ACTACTTCTAGAAGAACACGTAGGTCAACATCAGATTCAGTAAACACCTAC
2	45.60	yes	TQSRKSRRSVSEPVTTY	ACACAGTCAAGGAAATCACGCAGGTCGGTCTCTGAACCAGTAACAACCTAT
3	57.94	yes	TQSRRARASTSNSVTTY	ACACAGTCGAGAAGAGCACGTAGATCTACATCAAACTCAGTGACCACCTAC
4	36.25	no	TQSRRARRSTSNSVTTY	ACACAGTCGAGAAGAGCACGTAGATCTACATCAAACTCAGTGACCACCTAC
5	44.67	no	TQPRRSRRSTSNSVTTY	ACACATCCACGAAGATCGCGTAGGTCAACATCAAACTCTGTGACAACCTAT
6	45.98	no	TQPRRSRRSTSNSVTTY	ACACATCCACGAAGATCGCGTAGGTCAACATCAAACTCTGTGACAACCTAT
7	46.17	no	TQPRRSRRSTSNSVTTY	ACACATCCACGAAGATCGCGTAGGTCAACATCAAACTCTGTGACAACCTAT
8	46.21	no	TQSRRARRSTSNSVTTY	ACACAGTCGAGAAGAGCACGTAGATCTACATCAAACTCAGTGACCACCTAC
9	46.22	no	TQSRRARRSTSNSVTTY	ACACAGTCGAGAAGAGCACGTAGATCTACATCAAACTCAGTGACCACCTAC
10	46.36	no	TQPRRSRRSTSNSVTYY	ACACATCCACGAAGATCGCGTAGGTCAACATCAAACTCTGTGACAACCTAT
11	46.48	no	TQPRRSRRSTSNSVTTY	ACACATCCACGAAGATCGCGTAGGTCAACATCAAACTCTGTGACAACCTAT
12	46.54	no	TQPRRSRRSTSNSVTTY	ACACATCCACGAAGATCGCGTAGGTCAACATCAAACTCTGTGACAACCTAT
13	46.54	no	TQPRRSRRSTSNSVTTY	ACACATCCACGAAGATCGCGTAGGTCAACATCAAACTCTGTGACAACCTAT
14	46.67	no	TQPRRSRRSTSNSVTTY	ACACATCCACGAAGATCGCGTAGGTCAACATCAAACTCTGTGACAACCTAT
15	46.73	no	TQPRRSRRSTSNSVTTY	ACACATCCACGAAGATCGCGTAGGTCAACATCAAACTCTGTGACAACCTAT
16	46.78	no	TQSRRARRSTSNSVTTY	ACACAGTCGAGAAGAGCACGTAGATCTACATCAAACTCAGTGACCACCTAC
17	46.78	no	TQSRRARRSTSNSVTTY	ACACAGTCGAGAAGAGCACGTAGATCTACATCAAACTCAGTGACCACCTAC
18	46.85	no	TQSRRARRSTSNSVTTY	ACACAGTCGAGAAGAGCACGTAGATCTACATCAAACTCAGTGACCACCTAC
19	46.86	no	TQPRRSRRSTSNSVTTY	ACACATCCACGAAGATCGCGTAGGTCAACATCAAACTCTGTGACAACCTAT
20	46.98	no	TQPRRSRRSTSNSVTTY	ACACATCCACGAAGATCGCGTAGGTCAACATCAAACTCTGTGACAACCTAT
21	46.98	no	TQPRRSRRSTSNSVTTY	ACACATCCACGAAGATCGCGTAGGTCAACATCAAACTCTGTGACAACCTAT
22	46.99	no	TQSRRARRSTSNSVTTY	ACACAGTCGAGAAGAGCACGTAGATCTACATCAAACTCAGTGACCACCTAC
23	46.99	no	TQSRRARRSTSNSVTTY	ACACAGTCGAGAAGAGCACGTAGATCTACATCAAACTCAGTGACCACCTAC
24	47.06	no	TQSRRARRSTSNSVTTY	ACACAGTCGAGAAGAGCACGTAGATCTACATCAAACTCAGTGACCACCTAC
25	47.13	no	TQSRRARRSTSNSVTTY	ACACAGTCGAGAAGAGCACGTAGATCTACATCAAACTCAGTGACCACCTAC
26	47.24	no	TQSRRARRSTSNSVTTY	ACACAGTCGAGAAGAGCACGTAGATCTACATCAAACTCAGTGACCACCTAC
27	47.29	no	TQPRRSRRSTSNSVTTY	ACACATCCACGAAGATCGCGTAGGTCAACATCAAACTCTGTGACAACCTAT
28	47.36	no	TQPRRSRRSTSNSVTTY	ACACATCCACGAAGATCGCGTAGGTCAACATCAAACTCTGTGACAACCTAT
29	47.48	no	TQPRRSRRSTSNSVTTY	ACACATCCACGAAGATCGCGTAGGTCAACATCAAACTCTGTGACAACCTAT
30	47.54	no	TQPRRSRRSTSNSVTTY	ACACATCCACGAAGATCGCGTAGGTCAACATCAAACTCTGTGACAACCTAT
31	48.04	no	TQPRRSRRSTSNSVTTY	ACACATCCACGAAGATCGCGTAGGTCAACATCAAACTCTGTGACAACCTAT
32	48.64	no	TQSRRSRRSASNSVTTY	ACACAGTCACGAAGATCACGTAGGTCAGCATCAAATTCTGTAACAACCTAT
33	48.67	no	TQSRRSRRSASNSVKTY	ACACAGTCACGAAGATCACGTAGGTCAGCATCAAATTCTGTAACAACCTAT
34	48.92	no	TRPRRSRRSTSDSVTTY	ACACGGCCGCGAAGATCGCGTAGGTCAACATCAGACTCTGTGACAACCTAT
35	49.38	no	TRARRSRRSTSGSVTTY	ACACGGGCGCGAAGATCACGTAGGTCAGCATCGGGTTCTGTAACAACCTAT
36	50.10	no	TQSRRSRRSASNSVTTY	ACACAGTCACGAAGATCACGTAGGTCAGCATCAAATTCTGTAACAACCTAT
37	50.16	no	TQSRRSRRSASNSVTTY	ACACAGTCACGAAGATCACGTAGGTCAGCATCAAATTCTGTAACAACCTAT
38	50.41	no	TQSRRSRRSASNSVTTY	ACACAGTCACGAAGATCACGTAGGTCAGCATCAAATTCTGTAACAACCTAT
39	50.91	no	TKSRRARRSTPATLTTY	ACAAAGTCTAGAAGAGCACGTAGGTCAACACCAGCCACATTAACAACTTAC
40	51.10	no	TQSRRSRRSASNSVTTY	ACACAGTCACGAAGATCACGTAGGTCAGCATCAAATTCTGTAACAACCTAT
41	51.97	no	TKSRRARRSTPATLITY	ACAAAGTCTAGAAGAGCACGTAGGTCAACACCAGCCACATTAATAACTTAC
42	52.96	no	TQSRRARRSTSNSVTTY	ACACAGTCGAGAAGAGCACGTAGATCTACATCAAACTCAGTGACCACCTAC
43	53.38	no	TQSRRARRSTSNSVTTY	ACACAGTCGAGAAGAGCACGTAGATCTACATCAAACTCAGTGACCACCTAC
44	54.47	no	TSSKRSRRSIPETINTY	ACAAGTTCGAAAAGATCACGCAGGTCAATACCTGAAACAATAAATACCTAT
45	54.71	no	TQSRRARRSTSNSVTTY	ACACAGTCGAGAAGAGCACGTAGATCTACATCAAACTCAGTGACCACCTAC
46	54.99	no	TQSRRARRSTSNSVTTY	ACACAGTCGAGAAGAGCACGTAGATCTACATCAAACTCAGTGACCACCTAC
47	55.06	no	TQSRRARRSTSNSVTTY	ACACAGTCGAGAAGAGCACGTAGATCTACATCAAACTCAGTGACCACCTAC
48	55.06	no	TQSRRARRSTSNSVTTY	ACACAGTCGAGAAGAGCACGTAGATCTACATCAAACTCAGTGACCACCTAC
49	55.27	no	TQSRRARRSTSNSVTTY	ACACAGTCGAGAAGAGCACGTAGATCTACATCAAACTCAGTGACCACCTAC
50	55.62	no	TQSRRARRSTSNSVTTY	ACACAGTCGAGAAGAGCACGCAGATCTACATCAAACTCAGTGACCACCTAC
51	55.62	no	TQSRRARRSTSNSVTTY	ACACAGTCGAGAAGAGCACGTAGATCTACATCAAACTCAGTGACCACCTAC
52	55.69	no	TQSRRARRSTPNSVTTY	ACACAGTCTCGAAGAGCACGTAGGTCAACACCAAACTCAGTAACCACATAC
53	55.83	no	TQSRRARRSTSNSVTTY	ACACAGTCGAGAAGAGCACGTAGATCTACATCAAACTCAGTGACCACCTAC
54	55.98	no	TQSRRARRSTSNSVTTY	ACACAGTCGAGAAGAGCACGTAGATCTACATCAAACTCAGTGACCACCTAC
55	56.21	no	TQSRRARRSTSNSVTTY	ACACAGTCGAGAAGAGCACGTAGATCTACATCAAACTCAGTGACCACCTAC
56	56.26	no	TQSRRARRSTSNSVTTY	ACACAGTCGAGAAGAGCACGTAGATCTACATCAAACTCAGTGACCACCTAC
57	56.33	no	TQSRRARRSTSNSVTTY	ACACAGTCGAGAAGAGCACGTAGATCTACATCAAACTCAGTGACCACCTAC

Table 7.3.2.cont. FIP S1/S2 gene PCR products of the FIP-unbiased population.

FIP-unbiased specimen #	Probe T_m	Mutated fcS1/S2 motif	Peptide sequence	Nucleotide sequence
58	56.37	no	TQSRRARRSTSYSVTTY	ACACAGTCGAGAAGAGCACGTAGATCTACATCATACTCGGTGACCACCTAC
59	56.40	no	TQSRRARRSTSNSVTTY	ACACAGTCGAGAAGAGCACGTAGATCTACATCAAACTCAGTGACCACCTAC
60	56.40	no	TQSRRARRSTTNSVTTY	ACACAGTCTCGAAGAGCACGTAGGTCAACAACAAACTCAGTGACCACCTAC
61	56.54	no	TQSRRARRSTSNSVTTY	ACACAGTCGAGAAGAGCACGTAGATCTACATCAAACTCAGTGACCACCTAC
62	56.54	no	TQSRRARRSTSNSVTTY	ACACAGTCGAGAAGAGCACGTAGATCTACATCAAACTCAGTGACCACCTAC
63	56.54	no	TQSRRARRSTSNSVTTY	ACACAGTCGAGAAGAGCACGTAGATCTACATCAAACTCAGTGACCACCTAC
64	56.82	no	TQSRRARRSTSNSVTTY	ACACAGTCGAGAAGAGCACGTAGATCTACATCAAACTCAGTGACCACCTAC
65	56.89	no	TQSRRARRSTSNSVTTY	ACACAGTCGAGAAGAGCACGTAGATCTACATCAAACTCAGTGACCACCTAC
66	56.96	no	TQSRRARRSTSNSVTTY	ACACAGTCGAGAAGAGCACGTAGATCTACATCAAACTCAGTGACCACCTAC
67	56.96	no	TQSRRARRSTSNSVTTY	ACACAGTCGAGAAGAGCACGTAGATCTACATCAAACTCAGTGACCACCTAC
68	57.10	no	TQSRRARRSTSNSVTTY	ACACAGTCGAGAAGAGCACGTAGATCTACATCAAACTCAGTGACCACCTAC
69	57.10	no	TQSRRARRSTSNSVTTY	ACACAGTCGAGAAGAGCACGTAGATCTACATCAAACTCAGTGACCACCTAC
70	57.31	no	TQSRRARRSTTNSVTTY	ACACAGTCTCGAAGAGCACGTAGGTCAACAACAAACTCAGTGACCACCTAC
71	57.52	no	TQSRRSRRSTSNSITTY	ACACAGTCGAGAAGATCACGTAGGTCGACATCAAATTCTATTACGACCTAT
72	57.52	no	TQSRRARRSTPNSVTTY	ACACAGTCTCGAAGAGCACGTAGGTCAACACCAAACTCAGTAACCACATAC
73	58.22	no	TQSRRARRSTSNSVTTY	ACACAGTCGAGAAGAGCACGTAGATCTACATCAAACTCAGTGACCACCTAC
74	58.29	no	TQSRRARRSTSNSVTTY	ACACAGTCGAGAAGAGCACGTAGATCTACATCAAACTCAGTGACCACCTAC
75	58.32	no	TQSRRARRSTSNSVTTY	ACACAGTCGAGAAGAGCACGTAGATCTACATCAAACTCAGTGACCACCTAC
76	58.39	no	TQSRRARRSTSNSVTTY	ACACAGTCGAGAAGAGCACGTAGATCTACATCAAACTCAGTGACCACCTAC
77	58.43	no	TQSRRARRSTPNSVTTY	ACACAGTCTCGAAGAGCACGTAGGTCAACACCAAACTCAGTAACCACATAC
78	58.47	no	TQSRRARRSTSNSVTTY	ACACAGTCGAGAAGAGCACGTAGATCTACATCAAACTCAGTGACCACCTAC
79	58.49	no	TQSRRARRSTSNSVTTY	ACACAGTCGAGAAGAGCACGTAGATCTACATCAAACTCAGTGACCACCTAC
80	58.64	no	TQSRRARRSTPNSVTTY	ACACAGTCTCGAAGAGCACGTAGGTCAACACCAAACTCAGTAACCACATAC
81	58.85	no	TQSRRARRSTPNSVTTY	ACACAGTCTCGAAGAGCACGTAGGTCAACACCAAACTCAGTAACCACATAC
82	58.86	no	TQSRRARRSTSNSMTTY	ACACAGTCGAGAAGAGCACGTAGGTCTACATCAAACTCAATGACCACCTAC
83	59.13	no	TQSRRARRSTSNSVTTY	ACACAGTCGAGAAGAGCACGTAGATCTACATCAAACTCAGTGACCACCTAC
84	59.13	no	TQSRRARRSTPNSVTTY	ACACAGTCTCGAAGAGCACGTAGGTCAACACCAAACTCAGTAACCACATAC
85	59.20	no	TQSRRARRSTPNSVTTY	ACACAGTCTCGAAGAGCACGTAGGTCAACACCAAACTCAGTAACCACATAC
86	59.20	no	TQSRRARRSTPNSVTTY	ACACAGTCTCGAAGAGCACGTAGGTCAACCCCAAACTCAGTAACCACATAC
87	59.20	no	TQSRRARRSTPNSVTTY	ACACAGTCTCGAAGAGCACGTAGGTCAACACCAAACTCAGTAACCACATAC
88	59.34	no	TQSRRARRSTPNSVTTY	ACACAGTCTCGAAGAGCACGTAGGTCAACACCAAACTCAGTAACCACATAC
89	59.41	no	TQSRRARRSTPNSVTTY	ACACAGTCTCGAAGAGCACGTAGGTCAACACCAAACTCAGTAACCACATAC
90	59.56	no	TQSRRARRSTPNSVTTY	ACACAGTCTCGAAGAGCACGTAGGTCAACACCAAACTCAGTAACCACATAC
91	59.63	no	TQSRRARRSTPNSVTTY	ACACAGTCTCGAAGAGCACGTAGGTCAACACCAAACTCAGTAACCACATAC
92	59.70	no	TQSRRARRSTPNSVTTY	ACACAGTCTCGAAGAGCACGTAGGTCAACACCAAACTCAGTAACCACATAC
93	59.70	no	TQSRRARRSTSNSVTTY	ACACAGTCGAGAAGAGCACGTAGATCTACATCAAACTCAGTGACCACCTAC
94	59.74	no	TQSRRARRSTTNSVTTY	ACACAGTCTCGAAGAGCACGTAGGTCAACAACAAACTCAGTGACCACCTAC
95	59.77	no	TQSRRARRSTTNSVTTY	ACACAGTCTCGAAGAGCACGTAGGTCAACAACAAACTCAGTGACCACCTAC
96	59.84	no	TQSRRARRSTPNSVTTY	ACACAGTCTCGAAGAGCACGTAGGTCAACACCAAACTCAGTAACCACATAC
97	59.91	no	TQSRRARRSTTNSVTTY	ACACAGTCTCGAAGAGCACGTAGGTCAACAACAAACTCAGTGACCACCTAC
98	59.91	no	TQSRRARRSTTNSVTTY	ACACAGTCTCGAAGAGCACGTAGGTCAACAACAAACTCAGTGACCACCTAC
99	59.98	no	TQSRRARRSTPNSVTTY	ACACAGTCTCGAAGAGCACGTAGGTCAACACCAAACTCAGTAACCACATAC
100	59.98	no	TQSRRARRSTPNSVTTY	ACACAGTCTCGAAGAGCACGTAGGTCAACACCAAACTCAGTAACCACATAC
101	59.98	no	TQSRRARRSTPNSVTTY	ACACAGTCTCGAAGAGCACGTAGGTCAACACCAAACTCAGTAACCACATAC
102	59.98	no	TQSRRARRSTTNSVTTY	ACACAGTCTCGAAGAGCACGTAGGTCAACAACAAACTCAGTGACCACCTAC
103	60.05	no	TQSRRARRSTPNSVTTY	ACACAGTCTCGAAGAGCACGTAGGTCAACACCAAACTCAGTAACCACATAC
104	60.08	no	TQSRRARRSTTNSVTTY	ACACAGTCTCGAAGAGCACGTAGGTCAACAACAAACTCAGTGACCACCTAC
105	60.19	no	TQSRRARRSTTNSVTTY	ACACAGTCTCGAAGAGCACGTAGGTCAACAACAAACTCAGTGACCACCTAC
106	60.19	no	TQSRRARRSTTNSVTTY	ACACAGTCTCGAAGAGCACGTAGGTCAACAACAAACTCAGTGACCACCTAC
107	60.26	no	TQSRRARRSTPNSVTTY	ACACAGTCTCGAAGAGCACGTAGGTCAACACCAAACTCAGTAACCACATAC
108	60.26	no	TQSRRARRSTPNSVTTY	ACACAGTCTCGAAGAGCACGTAGGTCAACACCAAACTCAGTAACCACATAC
109	60.33	no	TQSRRARRSTSNSVTTY	ACACAGTCGAGAAGAGCACGTAGATCTACATCAAACTCAGTGACCACCTAC
110	60.40	no	TQSRRARRSTSNSVTTY	ACACAGTCGAGAAGAGCACGTAGATCTACATCAAACTCAGTGACCACCTAC
111	60.54	no	TQSRRARRSTPNSVTTY	ACACAGTCTCGAAGAGCACGTAGGTCAACACCAAACTCAGTAACCACATAC
112	60.75	no	TQSRRARRSTPNSVTTY	ACACAGTCTCGAAGAGCACGTAGGTCAACACCAAACTCAGTAACCACATAC
113	60.90	no	TQSRRARRSTPNSVTTY	ACACAGTCTCGAAGAGCACGTAGGTCAACACCAAACTCAGTAACCACATAC
114	61.52	no	TQSRRSRRSTSTSVTTY	ACACAGTCTCGAAGATCACGTAGGTCAACATCAACTTCTGTAACAACCTAT

In the FIP-biased population (**Table 7.3.2**), we performed the FCoV fcS1/S2 gene PCR on a total 252 FIP M gene mRNA positive specimens. Only 138 specimens (54.8%) were also positive in the FCoV fcS1/S2 gene PCR. We obtained a total of 107 sequences in this population after eliminating 31 specimens of which the sequence results was not readable. Among these 107 sequences of the FIP-biased population, 57.9% of the sequences harbor the mutated fcS1/S2 motif versus 42.1% of the sequences harbor the canonical motif. In contrast, 2.6% of the sequences harbor the mutated fcS1/S2 motif versus 97.4% of the sequences harbor the canonical motif in a total 114 sequences of the FIP-unbiased population. A two-tailed Fisher's Exact test was used to examine the differences in mutation frequency between the FIP-biased and -unbiased populations (**Table 7.3.3**). The test generates a *p*-value of less than 0.001, which indicates that the mutation frequency in the fcS1/S2 motif is highly significantly higher in the FIP-biased population than in the -unbiased population (**Table 7.3.3**).

Table 7.3.3. Statistical analysis of the fcS1/S2 motif mutation frequency between the FIP-biased versus -unbiased populations.

Population	Mutated fcS1/S2 motif	Canonical fcS1/S2 motif	Total sequences
FIP-biased	62 (57.9%)	45 (42.1%)	107
FIP-unbiased	3 (2.6%)	111 (97.4%)	114
Two-tailed Fisher's Exact test		P<0.001	

We then investigated whether the PCR target copy numbers (M gene mRNA copy/mL) of the cases with mutant sequences in the FIP-biased population differ from those with the canonical ones (**Table 7.3.4**). As shown in **Table 7.3.4**, the mean M gene mRNA copy number of the cases with the canonical fcS1/S2 motif is more than double

that of the sequence with the mutant fcS1/S2 motif. However, the data variance is too high for the difference of the means to achieve significance ($p = 0.31$, Student's *t*-test).

Table 7.3.4. Analysis of PCR target copy number of fcS1/S2 variants in the FIP-biased population.

fcS1/S2 motif	Total sequences	Mean M gene mRNA/mL	Std. Dev.
Mutated	62	3072.27	7813.39
Canonical	45	6545.96	25433.04
Student's *t*-test		P=0.31	

Peptide sequence results of the fcS1/S2 motif. When compared to the peptide sequences of the fcS1/S2 motif published by Licitra et al. (2013) (**Fig. 7.3.1**), we found that the sequences we obtained are substantially different (**Table 7.3.1 and 7.3.2**). The sequences of the FIP-biased population displayed substantially more overall diversity than those of the -unbiased population.

In the upstream fcS1/S2 region, sequences identified in our study generally start with TQ in both the FIP-biased and -unbiased populations. In the -unbiased population, only 6 non-canonical TR, TK, TT, and TS amino acids are interspersed. In the FIP-biased population, we observed 69 TQ initial amino acids, 17 TH, and additional 21 TR, TP, TS, TG, TA, TD, TY, KS, PH, or PQ sequences. The majority of the next 2 amino acids in both populations were SR, but also PR or few other amino acids. However, the TR sequence identified by Licitra et al. (2013) as canonical was only found in a small percentage (6.5%) of the FIP-biased population. In the furin cleavage recognition motif region, the mutated sequences in both populations demonstrate a distribution of the mutant amino acids across all five positions. In addition, for the complete FIP-biased population we found 71.0% of serine in the P3 position, identical to the 71.2% serine reported by

Licitra et al. (2013) in the combined FECV and FIP sequences. Interestingly however, for the FIP-unbiased population we found a significantly lower proportion with 24.6% of serine in the P3 position ($p < 0.001$; Fisher exact two-tailed test), while the remaining sequences contain alanine (and a single threonine) at the same position. Downstream of the fcS1/S2 motif, we found high sequence polymorphism, similar to what Licitra et al. (2013) report.

Peptide name	Sequence	%THTRRSRRSAPA Sequence *Vmax*
	P4 P3 P2 P1 P1'	
Canonical	THTRRSRRSAPA	100%
P1' SL	THTRRSRRLAPA	8%
P1 R-G	THTRRSRGSAPA	-2%
P1 R-M	THTRRSRMSAPA	-5%
P1 R-T	THTRRSRTSAPA	-5%
P2 R-H	THTRRSHRSAPA	0%
P2 R-L	THTRRSLRSAPA	52%
P2 R-P	THTRRSPRSAPA	129%
P2 R-S	THTRRSSRSAPA	19%
P3 S-A	THTRRARRSAPA	124%
P4 R-K	THTRKSRRSAPA	83%
P4 R-S	THTRSSRRSAPA	-3%
P5 R-K	THTKRSRRSAPA	149%
P6 T-F	THFRRSRRSAPA	162%
P7 H-Q	TQTRRSRRSAPA	186%
P7 H-Q P5 R-K	TQTKRSRRSAPA	232%

Figure 7.3.1. Cleavage efficiency of variant S1/S2 peptides determined by Licitra et al. (2013). Amino acids different from the canonical sequence THTRRSRRSAPA are underlined. Furin cleavage efficiencies were evaluated by the furin cleavage assays of the fluorogenic peptides.

As consequences for the S1/S2 furin cleavage efficiency, based on the analyses by Licitra et al. (2013), we assumed a generally high cleavage efficiency for the canonical RSRRS (P4-P1') motif, 186% of the nominal efficiency reported by Licitra et al. (2013) for their canonical sequence peptide, given the dominant Q at P7 in both populations. For mutations within the core S1/S2 motif, we assumed complete abrogation of cleavage for any mutation of the P1-P1' RS amino acids, at P2 only for R-S conversion, and for any

conversion other than to A or T at P3 and to K at P4. Under these assumptions, all 62 mutant S1/S2 motifs of the FIP-biased population, except for the four cases #8, 25, 32, and 51, are refractory to furin cleavage. In contrast, of the 3 mutant sequences of the FIP-unbiased population, only the single case #3 is refractory.

Melting temperature (T_m) analysis. To assess whether the PCR melting temperature differs between the mutated and canonical fcS1/S2 DNA sequences, a Student's *t*-test was performed on the data obtained from the FIP-biased and -unbiased populations (**Table 7.3.5**). The total of 221 FCoV fcS1/S2 sequences from both populations includes 65 mutated fcS1/S2 sequences and 156 canonical fcS1/S2 sequences. The T_m dispersion as measured by the standard deviation is almost equal in the mutated and canonical fcS1/S2 sequences. The Student's *t*-test generates a *p*-value less than 0.001 indicating that the T_m of the mutated sequences is highly significantly lower than that of the canonical sequences. However, Pearson's correlation analysis showed no significant correlation of the probe melting temperature (T_m) with the log-transformed FIP M gene mRNA copy numbers in the FIP-biased population. ($r^2 = 0.009$, p=0.33).

Table 7.3.5. Analysis of T_m data of the FIP-biased and -unbiased populations.

fcS1/S2 motif	Total sequences	Mean T_m	Std. Dev.
Mutated	65	50.29	5.28
Canonical	156	53.89	5.37
Student's *t*-test		P<0.001	

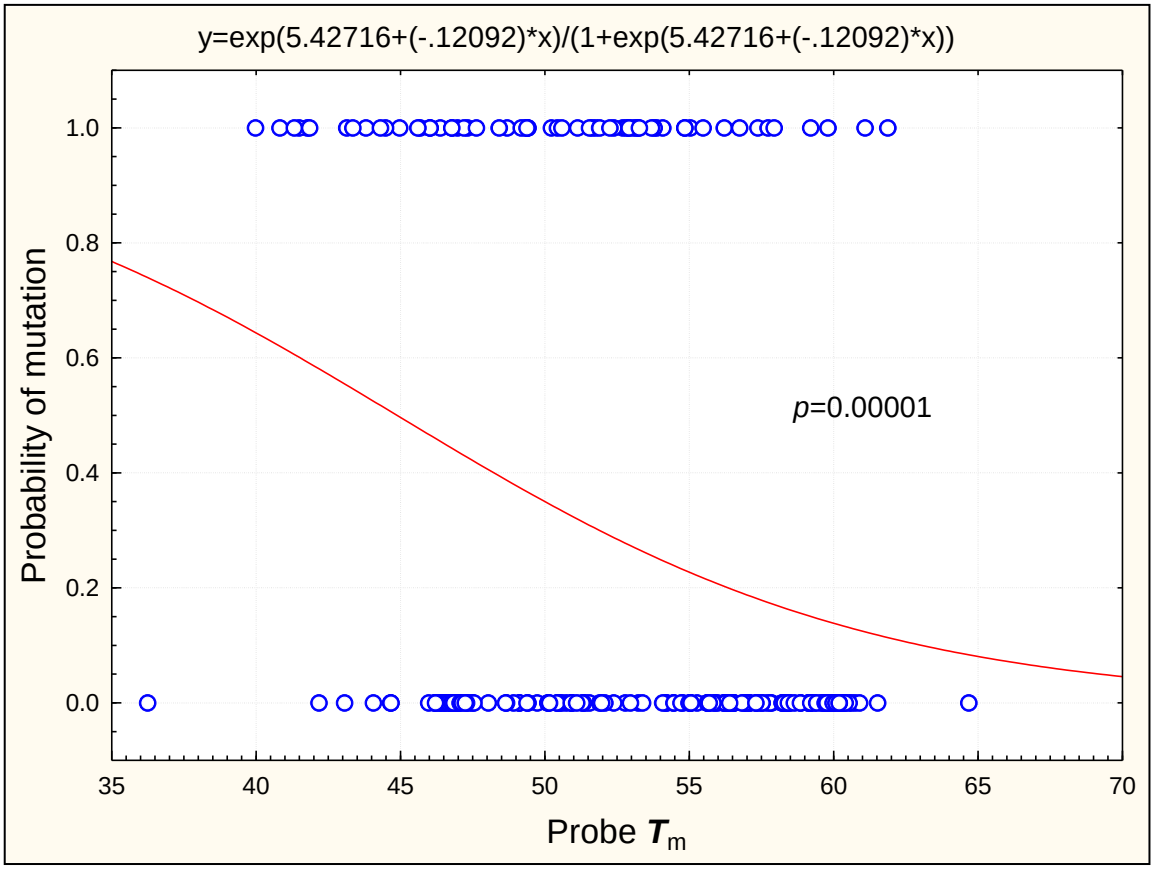

Figure 7.3.2. ***Logistic regression analysis of PCR melting temperature difference between the mutated and canonical fc S1/S2 motif.*** The PCR melting temperatures ($\boldsymbol{T}_m$) of the mutated fcS1/S2 motif sequences are more dispersed when compared to the canonical sequences. The probability of mutation of fc S1/S2 decreases as the melting temperature increases. The *p* value of 0.00001 generated by a *Chi*-square statistics indicates that there is a significant difference of melting temperature between the mutated and canonical fcS1/S2 sequences.

In addition, logistic regression analysis showed that the probability of a mutated fcS1/S2 motif highly significantly decreases as the probe melting temperature ($\boldsymbol{T}_m$) increases (**Fig. 7.3.1**). The $\boldsymbol{T}_m$ of the mutated fcS1/S2 motif sequences are more scattered than that of the canonical sequences, but the $\boldsymbol{T}_m$ standard deviation of the canonical sequences is marginally higher because of two outliers (**Fig. 7.3.1**; **Table 7.3.4**).

7.4. DISCUSSION

In this study, we investigated whether mutations of the FCoV furin cleavage site in the S1/S2 gene (fcS1/S2 motif) associate with FIP infection. We approached this aim by first developing the FCoV fcS1/S2 gene qRT-PCR that amplifies the FCoV fcS1/S2 motif identified by Licitra et al. (2013), followed by performing the PCR on two independent FCoV-infected cat populations, the FIP-biased and un-biased populations (**Table 7.3.1 and 7.3.2**). Among a total of 252 FIP M gene mRNA-positive specimens tested by the FCoV fcS1/S2 gene qRT-PCR, only 138 (54.8%) specimens were also positive for the FCoV fcS1/S2 gene. The low sensitivity of this PCR is likely the result of high polymorphisms in the spike protein gene, including the relatively conserved primer regions such that in many cases the primers fail to anneal to, and amplify, the cognate region of the S gene.

By DNA sequencing of the fcS1/S2 motif region, we determined mutation frequencies of the fcS1/S2 motif in both populations (**Table 7.3.3**). In the FIP-biased population, we identified among a total of 107 S1/S2 sequences 57.9% mutated versus 42.1% canonical fcS1/S2 motifs (**Table 7.3.3**). In contrast, only 2.6% of the FIP-unbiased population harbored a mutated fcS1/S2 motif among a total of 114 S1/S2 sequences (**Table 7.3.3**). A two-tailed Fisher's Exact test confirmed a highly significant difference in fcS1/S2 motif mutation frequencies between the two populations ($p<0.001$) (**Table 7.3.3**). These finding indicate that a mutant fcS1/S2 motif that modulated furin cleavage of the spike protein is highly significantly associated with FIP infection, consistent with literature findings (Licitra et al, 2013). However, the substantial portion of 42.1% of FIP-diagnosed cases with canonical fcS1/S2 motif in the FIP-biased population indicates that a fcS1/S2 motif mutation is not the sole mutation associated with FIP infection.

We further found that the M gene mRNA copy numbers of the canonical sequences was more than double that of the mutant sequences, but this difference was not significant (**Table 7.3.4**). While not significant, this result still is consistent with the hypothesis that FIP viruses in general replicate inefficiently, thus presenting a low antigenic exposure to the immune system that prevents elimination of the infection.

Next, we examined the differences between fcS1/S2 motif sequences in this study and the sequences reported by Licitra et al. (2013). In an overview, we found that the sequences of the FIP-biased population were considerably more diverse than that of the FIP-unbiased population. Also, we found a high percentage of serine in the P3 position in the FIP-biased population versus a high percentage of alanine in the same position in the -unbiased population, indicating a strong selection for lower furin cleavage efficiency in the FIP-biased population (**Fig. 7.3.1**).

On further examination of the differences to Licitra et al. (2013), the initial two amino acids of the upstream fcS1/S2 region were TQ at 80% versus Licitra's 56%. In addition, we only found 8% of the initial amino acids were TH, in contrast to 44% of Licitra's. For the next two amino acids, SR sequences were the majority in both FIP-biased and –unbiased populations, in agreement with Licitra's findings. We found, however, that Licitra's canonical TR sequence only accounted for a small percentage (7%) in the FIP-biased population and was absent in the -unbiased population. In the furin cleavage recognition motif region, our mutant sequences in both populations demonstrated a distribution of mutations across all five positions, which showed higher polymorphisms than those of Licitra et al. (2013). Finally, both studies found the downstream fcS1/S2 motifs highly polymorphic. Overall, the present study shows a broader spectrum of FCoV

fcS1/S2 motif sequences than the sequences reported by Licitra et al., 2013. These highly polymorphic fcS1/S2 sequences genuinely reveal the high mutation frequency of coronavirus, which inevitably imposes a substantial challenge to FIP diagnosis.

We then investigated furin cleavage efficiency of our data by using the data on S1/S2 peptide furin cleavage efficiency reported by Licitra et al. (2013). In our analysis, we assumed that any mutation of the P1-P1' RS amino acids, at P2 only R-S conversion, and any conversion other than to A or T at P3 and to K at P4 would be a lethal mutation that completely abrogates furin cleavage of FCoV. Under these assumptions, we found 58 out of 62 mutant sequences in the FIP-biased population and 1 out of 3 mutant sequences in the -unbiased population harbored mutations that render the spike protein refractory to furin cleavage. While the difference in the proportion of furin cleavage-refractory and -susceptible S1/S2 motifs between the FIP-biased and -unbiased populations is not significant, it nevertheless suggests that the abolished furin cleavage of the spike protein exerts a strong influence on the conversion of FECV to FIPV. However, it is also evident that the mutant fcS1/S2 motif of the FCoV spike protein is not the sole determinant for FIP etiology. Furthermore, other reports identify additional spike protein mutations outside the fcS1/S2 motif that also associate with FIP infection (Chang et al., 2012; Felten et al., 2017; Porter et al., 2014; Rottier et al., 2005). As a result, abolished furin cleavage of the FCoV spike protein clearly is not the sole determinant of FIP etiology. The fact that almost half of the sequences of the FIP-biased population did not harbor such a mutation further support this notion.

To investigate whether the PCR probe melting temperature ($\boldsymbol{T}_m$) can be used to differentiate the sequences that harbor either the mutant or the canonical fcS1/S2 motifs,

the probe mean $\boldsymbol{T}_m$ data were analyzed by Student's *t*-test ($p<0.001$) (**Table 7.3.5** and **Fig. 7.3.2**). The result indicated that the mutant sequences generated a highly significantly lower mean $\boldsymbol{T}_m$ than the canonical ones (**Table 7.3.5**). This finding is consistent with the fact that the more mismatches between the probes to the canonical template exist (indicating higher probability of fcS1/S2 nonsynonymous mutations), the easier the probes dissociate from the template, resulting in a lower probe melting temperature. A logistic regression analysis also demonstrated that the probability of a mutated fcS1/S2 motif substantially decreases as the probe $\boldsymbol{T}_m$ increases (**Fig. 7.3.2**). In this case, the probability of a mutated fcS1/S2 sequence can be determined solely by the probe $\boldsymbol{T}_m$ without examination of DNA sequencing results. For instance, a probe $\boldsymbol{T}_m$ of 58°C suggests an 18% probability of FCoV fcS1/S2 motif mutation; while a probe $\boldsymbol{T}_m$ of 40°C suggests a 65% probability (**Fig. 7.3.2**). The lower the probe melting temperature, the higher the probability is that the sequence harbors a fcS1/S2 mutation. However, there was no significant correlation between probe $\boldsymbol{T}_m$ and the log-transformed FIP M gene mRNA copy numbers in the FIP-biased population ($r^2 = 0.009$, $p=0.33$). This finding is consistent with the non-significantly increased M gene mRNA copy number of FIP cases with mutant fcS1/S2 motif, suggesting that data variance is too high to ascertain the notion that FIPV replicates less efficiently than FECV.

In conclusion, fcS1/S2 motif mutations that result in abrogation of furin cleavage are highly significantly associated with FIP infection. It is, however, not an exclusive mutation that converts FECV to FIPV. Rather, our evidence as well as that of others strongly suggests that mutations of multiple genes, and not single mutations within the FCoV genome, are the trigger for full conversion to FIP virus. Given that viral

polymorphisms can be modulated by the cellular environment (Sanjuán and Domingo-Calap, 2016), one can even assume that after an initial mutation that enables FECV to escape the intestinal habitat, the host immune response may orchestrate the entire FIP disease course by selecting for additional immune escape mutants within the initial FIPV population. An enabling factor is that coronavirus, as a positive-sense single-stranded RNA virus, is prone to mutate, generating 10^{-5} to 2×10^{-3} mutations per nucleotide per replication round (Holland et al., 1982; Drake, 1993; Duffy et al., 2008). The notion that multiple mutations within the FCoV genome are associated with FIP infection is consistent with reports of several such mutant loci (Borschensky et al., 2014;Chang et al., 2010, 2012; Dedeurwaeder et al., 2013; Licitra et al., 2013; Herrewegh et al., 1995; Hora et al., 2016; Rottier et al., 2015; Pedersen et al., 2009, 2012; Porter et al., 2014; Vennema et al.,1998).

On the basis of the results obtained in this study it is clear that FIP cannot be diagnosed via detection of, and polymorphisms within the FCoV S1/S2 motif. First, because of low conservation of the S protein gene, PCR detection of S gene mRNA is much less sensitive than of the M or N genes at 54.8% of the M gene mRNA detection rate. Assuming a 79.1% sensitivity of the M gene mRNA PCR (**Table 6.4.3**), this detection rate results in a disappointing 43.3% sensitivity of the FCoV fcS1/S2 gene qRT-PCR. Second, the probe $\boldsymbol{T}_{\mathrm{m}}$ allows only a very inaccurate estimation of S1/S2 motif mutation probability. Finally, even accurate detection of S1/S2 motif mutations by PCR product sequencing would be inconclusive because of the non-exclusive association of abolished furin cleavage with FIPV. Therefore, functional diagnosis of FIP by extra-intestinal presence of FCoV RNA and mRNA remains the method of choice for nucleic acid-based FIP diagnosis.

CHAPTER 8 Conclusions

8.1. SUMMARY AND CONCLUSIONS

Feline infectious peritonitis (FIP) is a fatal chronic progressive immune-pathological disease caused by feline coronavirus (FCoV), which affects mainly young cats (Cahn and Line, 2010; Pedersen, 2009). Feline coronavirus occurs as two pathotypes, the low-virulence feline enteric coronavirus virus (FECV) and the high-virulence feline infectious peritonitis virus (FIPV). It is widely believed that FIPV is an accumulation of mutations of the low-virulence FECV favored by a multi-cat environment (Chang et al., 2010; Pedersen et al., 2009; Poland et al., 1996; Vennema et al., 1998). However, the full scope of etiological mutations of FECV to FIPV conversion has remained unknown. The enigmatic pathogenesis of FIP also is a major impediment to accurate diagnosis of the disease. Therefore, an accurate ante-mortem diagnosis of FIP, currently unavailable, is essential.

What we did. The clinical challenge of accurately diagnosing FIP lies in the fact that there are no FIP-specific clinical manifestations and laboratory findings. Further diagnostic investigation of this disease is impeded by the absence of diagnostic assays that are capable of differentiating low-virulence FECV from high-virulence FIPV infection. To approach a solution to this diagnostic conundrum, we developed several real-time quantitative PCR assays to detect FIPV via either the detection of subgenomic FCoV mRNA, the replicating virus (FIP M gene mRNA qRT-PCR and FIP N gene mRNA qRT-PCR), or FCoV RNA, both the replicating virus and the viral particles (FIP MN gene qRT-PCR) in extra-intestinal specimens, i.e. detection of FIPV based on the functional characteristics of FIPV. Simultaneously, we developed as a gold-standard for the

performance analyses of the PCR assays a high quality FIP immunofluorescence (IF) assay with the capability of dual labeling FIPV-infected macrophages as well as FCoV in high resolution.

What we found. As a result, we were able to pinpoint the FIP MN gene qRT-PCR as the most sensitive among the three PCR assays based on the evaluations of PCR performance against the gold standard FIP IF assay (**Table 6.4.3**). Upon discovering a nearly mirror distribution of cases that were positive by one and negative by the other of either IF or MN gene PCR assay (**Table 6.3.1**), we reversed the performance analysis by using the MN gene PCR as the gold standard for IF assay performance evaluation (**Tables 6.4.4 and 6.4.5**). After initial re-evaluation, we converted all cases that had been scored as false-positive in either assay by virtue of a negative result in the other assay into true positive results. This was based on our gold standard-independent, absolute measure of specificity in both assays (PCR: positive amplification combined with specific melting point in high-resolution melting curve analysis; IF: positive detection of viral fluorescence, specifically localized to macrophages). This analysis showed that the two assays performed nearly indistinguishable (**Table 6.4.5**). Furthermore, by combining both the results of both 100%-specific assays, and assuming every single positive result as diagnosis of FIP disease, even of borderline cases 48-51 that were single-cell positive in the IF assay but negative in the MN gene qRT-PCR, we demonstrate in 63 specimens from FIP-suspicious cats that 55 cats were actually diseased with FIP (**Table 6.3.1**). These data further point to a more frequent occurrence of FIP than thought, and potentially a large number of falsely negative diagnosed cases.

What is the optimal single diagnostic assay? Based on the preceding analyses, it is clear that there is a pressing need for a single assay that quickly and reliably identifies FIP infection with absolute specificity of detection - to avoid erroneous euthanasia due to false-positive diagnosis, and highest possible sensitivity - to avoid suffering of cats due to falsely undetected FIP infection. To this end we extended the results of previous performance analyses to all 63 examined cases (**Table 6.3.1**), eliminating false-positive diagnoses and including all borderline cases. The results in **Tables 8.1.1** and 8**.1.2** indicate 83.6% sensitivity and 47.1% negative predictive value for the MN gene qRT-PCR, lower than the respective 92.7% and 66.7% of the IF assay. However, these analyses are misleading because they do not include the 52.3% of all cases that cannot be diagnosed with the IF assay to low cellularity of specimen cytospin preparations. Thus, we added 69 cases to the 63 diagnosed ones, and assumed results that were equally distributed as in the 63 cases, and all results of the IF assay were negative, due to the euthanasia consequence of a positive FIP test. (**Table 8.1.1**). Under these assumptions the sensitivity of the IF drops dramatically to 44.3% and the negative predictive value to 21%.

Table 8.1.1. Comprehensive distribution of FIP MN gene qRT-PCR and IF assay results.

MN gene PCR	Diseased[a]	Non-diseased	Positive with 69 IF-undiagnosable cases	Negative with 69 IF-undiagnosable cases
Positive	46	0	46+50 = 96	0
Negative	9	8	9+10 = 19	8+9 = 17
IF assay				
Positive	51	0	51	0
Negative	4	8	4+60 = 64	8+9 = 17

[a] Any positive test is assumed to indicate FIP disease.

Table 8.1.2. Comprehensive performance analysis of the FIP MN gene qRT-PCR and IF assays.

	Se	Sp	PPV	NPV	Accuracy
MN gene PCR	90.2%	100%	100%	61.5%	91.5%
MN gene PCR + 69 IF-undiagnosable cases	83.6%	100%	100%	47.1%	85.7%
IF assay	92.2%	100%	100%	66.7%	93.2%
IF assay + 69 IF-undiagnosable cases	44.3%	100%	100%	21.0%	51.5%

These result shows that if there were only one assay available for FIP testing, the FIP MN gene qRT-PCR is the assay of choice. It is more sensitive than FIP mRNA PCRs, with higher negative predictive value. Unlike the FIP IF assay, it is not influenced by specimen conditions and can be applied to any specimen. This makes it more sensitive, with higher negative predictive value and accuracy than the immunofluorescent assay that is applicable to less than 50% of specimens because of low numbers of retrievable cells. If such specimens still were scored in the FIP IF assay, 83% would be reported as false negatives (**Tables 8.1.1 and 8.1.2**). In clinical practice, the PCR assay is also more efficient owing to its technical ease and rapid turnaround time. For these reasons, we conclude that the FIP MN gene qRT-PCR is the best assay in this study for FIP diagnosis. In addition, this PCR demonstrates higher sensitivity and specificity compared to the available FIP diagnostic assays (Dye et al., 2008; Hartmann et al., 2003; Hornyák Á et al., 2012; Sharif et al., 2010; Simon et al., 2005;Soma et al., 2013).

In this study, we also investigated, by case-control study, the known critical clinical parameters that are associated with FIP. We determined that decreased red blood cell, decreased serum albumin concentration, and decreased serum albumin to globulin ratio (A/G) are associated with FIP, in agreement with literature reports (Norris et al., 2005;

Paltrinieri et al., 2001; Riemer et al., 2016; Tsai et al., 2011). In particular, the low serum albumin concentration genuinely reflects the chronic inflammatory course of FIP. However, since absolute albumin and globulin differ in dependence of cat genetics and nutrition, we believe that serum A/G may be best used as clinical FIP correlate. In our study, we identified A/G values of 0.5 or lower as clinical chemical parameter for FIP diagnosis.

Lastly, we investigated whether the mutation of the furin cleavage recognition motif of the FCoV spike protein, and consequently modified cleavage efficiency, are associated with FIP. We approached this aim by first developing the FCoV fcS1/S2 gene qRT-PCR that amplifies the FCoV fcS1/S2 motif reported by Licitra et al. (2013), followed by performing the PCR on two independent FCoV-infected cat populations, the FIP-biased and un-biased populations (**Table 7.3.1 and 7.3.2**). We then examined by PCR product DNA sequencing fcS1/S2 mutation frequencies between the two populations. The results led to the conclusion that the fcS1/S2 mutation is highly associated with FIP, it is, however, not the sole determinant of FECV to FIPV conversion. Analysis of the amino acid polymorphisms within and adjacent to the fcS1/S2 motif prompted us to conclude that mutations leading FIPV conversion are overwhelmingly associated with abrogation of furin cleavage of the FCoV spike protein.

In summary, our studies have confirmed serum albumin and serum albumin to globulin ratio as the most FIP-pertinent clinical parameters. We also conclude that mutations within the FCoV fcS1/S2 motif that largely abrogate furin cleavage of FCoV spike protein are associated with approximately 58% of FIP cases while 42% of FCoV associated with clinical FIP do not harbor such mutations. Most importantly, we have

established the FIP MN gene qRT-PCR as the most robust ante-mortem diagnosis of FIP, with a detection sensitivity of ~84% at 100% specificity, resulting in 100% positive and 47% negative predictive values. The relatively low negative predictive value of this optimized FIP assay is still unsatisfactory. It is a direct result of the nature of FIP as a chronic progressive disease with very low numbers of virus-infected macrophages. The only remedy to this unsatisfactory reliability of negative results is increasing sensitivity by increased the analyzed specimen volume by subjecting multiple extracted specimen aliquots to FIP MN gene qRT-PCR analysis.

References

Addie D, Belak S, Boucraut-Baralon C, Egberink H, Frymus T, Gruggydd-Jones T, Hartmann K, Hoise MJ, Radford AD, Thiry E, Truyen U, Horzinek MC. 2009. Feline infectious peritonitis ABCD guidelines on prevention and management. *J. Feline Med Surg* **11**: 594-604.

Addie DD, Schaap IAT, Nicolson L, Jarrett O. 2003. Persistent and transmission of natural type I feline coronavirus infection. *J Gen Virol* **84**: 2735-2744.

Amer A, Suri AS, Rhaman OA, Mohd HB, Faruku B, Saeed S, Azmi TIT. 2012. Isolation and molecular characterization of type I and type II feline coronavirus in Malaysia. *Virology* **9**: 1-6.

An D-J, Jeong H-Y, Jeong W, Park J-Y, Lee M-H, Park B-K. 2011. Prevalence of Korean cats with natural feline coronavirus infections. *Virol J* **8**: 455-461.

Bálint A, Farsang A, Zádori Z, Hornyák A, Dencso˝ L, Almazán F, Enjuanes L, Belák S. 2012. Molecular characterization of feline infectious peritonitis virus strain DF-2 and studies of the role of ORF3abc in viral cell tropism. *J Virol* **86**: 6258-6267.

Battilani M, Coradin T, Scagliarini A, Ciulli S, Ostanello F, Prosperi S, Morganti L. 2003. Quasispecies composition and phylogenetic analysis of feline coronaviruses (FCoVs) in naturally infected cats. *FEMS Immunol Med Microbiol* **39**: 141-147.

Benetka V, Kübber-Heiss A, Kolodziejek J, Nowotny N, Hofmann-Parisot M, Möstl K. 2004. Prevalence of feline coronavirus types I and II in cats with histologically verified feline infectious peritonitis. *Vet Microbiol* **99**: 31-42.

Borschensky and Reinacher. 2014. Mutations in the 3c and 7b genes of feline coronavirus in spontaneously affected FIP cats. *Res Vet Sci* **97**: 333-340.

Brown MA, Troyer JL, Pecon-Slattery J, Roelke ME, O'Brien SJ. 2009. Genetics and pathogenesis of feline infectious peritonitis Virus. *Emerg Infect Diseases* **15**: 1445-1452.

Bustin SA and Nolan T. 2004. Pitfalls of quantitative real-time reverse-transcription polymerase chain reaction. *J Biomol Tech* **15**:155-166.

Cahn CM and Line S (10th Ed.). 2010. *The Merck Veterinary Manual*. Whitehouse Station, NJ : Merck &Co., Inc.

Can-Sahna K, Ataseven VS, Pinar D, Oguzoglu TC. 2007. The detection of feline coronaviruses in blood samples from cats by mRNA RT-PCR. *J. Feline Med Surg* **9**: 369-372.

Chakraborty S. 2013. *Microfluidics and Microscale transport processes*. Boca Raton, FL. CRC Press.

Chang HW, Groot D, Egberink HF, Rottier PJ. 2010. Feline infectious peritonitis: insights into feline coronavirus pathogenesis and epidemiology based on genetic analysis of the viral 3c gene. *J Gen Virol* **91**: 415-420.

Chang HW, Groot D, Egberink HF, Rottier PJ. 2012. Spike protein fusion peptide and feline coronavirus virulence. *Emerg Infect Diseases* **18**: 1089-1095.

Cray C, Zaias J, Altman NF. 2009. Acute phase response in animals: a review. *Comp Med* **59**: 517–526.

Cunha NP, Giordano A, Caniatti Mario, Paltrinieri S. Analytical validation of the Sysmex XT-2000iV for cell counts in canine and feline effusions and concordance with cytologic diagnosis. *Vet Clinic Pathol* **44**: 295-302.

Dedeurwaerder A, Olyslaegers DA, Desmarets LM, Theuns S, Nauwynck HJ. 2014. ORF 7-encoded accessory protein 7a of feline infectious peritonitis virus as a counteragent against IFN-alpha-induced antiviral response. *J Gen Virol* **95**: 393-402.

Dedeurwaserder A, Desmarets LM, Olyslaegers DA, Vermeulen BL, Dewerchin HL, Nauwynck HJ. 2013. The role of accessory proteins in the replication of feline infectious peritonitis virus in peripheral blood monocytes. *Vet Microbio* **162**: 447-455.

DeDiego ML, Nieto-Torres JL, Jimenez-Guardeno JM, Regla-Nava JA, Alvarez E, Oliveros JC, Zhao J, Fett C, Perlman S, Enjuanes L. 2011. Severe acute respiratory syndrome coronavirus envelop protein regulates cell stress response apoptosis. *PLoS Pathog* **7**: e1002315.

Degraves FJ, Gao D, Kaltenboeck B. 2003. High sensitivity quantitative PCR platform. *Biotechniques* **34**: 106-110 112-115.

Di Ruffano LF, Hyde CJ, McCaffery KJ, Bossuyt PM, Deeks JJ. 2012. Assessing the value of diagnostics tests: a framework for designing and evaluating trials. *BMJ* **344**: 1-9.

Diaz JV and Poma R. 2009. Diagnosis and clinical signs of feline infectious peritonitis in the central nervous system. *Neurology* **50**: 1091-1093.

Doenges SJ, Weber K, Dorsch R, Fux R, Hartmann K. 2017. Comparison of real-time PCR transcriptase polymerase chain reaction of peripheral blood mononuclear cells, serum, and cell-free body cavity effusion for the diagnosis of feline infectious peritonitis. *J. Feline Med Surg* **19**: 344-350.

Donaldson JG, 2001. Immunofluorescence staining. *Curr Protoc Cell Biol* **4**: 4.3.

Drake JW. 2007. Too many mutants with multiple mutations. *Crit Rev Biochem Mol Biol*: **42**, 247–258.

Drechsler Y, Alcaraz A, Bossong F, Collisson EW, Diniz PP. 2011. Feline coronavirus in multicat environments. *Vet Clinc Small Anim* **41**: 1133-1169.

Duffy S, Shackelton LA, Holmes EC. 2008. Rates of evolutionary change in viruses: patterns and determinants. *Nat Rev Genet* **9**: 267–276.

Dye C, Helps CR, Siddell SG. 2008. Evaluation of real-time RT-PCR for the quantification of FCoV shedding faeces of domestic cats. *J. Feline Med Surg* **10**: 167-174.

Felten S, Weider K, Doenges S, Gruendl S, Matiasek K, Hermanns W, Mueller E, Matiasek L, Fischer A, Weber K, Hirschberger J, Wess G, Hartmann K. 2017. Detection of feline coronavirus spike gene mutations as a tool to diagnose feline infectious peritonitis. *J. Feline Med Surg* **19**: 321-335.

Fehr AR and Perlman S. 2015. Coronaviruses: An overview of their replication and pathogenesis. *Methods Mol Biol* **1282**: 1-23.

Fish EJ, Diniz PP, Juan Y-C, Bossong F, Collisson EW, Drechsler Y, Kaltenboeck B. 2017. A cross-sectional quantitative A cross-sectional quantitative viremia and replication in peripheral blood of healthy shelter cats in Southern California. *J. Feline Med Surg* **1**: 1-7.

Fleck A. **1989.** Clinical and nutritional aspects of changes in acute-phase proteins during inflammation. *Proc Nutr Soc* **48**: 347–354.

Fung S and Liu DX. 2014. Coronavirus infection, ER stress, apoptosis and innate immunity. *Front Microbiol* **5**: 1-13.

Gabay C and Kushner I. 1999. Acute-phase proteins and other systemic responses to inflammation. *N Engl J Med* **340**: 448–454.

Giordano A, Stranieri A, Rossi G, Paltrinieri S,. 2015. High diagnostic accuaracy of the Sysmex XT- 2000iV delta total nucleated cells on effusions for feline infectious peritonits. *Vet Clinic Pathol* **38**: 230-241.

Goodson TL, Tandell SC, Moore LE. 2009. Feline infectious peritonitis. *Compendium* **31**: 1-9.

Greene CE (4th Ed.) 2012. Section I: Viral, rickettsial, and chlamydial diseases. *Infectious diseases of the dogs and cats*. Philadelphia: Saunders.

Gruendl S, Matiasek K, Matiasek L, Fischer A, Felten S, Jurina K, Hartmann K. 2017. Diagnostic utility of cerebrospinal fluid immunocytochemistry for diagnosis of feline infectious peritonitis manifesting in the central nervous system. *J. Feline Med Surg* **19**: 576-585.

Hartmann K, Binder C, Hirschberger J, Cole D, Reinacher M, Schroo S, Frost J, Egberink H, Lutz H, Hermanns W. 2003. Comparison of different tests to diagnose feline infectious peritonitis. *J Vet Intern Med* **17**: 781–790.

Hartmann. 2005. Feline infectious peritonitis. *Vet Clin Small Anim* **35**: 39-79.

Herrewegh AA, Groot D. Cepica RJ, Egberink A, Horzinek MC, Rottier PJ. 1995. Detection of feline coronavirus RNA in feces, tissues, and body fluids of naturally infected cats by reverse transcriptase PCR. *J Clin Micobiol* **33**: 684-689.

Herrewegh AA, Smeenk I, Horzinek MC, Rottier PJ, Groot D. 1998. Feline coronavirus type II strains 79-1683 and 79-1146 originate from a double recombination between feline coronavirus type I and canine coronavirus. *J Virol* **72**: 4508-4514.

Hoffman GE, Le WW, Sita LV. 2008. The importance of titrating antibodies for immunocytochemical methods. *Curr Protoc Neurosci* **76:** 2.12. 1-2. 12.37.

Hok, 1989. Demonstration of feline peritonitis virus in conjunctival epithelial cells from cats. *APMIS* **97**: 820-824.

Holland J, Spindler K, Horodyski F, Grabau E, Nichol S, Van de Pol S. 1982. Rapid evolution of RNA genomes. *Science* **215**: 1577–1585.

Hora AS, Tonietti PO, Taniwaki SA, Asano KM, Maiorka P, Richtzenhain LJ, Brandão PE. 2016. Feline coronavirus 3c protein: a candidate for a virulence marker? *BioMed Res Int* **2016**: 1-9.

Horhogea C, Laiu I, Maciuca I, Rimbu C, Carp-Carare MC. 2011. Feline infectious peritonitis and anatomopathological aspects. *Bull UASVM Vet Med* **68**: 159-164.

Hornyák Á, Bálint Á, Farsang A, Balka G, Hakhverdyan M, Rasmussen TB, Blomberg J, Belák S. 2012. Detection of subgenomic mRNA of feline coronavirus by real-time polymerase chain reaction based on primer-probe energy transfer (P-sg-QPCR). *J Virol Methods* **18**:155-163.

Hsieh B, Burney DP. 2014 Feb. Feline infectious peritonitis. Retrieved from *http://www.clinicianbrief.com*.

Hugo TB and Heading KL. 2013. Prolonged survival of a cat diagnosed with feline infectious peritonitis by immunohistochemistry. *Can Vet J* **56**: 53-58.

Ives EJ, Vanhaesebrouck AE, Cian F. 2013. Immunocytochemical demonstration of feline infectious peritonitis virus within cerebrospinal fluid macrophages. *J. Feline Med Surg* **15**: 1149-1153.

Jeffery U, Deitz K, Hostetter S. 2012. Positive predictive value of albumin: globulin ratio for feline infectious peritonitis in a mid-western referral hospital population. *J. Feline Med Surg* **14**: 903-905.

Jeong YS, Makino S. 1994. Evidence for coronavirus discontinuous transcription. *J. Virol.* **68**: 2615-2623.

Kaltenboeck B and Wang C. 2005. Advances in real-time PCR: application to clinical laboratory diagnostics. *Adv. Clin. Chem.* **40**: 219-259.

Kaltenboeck B. 2007. U.S. Patent 7,252,937 B2.

Kim Y, Liu H, Kankanamalage ACG, Weerasekara S, Hua DH, Groutas WC, Chang KO, Pedersen NC. 2016. Reversal of the progression of fatal coronavirus infection in cats by a broad-spectrum coronavirus inhibitor. *PLoS Pathog* **12**: e1005531.

Kipar A, Meli ML, Baptiste KE, Bower LJ, Lutz H. 2010. Sites of feline coronavirus persistence in healthy cats. *J Gen Virol* **91**: 1698-1707.

Kipar A, Meli ML. 2014. Feline infectious peritonitis: still an enigma? *Vet Pathol* **51**: 505-526.

Kiss I, Kecskeméti S, Tanyi J, Klingeborn B, Belák S. 2000. Preliminary studies on feline coronavirus distribution in naturally and experimentally infected cats. *Res Vet Sci* **68**: 237-242.

Kleppe K, Ohtsuka E, Kleppe R, Molineux I, Khorana HG. 1971. Studies on polynucleotides. XCVI. Repair replications of short synthetic DNAs as catalyzed by DNA polymerases. J. Mol. Biol. **56**: 341–361.

Kroeber S, Schomerus C, Korf H-W. 1998. A specific double-immunofluorescence method for the demonstration of S-antigen and serotonin in trout and rat pinealocytes by means of primary antibodies from the same donor species. *Histochem Cell Biol* **109**: 309–317

Kummrow M, Meli ML, Haessig M, Goenczi, Poland A, Pedersen NC, Hofmann-Lehmann R, Lutz H. 2005. Feline coronavirus serotype 1 and 2: seroprevalence and association with disease in Switzerland. *Clin Diagn Lab Immunol* **12**: 120-1215.

Kuo L, Hurst-Hess KR, Koetzner CA, Paul SM. Analyses of coronavirus assembly interactions with interspecies membrane and nucleocapsid protein chimeras. *J Virol* **90**: 4357-4368.

Li X and Scott FW. 1994. Detection of feline coronaviruses in cell cultures and in fresh and fixed feline tissues using polymerase chain reaction. *Vet Microbiol* **42**: 65-77.

Li Y, Treffers EE, Napthine S, Tas A, Zhu L, Sun Z, Bell S, Mark BL, van Veelen PA, van Hemert MJ, Firth AE, Brierley I, Snijder EJ, Fang Y. 2013. Transactivation of programmed ribosomal frameshifting by a viral protein. *Proc Natl Acad Sci U S A* **111**: 2172-2181.

Licitra BN, Millet JK, Regan AD, Hamilton BS, Rinaldi VD, Duhamel GE, Whittaker GR. 2013. Mutation in spike protein cleavage site and pathogenesis of feline coronavirus. *Emerg Infect Diseases* **19**: 1066-1073.

Licitra BN. 2015. Role of the viral spike protein in feline and canine coronavirus pathogenesis. Cornell Univeristy, PhD.

Lin CN, Su BL, Huang HP, Lee JJ, Hsieh MW, Chueh LL. 2009. Field strain feline coronaviruses with small deletions in ORF7b associated with both enteric infection and feline infectious peritonitis. *J. Feline Med Surg* **11**: 413-419.

Litster AL, Pogranichniy R, Lin T-L. 2013. Diagnostic utility of a direct immunofluorescence test to detect feline coronavirus antigen in macrophages in effusive feline infectious peritonitis. *Vet J* **198**: 362-366.

Madias JE. 2013. Electrocardiogram voltage attenuation and shortening of the duration of P-waves, QRS complexes, and QT intervals. *Indian Heart J* **65**: 614-617.

Marioni-Henry K, Vite CH, Newton AL, Van WJ. 2004. Prevalence of disease of spinal cords of cats. *J Vet Intern Med* **18**: 851-858.

McAdam AJ. 2000. Discrepant analysis: How can we test a test? *J Clin Micobiol* **35**: 2027-2029.

McBride R, van zyl Marjorie, Fielding BC. 2014. The coronavirus nucelocapsid is a multifunctional protein. *Viruses* **6**: 2991-3018.

Mohan KH, Pal S, Rao R, Sripathi H. Prabhu S. 2008. Techniques of immunofluorescence and their significance. *Indian J Dermato Venereol Leprol* **74**: 415-419.

Motokawa K, Hohdatsu T, Hashimoto H, Koyama H. 1996. Comparison of the amino acid sequence and phylogenetic analysis of the peplomer, integral membrane and nucleocapsid proteins of feline, canine, porcine coronaviruses. *Microbiol Immunol* **40**: 425-433.

Neuman BW, Kiss G, Kunding AH, Bhella D, Baskh MF, Connelly S, Dorese B, Klaus JP, Makino S, Sawicki SG, Siddell SG, Stamou DG, Wilson IA, Kuhn P, Buchmeier. 2011. A sturcutral analysis of M protein in coronavirus assembly and morphology. *J Struct Biol* **174**: 11-22.

Norris JM, Bosward KL, White JD, Baral RM, Catt MJ, Malik R. 2005. Clinicopathological findings associated with feline infectious peritonitis in Sydney, Australia: 42 cases (1990-2002). *Aust Vet J* **83**: 666-673.

Paltrinieri S, Grieco V, Comazzi S, Parodi MC. 2001. Laboratory profiles in cats with different pathological and immunohistochemical findings due to feline infectious peritonitis (FIP). *J. Feline Med Surg* **3**: 149-159.

Paltrinieri S, Parodi MC, Cammarata G. 1999. In vivo diagnosis of feline infectious peritonitis by comparison of protein content, cytology, and direct immunofluorescence test on peritoneal and pleural effusions. *J Vet Diagn Inves* **11**: 358-361.

Parodi MC, Cammarate G, Paltrinieri S, Lavazza A, Ape F. 1993. Using direct immunofluorescence to detect coronaviruses in peritoneal and pleural effusions. *J Small Anim Prac* **34**: 609-613.

Pederden NC, Liu H, Dodd KA, Pesavento PA. 2009. Significance of coronavirus mutants in feces and diseased tissues of cats suffering from feline infectious peritonitis. *Viruses* **1**: 166-184.

Pedersen NC. 2014. An update on feline infectious peritonitis: Virology and immunopathogenesis. Veterinary Journal **201**: 123-132.

Pesteanu-Somogyi LD, Radzai C, Pressler BM. 2006. Prevalence of feline infectious peritonitis in specific cat breeds. *J. Feline Med Surg* **8**: 1-5.

Plant EP, Rakauskaite R, Taylor DR, Dinman JD. 2010. Achieving a golden mean: mechanisms by which coronaviruses ensure synthesis of the correct stoichiometric ratios of viral proteins. *J Virol* **84**: 4330-4340.

Poland AM, Vennema H, Foley JE, Pedersen NC. 1996. Two related strains of feline infectious peritonitis virus isolated from immunocompromised cats infected with a feline enteric coronavirus. *J Clin Micobiol* **34**: 3180-3184.

Poncelet L, Coppens A, Peters D, Bianchi E, Grant CK, Kadhim H. 2008. Detection of antigenic heterogeneity in feline coronavirus nucleocapsid in feline pyogranulomatous meningoencephalitis. *Vet Pathol* **45**: 140-153.

Porter E, Tasker S, Day MJ, Harley R, Kipar A, Siddell SG, Helps CR. 2014. Amino acid changes in the spike protein of feline coronavirus correlate with systemic spread of virus from the intestine and not with feline infectious peritonitis. *Vet Res* **45**:49.

Rand JS, Parent J, Percy D, Jacobs R. 1994. Clinical, cerebrospinal fluid, and histological data from twenty-seven cats with primary inflammatory disease of the central nervous system. *Can Vet J* **35**: 103-110.

Riemer F, Kuehner KA, Ritz S, Sauter-Louis C, Hartmann K. 2016. Clinical and laboratory features of cats with feline infectious peritonitis- a retrospective study of 231 confirmed cases (2000-2010). *J. Feline Med Surg* **18**: 348-356.

Rohrbach BW, Lefendre AM, Baldwin CA, Lein DH, Reed WM, Wilson RB. 2001. Epidemiology of feline infectious peritonitis among cats examined at veterinary medical teaching hospitals. *JAVMA* **218**: 1111-1115.

Rottier PJM, Nakamura K, Schellen P, Volders H, Haijema BJ. **2005.** Acquisition of macrophage tropism during the pathogenesis of feline infectious peritonitis is determined by mutations in the feline coronavirus spike protein. *J of Virol* **79**: 14122-14130.

Ruch TR and Machamer CE. 2012. The coronavirus E protein: assembly and beyond. *Viruses* **4**: 363-382.

Saitou N and Nei M, 1987. The neighboring-joining method: a new method for reconstructing Guide Trees. *Mol. Biol. Evol* **4**: 406-425.

Sanjuán R and Domingo-Calap P. 2016. Mechanism of viral mutation. *Cell Mol Life Sci* **73**: 4433-4448.

Sawicki SG, Sawicki DL, Siddell SG. 2007. A contemporary view of coronavirus transcription. *J of Virol* **81**: 20-29.

Sethna PB, Hoffman MA, Brian DA. 1991. Minus-strand copies of replicating coronavirus mRNAs contain antileaders. *J of Virol* **65**: 320-325.

Sharif S, Arshad SS, Hair-Bejo M, Omar AR, Zeenathul NA, Alazawy A. 2010. Diagnostics methods for feline coronavirus. *Vet Med Int* **2010**: 1-7.

Sharif S, Arshad SS, Hair-Bejo M, Omar A-R, Zeenathul NA, Rahman N-A, Alazawy A. 2011. Evaluation of feline coronavirus viremia in clinically healthy and ill cats with feline infectious peritonitis. *J Anim Vet Adv* **10**: 18-22.

Simons, FA, Vennema H, Rofina, JE, Pol, JM, Horzinek, MC, Rottier, PJ, and Egberink, HF. 2005. A mRNA PCR for the diagnosis of feline infectious peritonitis. *Journal of Virological Methods* **124**: 111–116.

Siu YL, Teoh KT, Lo J, Chan CM, Kien F, Escriou N, Tsao SW, Nichollas JM, Altmeyer R, Peiris JSM, Bruzzone R, Nal B. 2008. The M, E, and N structural proteins of the severe acute respiratory syndrome coronavirus are required for efficient assembly trafficking, release of virus-like particles. *J Virol* **82**: 11318-11330.

Soma T, Wada M, Taharaguchi S, Tajima T. 2013. Detection of ascitic feline coronavirus RNA from cats with clinically suspected feline infectious peritonitis. *Virology* **75**: 1389-1392.

Tamke PG, Petersen MG, Dietze AE, deLahunta A. 1988. Acquired hydrocephalus and hydromyelia in a cat with feline infectious peritonitis: A case report and brief review. *Can Vet J* **29**: 997-1000.

Thiel V, Thiel HJ, Tekes G. 2014. Tackling feline infectious peritonitis via reverse genetics. *J Virol* **86**: 6994-6998.

Thompson JD, Higgins DG, Gibson TJ. 1994. CLUSTAL W: improving the sensitivity of progressive multiple sequence alignment through sequence weighting, position-specific gap penalties and weight matrix choice. *Nucleic Acid Res.* **22**: 4673-4680.

Timmann D, Cizinauskas S, Tomek L, Doherr M, Vandevelde M, Jaggy A. 2008. Retrospective analysis of seizures associated with feline infectious peritonitis in cats. *J. Feline Med Surg* **10**: 9-15.

Tresnan DB, Levis R, Holmes KV. 1996. Feline Aminopeptidase N Serves as a Receptor for Feline, Canine, Porcine, and Human Coronaviruses in Serogroup I. *J Virol* **70**: 8669-8674.

Trotman TK, Mauldin E, Hoffmann V, Piero FD, Hess RS. 2007. Skin fragility syndrome in a cat with feline infectious peritonitis and hepatic lipidosis. *Vet Dermatol* **5**: 365-369.

Tsai H-Y, Chueh L-L, Lin C-N, Su B-L. 2011. Clinicopathological findings and disease staging of feline infectious peritonitis: 51 cases from 2003 to 2009 in Taiwan. *J. Feline Med Surg* **13**: 74-80.

Utans U, Arceci RJ, Yamashita T, Russell ME. 1995. Cloning and characterization of Allograft Inflammatory Factor-1: A novel macrophage factor identified in rat cardiac allografts with chronic rejection. *J Clin Invest* **95**: 2954-2962.

Vennema H, Poland A, Foley J, Pedersen NC. 1998. Feline infectious peritonitis viruses arise by mutation from endemic feline enteric coronaviruses. *Virology* **243**: 150-157.

Vennema H. 1999. Genetic drift and genetic shift during feline coronavirus evolution. *Vet Microbio* **69**: 139-141.

Vermeulen BL, Devriendt B, Olyslaegers DA, Dedeurwaerder A, Desmarets LM, Favoreel HW, Dewerchin HL, Nauwynck HJ. 2013. Supression of NK cells and regulatory T lymphocytes in cats naturally infected with feline infectious peritonitis virus. *Vet Micobiol* **164**: 46-59.

Viana MB. 2011. Anemia and infection: a complex relationship. Rev Bras Hematol Hemoter **33**: 90-92.

Wang C, Gao D, Vaglenov A, Kaltenboeck B. 2004. One-step real-time duplex reverse transcription PCRs simultaneously quantify analyte and housekeeping gene mRNAs. *Biotechniques* **36**: 508-519.

Wang Y-T, Chueh L-L, Wan C-H. 2014. An eight-year epidemiologic study based on baculovirus-expressed type-specific spike proteins for the differentiation of type I and II feline coronavirus infections. *BMC Vet Res* **10**: 1-8.

Wesseling JG, Vennema H, Godeke G-J, Horzinek MC, Rottier JM. 1994. Nucleotide sequence and expression of the spike (S) gene of canine coronavirus and comparison with the S proteins of feline and porcine coronavirus. *J Gen Virol* **75**: 1789-1794.

Wester K, Asplund A, Bäckvall H, Micke P, Dervenience A, Hartmane I, Malmström P-U, Pontén. 2003. Zinc-based fixative inproves preservation of genomic DNA and proteins in histoprocessing of human tissues. *Lab Invest* **83**: 889-899.

Wolfe LG and Griesemer RA. 1966. Feline infectious peritonitis. *Path Vct* **3**: 255-270.

Worthing KA, Wigney DI, Dhand NK, Fawcett A, McDonagh P, Malik R, Norris JM. 2012. Risk factors for feline infectious peritonitis in Australian cats. *J. Feline Med Surg* **14**: 405-412.

Wu H-Y and Brian DA. 2010. Subgenomic messenger RNA amplification in coronaviruses. *Proc Natl Acad Sci U S A* **107**: 12257-12262.

Wu K, Peng G, Wilken M, Geraghty RJ, Li F. 2012. Mechanism of host receptor adaptation by SARS coronavirus. *J Biol Chem* **287**: 8904-8911.